Analysis of Neil DNA glycosylases during early *Xenopus* development

Dissertation

Zur Erlangung des Grades

Doktor der Naturwissenschaften

Am Fachbereich Biologie

Der Johannes Gutenberg-Universität Mainz

Dandan Han

Mainz, 2018

Dekan:

1. Berichterstatter:

2. Berichterstatter:

Tag der mündlichen Prüfung: 30.10.2018

Table of Contents

1. Summary

DNA demethylation plays an important role in development and vertebrate physiology. In active DNA demethylation, 5-methylcytosine (5mC) is iteratively oxidized into 5-hydroxylmethylcytosine (5hmC), 5-formylcytosine (5fC) and 5-caboxylcytosine (5caC) by Ten-eleven-translocation (TET) enzymes. Subsequently, 5fC and 5caC are removed by Thymine DNA glycosylase (TDG) and base excision repair (BER) proteins. *In vitro* data indicate that Nei-like (NEIL) glycosylases play a crucial role in this context by increasing the enzymatic turnover of TDG in BER. In the first part of my thesis, I analyzed the role of Tet3, Tdg, and especially Neil proteins in active DNA demethylation in *Xenopus laevis* embryos. Expression analysis showed that *tet3, tdg*, *neil1* and *neil3* are expressed during the embryonic development of the central nervous system. *Neil2* mRNA is maternally supplied, and its expression level is decreased drastically upon zygotic genome activation (ZGA). Analysis of 5mC and its oxidative derivatives by mass spectrometry supports the cooperation of Tet3, Tdg, and Neil2 in active DNA demethylation *in vivo*. Antisense Morpholino (MO) knockdown of Tet3, Tdg, Neil2 and Neil3 induces neural crest defects and microcephaly.

In the second part of my thesis, I examined the mechanisms leading to the neural crest cell (NCC) defects and microcephaly phenotypes of *neil2* MO injected embryos (Neil2 morphants). Whole transcriptome analysis and qPCR expression analysis show that the Tp53 DNA damage pathway is activated in Neil2 morphants. In Neil2 morphant neural plates, pS345 Chk1, Tp53, and active caspase-3 accumulate during NCC differentiation. Knockdown of Tp53 reduces apoptotic cell death and rescues microcephaly in Neil2 morphants. Neural crest defects and microcephaly are recapitulated by treating embryos with the reactive oxygen species (ROS) inducer pyocyanin. This treatment upregulates protein levels of pS345 Chk1, Tp53, and active caspase-3, and activates expression of Tp53 target genes. Pyocyanin and *neil2* MO injection show synergistic effects in inducing microcephaly. Furthermore, Neil2 morphants display craniofacial abnormalities, mimicking Treacher-Collins-Syndrome.

In summary, my study demonstrates a novel role of Neil2 in cooperation with Tet3 and Tdg in active DNA demethylation during *Xenopus* embryogenesis. In addition, Neil2 deficiency elicits an oxidative stress-induced, Tp53-dependent DNA damage response, which impairs NCC differentiation. My work emphasizes how defects in BER can lead to a selective lineage defect during embryogenesis.

2. Zusammenfassung

DNA-Demethylierung spielt eine wichtige Rolle in der Entwicklung und Physiologie von Vertebraten. Während der aktiven DNA-Demethylierung wird 5-Methylcytosin (5mC) von Ten-eleven-translocation (TET) Enzymen iterativ zu 5-Hydroxymethylcytosin (5hmC), 5-Formylcytosin (5fC), sowie 5-Carboxylcytosin (5caC) oxidiert. 5fC und 5caC werden daraufhin von Thymine DNA Glycosylase (TDG) und Enzymen der Basenexzisionsreparatur (BER) aus der DNA entfernt. *In vitro* Daten belegen, dass Nei-like (NEIL) Glykosylasen eine entscheidende Rolle in diesem Prozess spielen, indem sie den enzymatischen Durchsatz von TDG erhöhen. In dieser Arbeit habe ich die Rolle von Tet3, Tdg und insbesondere der Neil Glykosylasen während der aktiven DNA-Demethylierung in *Xenopus laevis* Embryonen analysiert. *Tet3*, *tdg*, *neil1* und *neil3* werden während der embryonalen Entwicklung des zentralen Nervensystems exprimiert. *Neil2* mRNA wird maternal bereitgestellt und verringert sich drastisch nach der zygotischen Genomaktivierung (ZGA). Eine massenspektrometrische Analyse von 5mC und seinen oxidativen Derivaten bestätigt die Kooperation von Tet3, Tdg und Neil2 während der aktiven DNA-Demethylierung *in vivo*. Ein *Antisense*-Morpholino vermittelter *Knockdown* von Tet3, Tdg, Neil2 und Neil3 führt zu Defekten in der Neuralleistenentwicklung und Mikrozephalie.

Im zweiten Teil meiner Arbeit untersuchte ich die Mechanismen, die zu den erwähnten Phänotypen der *neil2*-Morpholino injizierten Embryonen führen. Transkriptom, sowie qPCR-Analysen zeigen eine Aktivierung der Tp53-abhängigen DNA-Schadens-Antwort in *neil2*-Morpholino injizierten Embryonen. In den Neuralplatten dieser Embryonen ist pS345 Chk1, Tp53 und aktive Caspase-3 erhöht. Ein *Knockdown* von Tp53 vermindert Apoptose und den Mikrozephalie-Phänotyp der *neil2*-Morpholino injizierten Embryonen. Neuralleistendefekte und Mikrozephalie werden in Wildtyp-Embryonen durch Zugabe von Pyocyanin, einem Produzenten von reaktiven Sauerstoffspezies, imitiert, einhergehend mit erhöhter Proteinmenge von Tp53 und Expression von Tp53-Zielgenen. Pyocyanin und *neil2*-Morpholinoinjektion erzielen einen synergistischen Effekt bei der Induzierung von Mikrozephalie. Des Weiteren weisen *neil2*-Morpholino injizierte Embryonen kraniofaziale Fehlbildungen auf, die dem Treacher-Collins-Syndrom ähneln.

Zusammenfassend demonstriert meine Arbeit eine bisher unbekannte Rolle von Neil2, in Kooperation mit Tet3 und Tdg bei der aktiven DNA-Demethylierung während der *Xenopus*-Embryogenese. Zudem induziert der Verlust von Neil2 eine durch oxidativen Stress verursachte, Tp53-abhängige DNA-Schadens-Antwort, welche die Neuralleisten-differenzierung beeinträchtigt. Meine Arbeit verdeutlicht, wie BER-Defekte zu selektiven Differenzierungsdefekten während der Embryogenese führen können.

3. Introduction

3.1 DNA methylation and demethylation

3.1.1 DNA methylation

Embryogenesis is delicately regulated by transcription factors and epigenetic modifications, such as DNA methylation, histone modification, and non-coding RNA [1]. DNA methylation plays key roles in cell differentiation, carcinogenesis, aging and embryonic development, especially in vertebrates [2, 3]. In DNA methylation, *de novo* DNA methyltransferases (DNMTs) DNMT3a and DNMT3b covalently transfer a methyl group to the fifth position of cytosine, predominantly at cytidine-guanosine (CpG) dinucleotides. After DNA replication, the parent DNA strands retain their methylation patterns, but the newly synthesized daughter strands are unmethylated. The maintenance DNA methyltransferase DNMT1 preferentially binds to the hemi-methylated DNA, and catalyzes DNA methylation on the opposite cytosine in the CpG dinucleotide of the daughter strand [4, 5].

DNA methylation is mainly involved in repressive gene regulation, which is achieved either by repelling transcription factors from binding to the regulatory DNA elements directly [6, 7], or by recruiting methylated DNA binding proteins to the sites, which further inhibits the binding of specific transcription factors, or generally form a repressive, inaccessible chromatin structure [8–10]. DNA methylation may however also activate gene expression by inhibiting the binding of transcriptional repressors to regulatory elements within the DNA [11].

3.1.2 DNA demethylation

DNA methylation was considered a stable epigenetic mark for a long time. Direct removal of methyl groups from cytosine requires the break of a carbon-carbon bond, which is thermodynamically unfavorable. Although one study showed that Methyl-CpG-binding domain protein 2 (MBD2) achieves the direct removal of methyl groups by releasing them in the form of methanol [12], these results so far have not been reproduced. Passive DNA demethylation and other active DNA demethylation pathways, however, have been well characterized by now. Passive DNA demethylation is replication dependent. In the absence of DNMT1, the newly synthesized DNA cannot be methylated and methylation is passively diluted after several rounds of DNA replication [13]. The ten-eleven translocation (TET)

family proteins initiate active DNA demethylation by iteratively oxidizing 5-methylcytosine (5mC) into 5-hydroxymethylcytosine (5hmC) [14, 15], 5-formylcytosine (5fC) and 5-carboxylcytosine (5caC) [16]. These oxidized 5mC derivatives are either passively diluted through DNA replication, or actively removed via thymine DNA glycosylase (TDG) initiated base excision repair (BER) [17, 18]. In active DNA demethylation, TDG excises 5fC and 5caC and generates apurinic/apyrimidinic (AP) sites. Subsequently, AP sites are repaired by other BER factors to restore the site with an unmodified cytosine, resulting in DNA demethylation (Figure 3.1).

Evidence is emerging to support that oxidative 5mC products might play roles other than merely acting as active DNA demethylation intermediates. In neuronal cells, 5hmC is abundantly distributed in the genome, which indicates it might act not only as a transient intermediate, but also as a stable epigenetic mark affecting neuronal function [19, 20]. Also quantitative mass-spectrometry-based proteomics have identified specific readers for the oxidized derivatives [21]. The readers show not only cell type specificity, but also modification specificity, hinting that not only 5mC, but also its oxidized derivatives may play specific roles in regulating cell proliferation and differentiation. Interestingly, many DNA repair proteins are identified as readers for 5mC oxidized derivatives, revealing the involvement of DNA damage response (DDR) in active DNA demethylation or epigenetic regulation based on 5hmC, 5fC and 5caC [21].

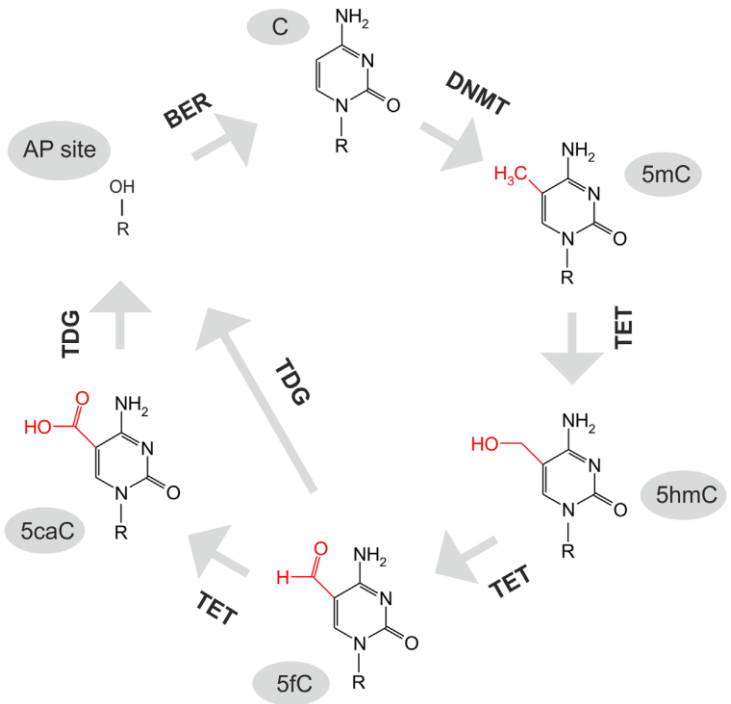

Figure 3.1 Ten-Eleven Translocation-Thymine DNA Glycosylase (TET-TDG) mediated active DNA demethylation.

Unmodified cytosine is methylated by DNMTs (DNMT3a/b for *de novo* or DNMT1 for maintenance methylation) to 5-methylcytosine (5mC) and iteratively oxidized by TET(1–3) to 5-hydroxymethycytosine (5hmC), 5-formylcytosine (5fC), and 5-carboxylcytosine (5caC), respectively. 5fC and 5caC are excised by TDG and the generated abasic (AP) site is repaired by base excision repair (BER) to restore DNA with an unmodified cytosine (From ref. [22]).

3.2 Base excision repair

3.2.1 Mechanism of base excision repair

Base excision repair (BER) efficiently excises and repairs DNA damage derived from deamination, oxidation, alkylation, methylation, and ionizing radiation, thereby helping to maintain genomic stability [23]. DNA glycosylases, AP endonucleases, DNA polymerases, and DNA ligases cooperate to accomplish BER [24]. DNA glycosylases initiate BER by recognizing and excising the damaged bases from the DNA. DNA glycosylases cleave the N-glycosidic bond between the damaged DNA base and the sugar phosphate backbone, which generates an abasic (AP) site. Then the AP endonuclease induces a nick on the DNA phosphodiester backbone at the AP site. Finally, DNA polymerase incorporates an undamaged nucleotide to fill the gap and DNA ligase mends the phosphodiester bond. There are two types of DNA glycosylases: monofunctional and bifunctional DNA glycosylases. Bifunctional DNA glycosylases also possess DNA lyase activity, which incises the phosphodiester backbone via a β-elimination reaction [25–27].

In mammals, eleven DNA glycosylases have been described. Among those eleven DNA glycosylases (Table 3.1 [25]), TDG is the DNA glycosylase best characterized to be involved in active DNA demethylation (see in 3.1.2). Additionally, TDG and MBD4 were reported to participate in active DNA demethylation by excising thymine (T) or 5-hydroxymethyluracil (5hmU). TDG and MBD4 mediated active DNA demethylation is initiated by AID/APOBEC, which deaminates 5mC into T, and 5hmC into 5hmU [28–31]. However, AID possesses lower deaminase activity towards 5mC than towards unmethylated cytosine. Thus, it is unlikely that AID directly deaminates 5mC to mediate DNA demethylation *in vivo*. In addition, research concerning DNA demethylation mediated by 5mC deamination coupled with DNA glycosylases MBD4/TDG yielded contradictory results [32, 33].

To better characterize whether other glycosylases, apart from the well characterized TDG, are also involved in active demethylation and more specifically to search for other glycosylases that function in 5fC and 5caC removal, an siRNA screen was performed in HeLa cells in this laboratory. Analysis of the screen showed that knockdown of *Nei-Like DNA Glycosylases1* and *2* (*NEIL1* and *2*) inhibited 5fC and 5caC removal, pointing to a role of these proteins in active DNA demethylation pathways. Moreover, DNA glycosylases NEIL1 and NEIL3 have also been identified as readers for 5hmC, 5fC and 5caC in an independent study [21].

Type of base lesion	DNA glycosylase		Physiological substrates	M/B	Mouse knockout (ko)/ knockdown (kd) phenotype
Uracil in ssDNA dsDNA	UNG	Uracil-N glycosylase	U, 5-FU, ss and dsDNA	M	ko: viable, B-cell lymphomas, disturbed antibody diversification
	SMUG1	Single-strand-specific monofunctional uracil DNA glycosylase 1	U, 5-hmU, 5-FU, ss and dsDNA	M	kd: moderate increase in mutation frequency (C → T)
Pyrimidine derivates in mismatches	MBD4	Methyl-binding domain glycosylase 4	T, U, 5-FU, εC, opposite G, dsDNA	M	ko: viable, elevated mutation frequency (C → T)
	TDG	Thymine DNA glycosylase	T, U, 5-FU, εC, 5-hmU, 5-fC, 5-caC; opposite G, dsDNA	M	ko: embryonic lethal, aberrant DNA methylation and imbalanced chromatin marks in CpG-rich promoters
Oxidative base damage	OGG1	8-OxoG DNA glycosylase 1	8-oxoG, FaPy, opposite C, dsDNA	B	ko: viable, accumulation of 8-oxoG, elevated mutation frequency (G → T)
	MYH	MutY homolog DNA glycosylase	A opposite 8-oxoG, C or G, 2-hA opposite G, dsDNA	M	ko: viable, see OGG1
Alkylated purines	MPG	Methylpurine glycosylase	3-meA, 7-meG, 3-meG, hypoxanthine, εA, ss and dsDNA	M	ko: viable, elevated levels of ethenoA and hypoxanthine
Oxidized, ring-fragmented or -saturated pyrimidines	NTHL1	Endonuclease III-like 1	Tg, FaPyG, 5-hC, 5-hU, dsDNA	B	ko: viable
	NEIL1	Endonuclease VIII-like glycosylase 1	Tg, FaPyG, FaPyA, 8-oxoG, 5-hU, 5-hC, ss and dsDNA	B	ko: metabolic syndrome, increased damage levels in mitochondrial DNA; kd: hypersensitive to γ radiation
	NEIL2	Endonuclease VIII-like glycosylase 2	As NTHL1 and NEIL1	B	ko: susceptible to inflammation
	NEIL3	Endonuclease VIII-like glycosylase 3	FaPyG, FaPyA, prefers ssDNA	B	ko: viable and no apparent phenotype

Table 3.1 Mammalian DNA glycosylases, their main substrates, modes of action, and mutant phenotypes

M/B, Monofunctional/Bifunctional; U, uracil; A, adenine; T, thymine; C, cytosine; G, guanine; ss, single stranded; ds, double stranded; 5-hm, 5-hydroxymethyl; 5-FU, 5-fluorouracil; ε, etheno; 5-fC, 5-formylcytosine; 5-caC, 5-carboxylcytosine; 8-oxoG, 8-oxo-7,8-dihydroguanine; Tg, thymine glycol; FaPy, 2,6-diamino-4-hydroxy-5-N-methylformamidopyrimidine; me, methyl; h, hydroxyl. Retrieved and modified from reference [25]**.**

3.2.2 The NEIL family of DNA glycosylases/AP lyases

NEILs are bifunctional DNA glycosylases that possess both DNA glycosylase and AP lyase activity [34, 35]. Oxidized pyrimidines are known substrates for NEILs, as listed in table 3.1 [25, 36]. The N-terminal proline of NEIL1 and NEIL2 and the N-terminal valine of NEIL3 are vital for their enzymatic activity, as they form Schiff bases with oxidized DNA lesions [36, 37].

In rats, *Neil1* and *Neil2* are highly expressed in both the embryonic and the adult brain, indicating that Neil1 and Neil2 might be involved in protecting genomic stability in neuronal lineages [38, 39]. In some cancer cells, expression of *NEIL1* and *NEIL2* is downregulated, hinting that NEILs protect cells from the accumulation of mutagenic DNA lesions [40].

Neil deficient mice were generated to better characterize the physiological roles of NEILs. In *Neil1* deficient mice, 4,6-diamino-5-formamidopyrimidine (FapyA) and 2,6-diamino-4-hydroxy-5-formamidopyrimidine (FapyG) levels are elevated [41]. Phenotypically, *Neil1* deficient mice develop metabolic syndrome [42], which is thought to be caused by a failure to remove mitochondrial oxidative DNA damage [43]. In another study, *Neil1* deficient mice exhibit disability to cope with ischemic stroke induced brain damage, highlighting the involvement of NEIL1 in maintaining proper neuronal function [39]. *Neil2* deficient mice are more susceptible to inflammation [44]. *Neil3* deficient mice display defects in both hippocampal adult neurogenesis [45] and hypoxia-ischemia induced neurogenesis [46]. Surprisingly, *Neil1/2/3* triple knockout mice show no accumulation of oxidized DNA lesions, no increase in tumor formation, no elevated frequency of spontaneously occurring mutations, and no decrease of telomere length [47], which is in contradiction to observations in the Neil single knockout mice.

3.3 Neural crest development

3.3.1 Neural crest induction, specification, delamination, migration and differentiation

Neural crest cells (NCCs) are a group of multipotent and migratory cells that originally arise from the ectoderm of the neural plate border [48–50]. According to their final destination localizations, NCCs are classified as cranial NCCs or trunk NCCs. The prospective NCCs undergo delamination to leave the neuroepithelium. During epithelial to mesenchymal transition (EMT), NCCs develop reduced cell-cell adhesion, increased mobility, and

multipotency. Then NCCs migrate to their final destination, and differentiate into diverse cell types and tissues, such as craniofacial cartilages, neurons and glial cells of the peripheral nervous system, connective tissue, smooth muscle cells, and pigmented cells [51]. In different model systems, NCC delamination, EMT and neural tube closure take place in variable fashions. In *Xenopus* and mouse, cranial NCCs delaminate and migrate while the neural plate is still open [52, 53]. In chicks, cranial NCC delamination, EMT, and migration take place coinciding with neural tube closure [54]. In contrast, trunk NCCs of all model systems initiate delamination, EMT, and migration after neural tube closure. Neural tube closure and NCC delamination are not functionally coupled [55, 56]. Another difference between cranial and trunk delamination is that cranial NCCs delaminate all together at once, while trunk NCCs delaminate one by one in a dripping manner [48, 57] (Figure 3.2).

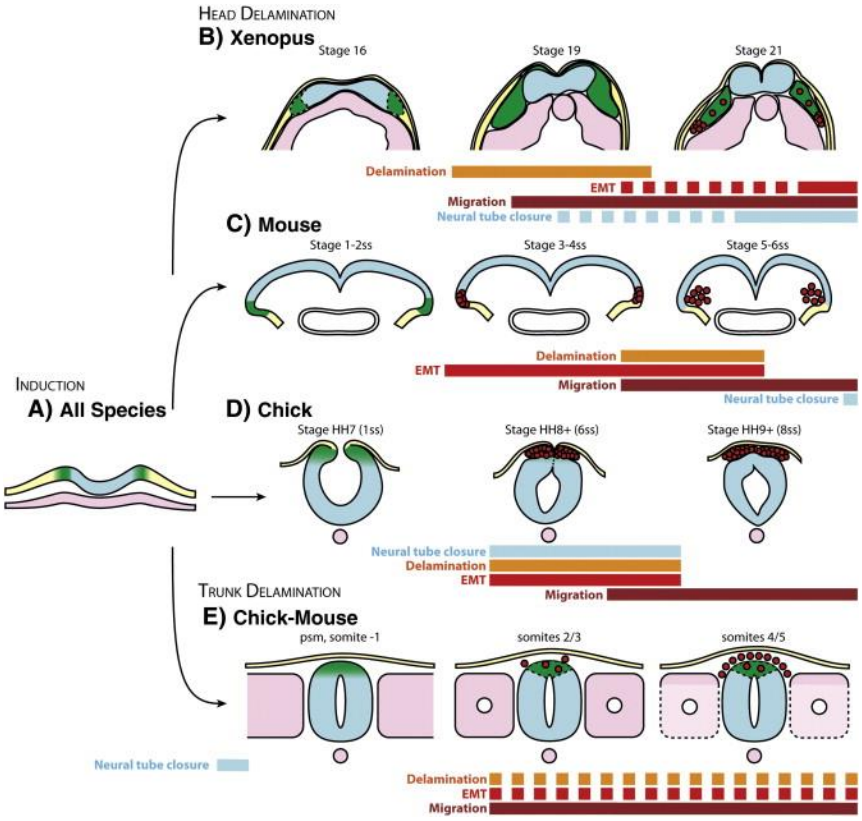

Figure 3.2 Delamination of the cranial and trunk neural crest cells

A. Basic organization of the dorsal region of a vertebrate embryo at early neurula stage. **B**. Delamination of *Xenopus* cranial NCCs. **C**. Delamination of mouse cranial NCCs. **D**. Delamination of chick cranial NCCs. **E**. Delamination of chick/mouse rostral trunk. NCCs, green; migrating NCCs, red; neural plate, blue (From ref. [48]).

The spatiotemporally regulated Wnt, bone morphogenetic protein (BMP) and fibroblast growth factor (FGF) signaling pathways modulate NCC induction [50]. The involvement of FGF signaling in NCC induction is generally considered Wnt-dependent [58–60], although

there are also results supporting a Wnt-independent activity of FGF [61–63]. In competent ectoderm, overexpression of certain factors from the Wnt, BMP and FGF signaling pathways is sufficient to induce NCCs [64]. For example, co-overexpression of BMP antagonists *noggin* and *wnt8* efficiently induces NCCs in *Xenopus* animal cap ectoderm [65, 66].

Given that NCCs arise from the neural plate border, specification of the neural plate border is a prerequisite for NCC specification. *Pax3*, *myc*, *msx1*, *zic1*, *tfap2a* and *hes4/hairy2* are neural plate border specifiers. Expression of these genes is essential for the establishment of the neural plate border and the induction of NCCs, but their expression is not maintained in NCCs, except for *tfap2a* [60, 67–70]. Neural plate border specifiers further activate expression of *snai2/slug*, *foxd3*, *twist*, and *soxE* (*sox8*, *sox9*, *sox10*). These genes lying downstream of neural plate border specifiers are defined as NCC specifiers. NCC specifiers are highly expressed in NCCs and are used as NCC marker gene [71].

3.3.2 Cranial NCC differentiation in *Xenopus* embryos

During *Xenopus* embryogenesis, cranial NCCs migrate anteriorly in a pattern of three main streams: the mandibular (MA), hyoid (HY), and branchial (BR) streams. MA, HY and BR later develop into the craniofacial skeleton: Meckel's cartilage (ME), ceratohyal cartilage (CE), branchial cartilage (BR), and basihyal cartilage (BA) (Figure 3.3) [64, 72]. A failure of cranial NCC differentiation leads to a series of syndromes called neurocristopathies (NCP), such as 3MC syndrome, Auriculo-Condylar syndrome (ACS), Craniosynostosis (CS), Treacher-Collins-syndrome (TCS), and others. Twenty-nine NCPs are classified as NCPs originating from disturbed cranial NCCs [73]. Cranial NCPs are one of the major causes of newborn mortality in humans. In addition, surviving patients' quality of life depends on plastic surgery, psychological therapy, dental therapy, or rehabilitation therapy [74]. Therefore, a better understanding of cranial NCC differentiation and craniofacial structure formation may provide solutions to reduce the occurrence of NCPs.

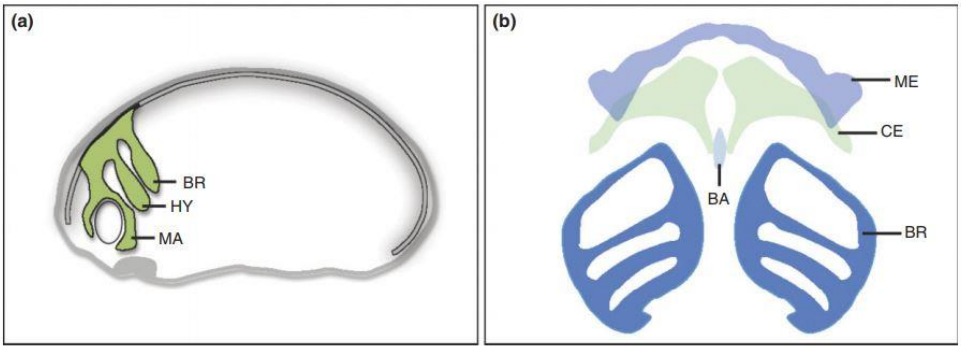

Figure 3.3 Cranial neural crest migration and cartilage differentiation in *Xenopus* embryos.

A. Cranial neural crest cells migrate anteriorly in the embryos, forming three main streams of migration: the mandibular (MA), hyoid (HY), and branchial streams (BR). Scheme drawn after *sox10* expression in a stage (st) 22 embryo. **B**. Cells from these streams differentiate into head skeleton elements: Meckel's cartilage (ME), ceratohyal cartilage (CE), branchial cartilage (BR), basihyal cartilage (BA). Scheme drawn after an alcian blue-stained preparation of the cranial and ventral cartilage from a st45 embryo (From ref. [64]).

3.3.3 Treacher-Collins-syndrome (TCS)

TCS, also called mandibulofacial dysostosis, is a NCP, which was first described by Edward Treacher Collins [75] in 1900. It is a congenital craniofacial disorder that manifests in external ear anomalies, defects or absence of facial bones, airway blockage, hearing loss, or a cleft lip/ palate [73]. The high mortality of infants born with TCS is mostly caused by airway blockage. Most surviving patients have normal cognition and intelligence, although some clinical records show cases of defects in brain development, microcephaly and mental retardation. The incidence of TCS is 1/50,000 [76].

At least, three different genes are associated with TCS: *Treacle ribosome biogenesis factor 1 (TCOF1), RNA polymerase I and III subunit C,* and *D (POLR1C* and *POLR1D).* Approximately 78%-93% of TCS patients bear mutations in *TCOF1*, while 8% of TCS patients bear mutations in *POLR1C* or *POLR1D* [77, 78]. TCSs caused by mutations in *TCOF1*, *POLR1C* and *POLR1D* are classified as TCS1, TCS3, and TCS2, respectively [78]. Mutations in *TCOF1* are inherited in an autosomal dominant mode [79–82], while mutations in *POLR1C* are inherited in an autosomal recessive mode. It is so far not clear whether mutations in *POLR1D* are inherited in an autosomal dominant or in an autosomal recessive mode [83, 84]. In mice, *in situ* hybridization shows that *Tcof1* is strongly expressed in neuroepithelium, migrating neural crest cells, craniofacial mandibular mesenchyme, and sensory ganglia, indicating that Tcof1 might execute its function in a cell autonomous fashion. Haploinsufficiency of *Tcof1* in mice reveals no migration defects in NCCs. However, fewer migrating NCCs are found in *Tcof1* haploinsufficient embryos compared to wild type embryos, indicating that Tcof1 might play roles in regulating NCC formation, proliferation, and/ or viability. Tcof1 is a putative nucleolar phosphoprotein, which shows co-localization with upstream-binding factor 1 (UBF1) in the nucleolus [85, 86]. Further experiments demonstrated that *Tcof1* deficiency inhibits ribosome biogenesis, which triggers cell apoptosis and cell cycle arrest in the neuroepithelium and in NCCs, resulting in craniofacial anomalies [85, 87]. POLR1C and POLR1D are subunits of RNA polymerases I and III. Both RNA polymerase I and III complexes participate in rRNA synthesis, which is the rate-limiting step

in ribosome biogenesis [81, 83]. In conclusion, all three genes implicated in TCS are functionally involved in ribosome biogenesis. Therefore, TCS is also defined as a ribosomopathy [88, 89].

Disruption of ribosome biogenesis by preventing rRNA transcription or ribosome assembly elevates nucleolar stress, inducing NCC-specific apoptosis and cell cycle arrest in a Tp53-dependent manner [90–92]. Inhibition of *Tp53* rescues craniofacial anomalies by reducing cell apoptosis in the neuroepithelium of *Tcof1* haploinsufficient mice, but does not restore ribosome biogenesis [93, 94]. This indicates that a failure of ribosome biogenesis might not be the direct cause for craniofacial anomalies in TCS, but rather the activation of Tp53 signaling. Consistent with this hypothesis, treatment with antioxidants significantly diminishes cell apoptosis in the neuroepithelium, and rescues craniofacial anomalies in *Tcof1* haploinsufficient mice in a Tp53-dependent manner [92].

3.4 DNA damage response

3.4.1 Tp53-dependent DDR

3.4.1.1 DNA damage

Cells in multicellular organisms are continuously confronting DNA damage introduced by either exogenous sources, such as ionizing irradiation (IR) and UV light from sunlight, X-ray and IR used in cancer therapies, and chemicals used as chemotherapeutic drugs, or reactive oxygen species (ROS) and reactive nitrogen species (RNS) originating from the cellular metabolism [95, 96]. IR and UV light introduce single strand breaks (SSBs) or double strand breaks (DSBs) to DNA. DSBs are extremely toxic to cells due to the difficulty to repair them, and if left unrepaired, might induce deletion, amplification, or translocation of chromosomes, leading to aging, carcinogenesis, or cell death [97–99]. Besides, UV light generates pyrimidine dimers and oxidative damages to DNA. Cyclobutane pyrimidine dimers (CPD) generated by UV light are frequently found in melanoma and are correlated to the genetic mutations involved in development of melanoma [100–102]. Superoxide anions ($O^{\bullet-}_2$), hydroxyl radicals ($^{\bullet}OH$), singlet oxygen ($^1O_2$), and hydrogen peroxide (H_2O_2) are ROS that can introduce oxidative damage to specific DNA bases, or initiate $^{\bullet}OH$ attacks leading to DNA strand breaks, deamination, or generation of AP sites [103–106]. 8-oxoguanine (8-oxoG) is one of the major oxidative DNA lesions. Accumulation of 8-oxoG is positively correlated with neurodegeneration, carcinogenesis, and aging [107–109]. Deaminated bases and AP sites in DNA are mutagenic to cells [110–112]. Nitric oxide ($NO^{\bullet}$), nitric dioxide ($NO_2^{\bullet}$), and

peroxynitrite ($ONOO^-$) are RNS that damage DNA oxidatively and nitratively, generating mutagenic DNA damage involved in carcinogenesis [113]. In addition to cell metabolism, infections and chronic inflammation also generate ROS/RNS to regulate blood pressure, repair wounds, and defend the host against pathogens under physiological conditions [114].

To counteract DNA damage and protect genomic integrity, cells have evolved DDR. DDR is a complex process, which involves damage recognition, signal transduction, and action execution, leading to either cell cycle arrest, DNA damage repair, or cell apoptosis in case of irreparable damage [115]. In DDR, Tp53 is the most extensively characterized factor and is considered to be a key player [96, 116].

3.4.1.2 Tp53

Tp53 is a well-studied tumor suppressor, which responds to various cellular stresses that contribute to tumorigenesis [117, 118]. Under physiological conditions, Tp53 is maintained at a low level and in an inactive state. Cellular stresses elevate Tp53 levels and post-translationally modify Tp53 to enable its binding to downstream target genes [119, 120].

Multiple post-translational modifications can be deposited on Tp53, such as phosphorylation, acetylation, ubiquitination, methylation, and ADP-ribosylation [121–125]. Phosphorylation sites are mostly located towards the N-terminus of Tp53. Kinases such as ATM/ATR and CHK1/CHK2 rapidly phosphorylate Tp53 under stress conditions to activate Tp53. Tp53 phosphorylation also repels the protein's negative regulators and thus stabilizes Tp53 activity. Phosphorylation of Tp53 at the N-terminus is highly redundant. The same kind of stress might induce phosphorylation at different sites, and phosphorylation at different sites might serve the same physiological function [126–128]. Tp53 ubiquitination mediated by MDM2/MDMX leads to protein degradation [129–131]. Given that Tp53 acetylation and ubiquitination sites are shared, acetylation stabilizes Tp53 by inhibiting ubiquitination-mediated degradation [132]. EP300 and CREB-binding protein (CBP) are responsible for Tp53 acetylation at the C-terminus [132–134], while histone deacetylases (HDACs) such as HDAC1 and Sirtuin1 (SIRT1) deacetylate Tp53 [135–138]. Methylation and ADP-ribosylation can both promote and suppress expression of Tp53 target genes [121, 139–143].

Tp53 performs its cellular functions primarily as a transcription factor. By combining Tp53-dependent transcriptome analysis and Tp53 chromatin immunoprecipitation sequencing (ChIP-Seq), Tp53 target genes were comprehensively studied [144–146]. With the help of data mining, top Tp53 target genes, which are identified to be activated by Tp53 reproducibly

by different studies, can be determined, including *AEN*, *CCNG1*, *SESN1*, *MDM2*, *FBXW7*, *Tp53INP1*, *PLK2*, and *ULK*. These genes can be categorized according to their functions in various processes. For example, BAX, AEN, BBC3, SUSD6 are involved in cell apoptosis; XPC, PCNA, and DDB2 participate in DNA repair; GADD45A and CDKN1A mediate cell cycle arrest; MDM2 and CCNG1 function in feedback regulation of Tp53 [147–150]; PRKAB1 and DRAM1 induce autophagy; and GLS2, FDXR, and PRKAB1 regulate cellular metabolism [151] (Figure 3.4).

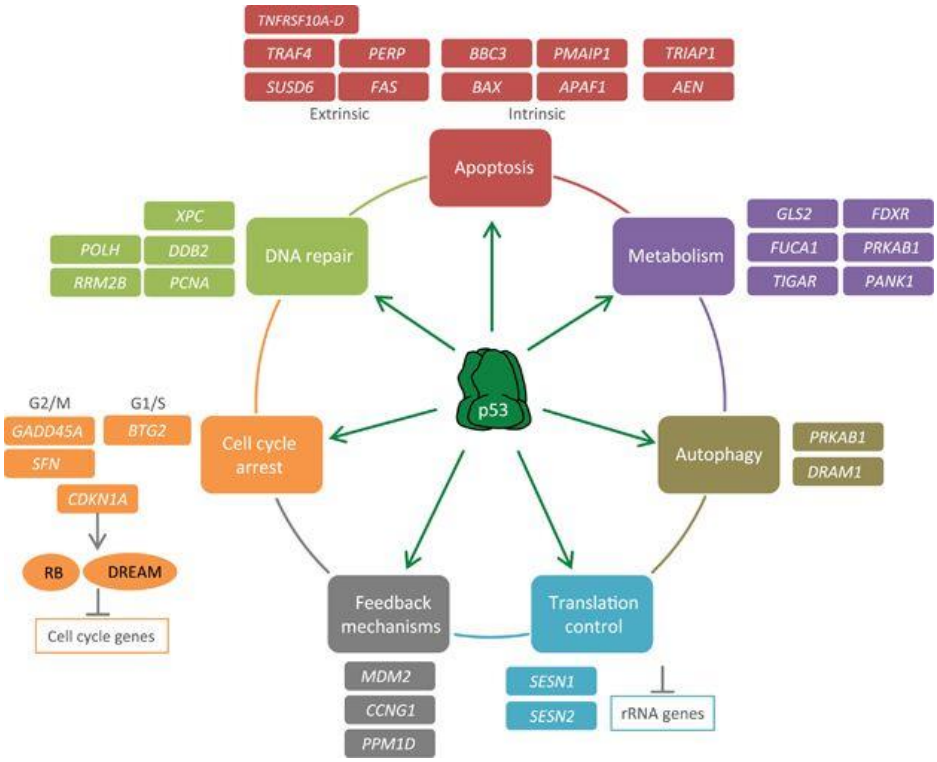

Figure 3.4 Tp53 directly activates target genes that mediate various functions.

Proteins encoded by Tp53 target genes function in multiple processes that include, but are not limited to, cell cycle arrest, DNA repair, apoptosis, metabolism, autophagy, translation control and feedback mechanisms (From ref. [151]).

3.4.1.3 Tp53-dependent DDR

Tp53-dependent DDR is initialized by signal transducers that sense and transduce the stress signals to activate the core factor of the pathway, Tp53. This active form of Tp53 is more stable and shows higher binding activity to its target genes. These target genes can be defined as feedback regulators and output regulators. The feedback regulators negatively regulate both Tp53 and its upstream signal transducers, while the output regulators "instruct" the cell to take specific actions [120] (Figure 3.5). Variable signal transducers, feedback regulators, and output regulators are employed in response to different cellular stresses.

Depending on the damage type and amount, cells are destined to different fates: cell cycle arrest to allow time to repair the damage, or cell apoptosis to eliminate severely damaged cells from the tissue [152, 153]. Tp53, as the central player of DDR, integrates various damage signals and determines cell fates. Mild DNA damage induces moderate levels of Tp53, which leads to cell cycle arrest and DNA repair. Accumulation of irreparable DNA damage increases Tp53 to a relatively high level, upregulating expression of apoptotic Tp53 target genes [115]. The necessity of high Tp53 levels to trigger apoptosis might be due to the promoters of apoptotic Tp53 targets possessing lower binding affinity for Tp53, thus requiring higher Tp53 levels for their transcriptional activation [154]. Post-translational modification including phosphorylation and acetylation at specific sites of Tp53 also affects cell fate determination. For example, most Tp53 phosphorylation events are crucial for inducing p21 mediated cell cycle arrest [155, 156], while Tp53 phosphorylation at S46, or Tp53 acetylation at K164 and K120 activate expression of apoptotic Tp53 target genes instead [157–161].

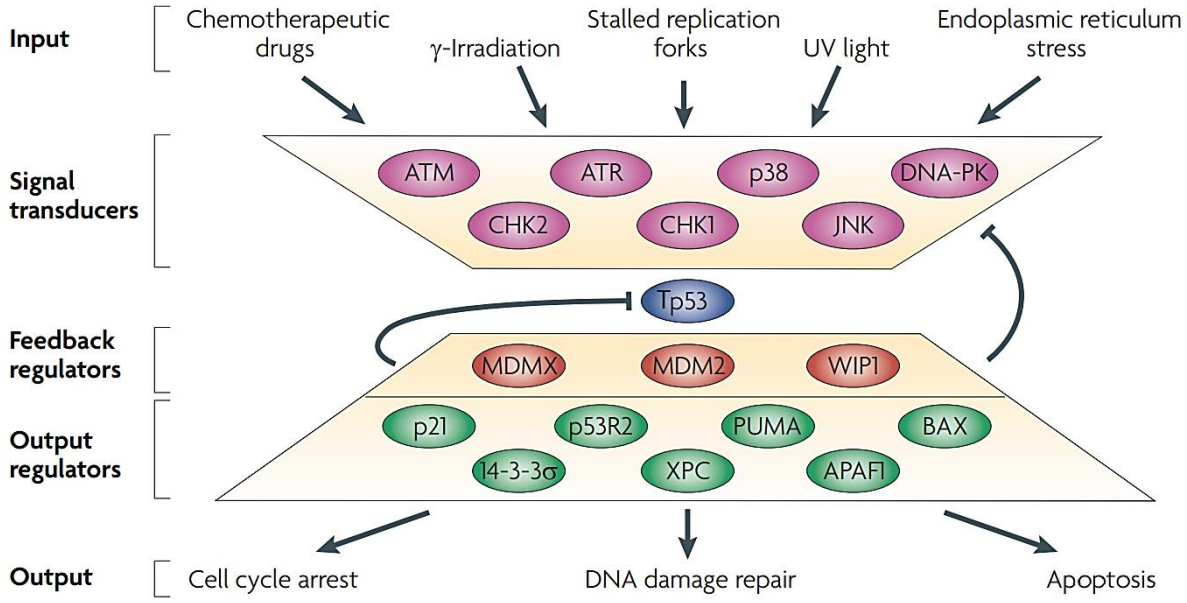

Figure 3.5 The Tp53 signaling network.

Stress signals (inputs) are detected and transduced to Tp53 through several kinases (signal transducers). On activation, Tp53 upregulates the transcription of numerous genes. Some Tp53 targets act as feedback regulators, altering the activity of the kinases or the stability of Tp53 itself. Other Tp53 targets are output regulators that trigger specific cellular outcomes, including cell cycle arrest and apoptosis. APAF1, apoptotic protease-activating factor; ATM, ataxia telangiectasia mutated; ATR, ataxia telangiectasia and rad3 related; CHK, checkpoint kinase; DNA-PK, DNA-dependent protein kinase; JNK, JUN N-terminal kinase; p53R2, Tp53-inducible ribonucleotide reductase small subunit 2-like protein; UV, ultraviolet (From ref. [120]).

3.4.2 Cell cycle arrest and DNA repair in DDR

3.4.2.1 Cell cycle arrest

The primary goal of DDR is to repair DNA damage to protect genomic integrity. To this end, when DNA damage occurs, DDR slows or arrests cell cycle progression, allowing recruitment of DNA repair factors to the sites of damage and execution of their repair functions. Cells have evolved sophisticated cell cycle checkpoints to prevent inaccurate duplication of damaged DNA, which usually take place at transitions between cell cycle phases. DNA damage checkpoints are categorized according to the cell cycle phases into G1/S, S, and G2/M checkpoints [162].

DNA damage introduced during the G1 phase triggers the G1/S checkpoint, where Tp53 transcriptionally activates expression of *p21*. P21 inhibits activity of cyclin E-Cdk2, which is crucial for cell cycle progression into S phase. Cell cycle arrest in G1 protects cells from replicating the damaged DNA [155, 156]. A Tp53-independent G1/S arrest is mediated by inhibition of cyclin D-CDK4/6 via ATR-CHK1 regulated CDC25A degradation [163–165].

DNA damage introduced during the S phase activates the S phase checkpoint, which inhibits DNA replication to minimize the propagation of damaged DNA. Compared to the G1/S arrest, the S phase arrest is of transient nature. If the damage cannot be repaired quickly enough, the cell enters the G2 phase and later arrests at the G2 checkpoint [163, 166, 167]. Upon S phase checkpoint activation, CHK2 stimulates ATR-CHK1 dependent CDC25A turnover, which speeds up the proteolysis of CDC25A, and eventually inhibits cyclin E/A-CDK2. This, in turn, prevents DNA replication. It seems that the S phase arrest is Tp53 independent [168–170], although some reports indicated that Tp53 might be involved after all [171–173].

The G2/M checkpoint allows time to repair DNA damage introduced in late S phase or G2, protecting the cell from transmitting faulty genomic information to the daughter cells during mitosis. Like the G1/S arrest, G2/M arrest is also divided into a Tp53 dependent or independent arrest. In the Tp53 dependent G2/M arrest, Tp53 induced Gadd45a either destabilizes CDC2/Cyclin B complexes, or transcriptionally inhibits expression of *cdc2* and *cyclin B*. Activation of CDC2/Cyclin B is essential for cells to enter mitosis. In the Tp53 independent G2/M arrest, the ATR-CHK1 phosphorylates CDC25C, which then inhibits the dephosphorylation of CDC2, also resulting in cell cycle arrest in G2 phase [174–177].

Deficiency of proteins involved in DNA damage checkpoints tends to induce neurodegeneration, immunodeficiency, and tumorigenesis [163].

3.4.2.2 DNA damage repair

DNA repair takes action once the cell cycle progression is halted. Based on the type of DNA damage repaired, DNA repair processes are categorized into BER, nucleotide excision repair (NER), mismatch repair (MMR), and DSB repair. Different DNA lesions are sensed by distinct DNA repair factors. For instance, Mutator S (MutS) proteins bind to mismatched bases, Ku heterodimers bind to DSBs, and XPC involved in NER binds to UV-induced DNA photo products. Once the lesions are removed, or repaired, cells end the cell cycle arrest and proceed to normal cell cycle progression. Irreparable cells are destined for cell senescence, or cell apoptosis [178–180]. The mechanistic details of these various DNA repair pathways are well described in reviews [96, 180].

3.4.3 Cell apoptosis in DDR

Cell apoptosis eliminates cells containing excessive unrepaired DNA damage to prevent tumorigenesis [181–184]. As introduced in section 3.4.1.3, high levels of Tp53 or specific post-translational modifications of Tp53 induce cell apoptosis. Two apoptotic signaling pathways are characterized, the extrinsic pathway and the intrinsic pathway. Both pathways converge at the level of activating effector caspases (caspase-3, 6 and 7) [185–187].

Tp53 triggers extrinsic apoptosis either by transcriptionally activating the expression of death domain containing receptors, such as, Fas, Killer/DR5, and PERP [188], or by trafficking Fas receptors from the Golgi complex to the cell membrane to accelerate Fas-mediated apoptosis by bypassing transcription [189–191]. After binding to its specific death ligand FasL, which is expressed predominantly by activated T lymphocytes and natural killer (NK) cells, Fas forms a homotrimer. Trimerized Fas further recruits the adaptor protein Fas-associated death domain (FADD) to form a death inducing signaling complex (DISC) with the initiator caspase, procaspase-8. Within DISC, procaspase-8 is activated via dimerization induced autocatalytic cleavage. Active caspase-8 triggers execution of apoptosis by cleaving effector caspases (caspase-3, 6 and 7) into their active forms (Figure 3.6).

Intrinsic apoptosis, also called the mitochondrial apoptotic pathway, involves the release of cytochrome c (cyt c) from the mitochondrial intermembrane space into the cytoplasm. Released cyt c binds to apoptotic protease-activating factor 1 (APAF-1) and procaspase-9 in

the cytoplasm to form the apoptosome, where procaspase-9 is activated. Then, active caspase-9 triggers execution of apoptosis by cleaving effector caspases similar to caspase-8 during extrinsic apoptosis. Tp53 participates in intrinsic apoptosis by transcriptionally regulating expression of *APAF-1* and Bcl-2 family members *Bax*, *Noxa*, *PUMA*, and *Bid* [192–194]. Bax, Noxa, and PUMA as pro-apoptotic Bcl-2 family members, promote the release of cyt c, while Bid serves as a link that connects extrinsic and intrinsic apoptosis. Active caspase-8 from the extrinsic apoptotic pathway cleaves cytoplasmic Bid into truncated Bid (tBid) that translocates into mitochondria to initiate the intrinsic/mitochondrial apoptotic pathway [185, 195, 196] (Figure 3.6).

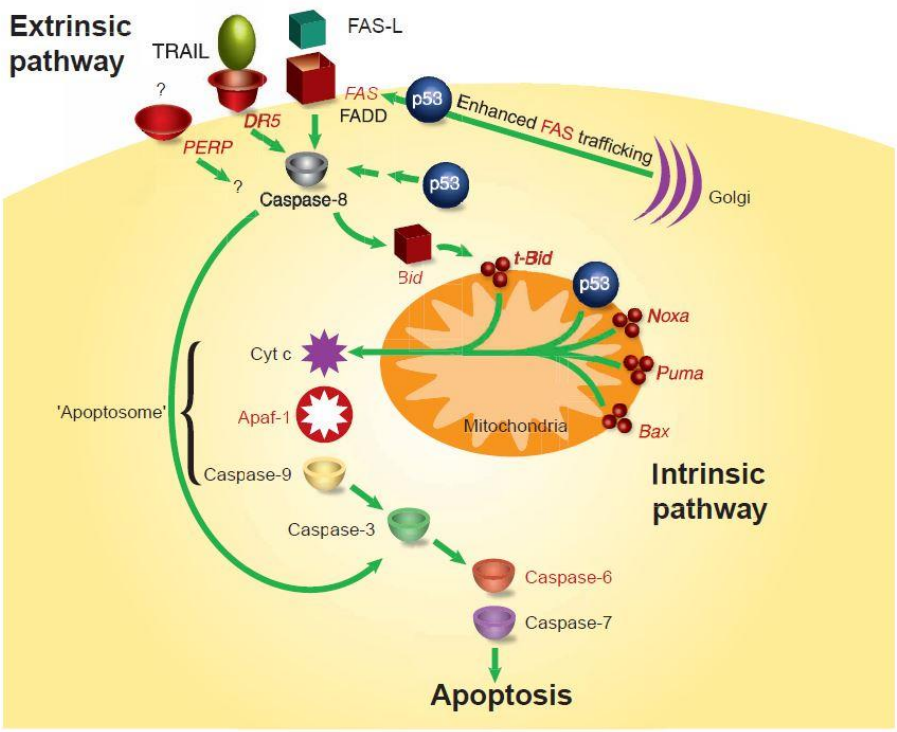

Figure 3.6 A model for Tp53-mediated apoptosis.

This model depicts the involvement of Tp53 in the extrinsic and intrinsic apoptotic pathways. Tp53 target genes are shown in red. The convergence of the two pathways through Bid is shown (From ref. [185]).

Apoptotic cells exhibit specific morphological features: cell shrinkage and retraction from neighboring cells, nuclear chromatin condensation and fragmentation, and continuous cell membrane blebbing. Eventually, cells form apoptotic bodies comprised of plasma membrane and fragmented nuclear DNA to ensure that no cellular contents leak into the surrounding tissue. Apoptotic bodies are subsequently engulfed and digested by phagocytes [197–199]. To detect cell apoptosis, several methods have been developed. Agarose gel electrophoresis of apoptotic DNA exhibits a ladder-like pattern due to internucleosomal fragmentation [200]. The terminal deoxynucleotidyl transferase dUTP nick end labeling (TUNEL) assay makes cell

containing fragmented DNA visible for microscopy analysis [201, 202] [203]. In addition, antibodies against active caspase-3 are also frequently employed as markers for apoptotic cells [204, 205].

Properly regulated cell apoptosis plays important roles in embryogenesis: It 1) sculpts structures; 2) eliminates unwanted structures; 3) adjusts cell numbers; 4) removes damaged or injured cells; and 5) produces differentiated cells without organelles. For example, apoptosis eliminates interdigital cells to sculpt limbs of all amniotes [206]and removes structures like frog tails, and fly midguts, hindguts and salivary glands in the metamorphosis of amphibians and insects [206, 207]. However, inaccurately regulated cell apoptosis can induce neurodegeneration, autoimmune disease, ischemia, and cancer [208–210].

3.4.4 DDR and embryogenesis

As mentioned, cellular metabolism generates ROS that introduce various DNA damage, and if left unrepaired, those damage may trigger DDR. ROS generation is highly correlated with oxygen levels of the environment in which embryos develop [211–213]. Mammalian embryos developing inside wombs face much lower oxygen levels (1%-9%) than amphibian and fish embryos developing in water (up to 20% O2) [214–217]. Viability of mammalian embryos decreases significantly when they are cultured *in vitro* with elevated oxygen levels. Consistent with reduced embryo viability, DNA damage levels are elevated in these embryos [213, 218–220]. Multicellular organisms have evolved different antioxidant defenses or repair machineries to adapt to the variable environmental oxygen levels that they develop and live in [221–223]. Some amphibians, fishes and reptiles regulate their antioxidant enzymes flexibly in reaction to changes in environmental oxygen levels. Also, some species constantly maintain a pool of antioxidant enzymes at a relatively high level [222].

Disruption of antioxidant defenses or repair machineries during embryonic development leads to accumulation of DNA damage, which triggers DDR. As introduced above, DDR induces either cell cycle arrest to repair DNA damage, or cell apoptosis to eliminate damaged cells, both of which might impact embryonic development. Given that Tp53 is the central player of DDR, does Tp53-dependent-DDR affect embryonic development? Does Tp53-dependent-DDR exhibit cell-type specificity?

During early embryogenesis, the NCC progenitors and neuroepithelial cells endogenously generate higher levels of ROS compared to other tissues [92, 224]. Besides, *tp53* mRNA is

expressed in the developing brain and NCCs of mouse, chick, fish, and frog embryos [225–227]. Consistent with the expression pattern of *tp53*, Tp53 target genes involved in promoting cell apoptosis, cell cycle arrest, and maintaining genomic integrity are also highly expressed in the developing brain and in NCCs [227]. The precisely and strictly regulated spatiotemporal expression patterns of *tp53* and its target genes in developing brain and NCCs could hint at regulatory functions in neural lineage cell differentiation and migration [225, 227–229]. Under physiological conditions, *tp53* is lowly expressed due to the negative feedback loops introduced earlier. Upon DNA damage, DDR triggered upregulation or stabilization of Tp53 induces apoptotic removal of damaged *tp53*-expressing cells. *Tp53* is specifically expressed in NCCs and enteric nervous system (ENS), thus DDR-triggered Tp53-dependent apoptosis leads to defects in NCC cell differentiation, causing craniofacial anomalies and ENS anomalies [230–233]. Under physiological conditions, Tp53 regulates G1 to S phase transition, which is crucial for the EMT of NCC precursors [234–236]. Whether DDR induced cell cycle arrest affects NCC differentiation is yet unknown.

3.5 Aim of the thesis

The DNA glycosylase TDG is involved in active DNA demethylation by excising 5mC's oxidative derivatives, 5fC and 5caC, from the DNA. In a search for other DNA glycosylases that also participate in 5fC and 5caC removal, Neil1 and Neil2 were identified in an siRNA screen in HeLa cells in this laboratory. *In vitro* experiments revealed that Neil1 and Neil2 are incapable of excising 5fC or 5caC directly, and instead execute their function by stimulating substrate turnover of TDG. This is due to their high affinity to AP sites generated by TDG during 5fC and 5caC excision.

The overarching goal of my PhD thesis was to validate the *in vitro* results of our laboratory *in vivo*, specifically in *Xenopus* embryos. The Results are presented in two Chapters.

In Chapter 1, I characterized the phenotype of *Xenopus laevis* embryos after Neil1, Neil2, Neil3, Tdg, and Tet3 knockdown or overexpression, respectively. This led to the discovery of a NCC phenotype in Neil2, Neil3, Tdg, and Tet3 deficient embryos. Chapter 1 was published in *Nature Structural & Molecular Biology* (2016). The publication is attached in the format as submitted to the journal. References in Chapter 1 are separated from the rest of the thesis. I carried out all *Xenopus* experiments for this publication.

In Chapter 2, I addressed the question what the underlying mechanism of the NCC defects described in Chapter 1 is. Unless specified, I performed all the experiments described in this Chapter.

4. Results

4.1 Chapter 1. Neil DNA glycosylases promote substrate turnover by Tdg during DNA demethylation (Schomacher, et al. Nat. Struct. Mol. Biol. 23, 116–124 (2016))

Lars Schomacher[1,3,], Dandan Han[1,3], Michael U. Musheev[1,3], Khelifa Arab[1], Sabine Kienhöfer[1], Annika von Seggern[1], and Christof Niehrs[1,2,]

[1] Institute of Molecular Biology (IMB), Mainz, Germany

[2] Division of Molecular Embryology, German Cancer Research Center-Zentrum für Molekulare Biologie der Universität Heidelberg (DKFZ-ZMBH) Alliance, Heidelberg, Germany

[3]These authors contributed equally.

Corresponding authors:

Phone: 49-6131-39-21402 / 00

Fax: 49-6131-39-21421

E-mail: l.schomacher@imb-mainz.de / c.niehrs@imb-mainz.de

Abstract

DNA 5-methylcytosine is a dynamic epigenetic mark which plays important roles in development and disease. In the Tet-Tdg demethylation pathway, methylated cytosine is iteratively oxidized by Tet dioxygenases and unmodified cytosine is restored via thymine DNA glycosylase (Tdg). Here we show that human NEIL1 and NEIL2 DNA glycosylases coordinate abasic site processing during TET–TDG DNA demethylation. NEIL1 and NEIL2 cooperate with TDG during base excision: TDG occupies the abasic site and is displaced by NEILs, which further process the baseless sugar, thereby stimulating TDG substrate turnover. In early *Xenopus* embryos Neil2 cooperates with Tdg to remove oxidized methylcytosines and to specify neural crest development together with Tet3. Thus, Neils function as AP lyases in the coordinated AP site hand-over during oxidative DNA demethylation.

Introduction

DNA 5-methylcytosine (5mC) is an epigenetic mark which plays important regulatory roles in development and is involved in disease[1,2]. It has become clear that DNA methylation in animal cells is reversible by an enzymatic demethylation process involving oxidation of 5mC by the Ten-eleven translocation (Tet) family of dioxygenases[3-7]. Tet enzymes iteratively oxidize 5mC to form 5-hydroxymethylcytosine (5hmC), 5-formylcytosine (5fC) and 5-carboxylcytosine (5caC). The oxidation products act as intermediates in DNA demethylation by both active and passive modes (reviewed in[8,9]). The active mode involves thymine DNA glycosylase (Tdg), which recognizes and excises higher oxidation products and initiates downstream base excision repair (BER) to restore unmodified cytosines[5,10]. This Tet–Tdg demethylation pathway is involved in gene specific, not global DNA demethylation. Tdg null mice die around embryonic day E12.5 and show a modest 5mC increase at CpG-rich gene promoters[11,12]. Base resolution sequencing of Tdg knockdown cells confirmed highly gene-specific hypermethylation[13-15].

Early discovery of a role for Tdg in active DNA demethylation suggested that the enzyme might promote DNA demethylation through direct excision of 5mC[16]. However, Tdg processes 5fC and 5caC, but not 5hmC or 5mC[5,10,11]. Tdg acts as a monofunctional DNA glycosylase cleaving the N-glycosidic bond between the base and the sugar at 5fC and 5caC residues within double stranded DNA to generate abasic (apyrimidinic, AP) sites. It is assumed that the AP site intermediate is subsequently processed by the canonical BER pathway: AP endonuclease 1 (Apex1) cleaves the phosphodiester bond to generate a 3'-hydroxyl and 5'-deoxyribose phosphate; DNA polymerase β removes the sugar phosphate moiety and incorporates an unmodified cytosine; DNA ligase I or IIIα seals the nick[17]. However, which BER components indeed function in the Tet–Tdg pathway has remained unexplored.

DNA repair intermediates are often unstable and can cause genomic instability, cell cycle arrest, cell death, or cell transformation. It is thought that DNA repair pathways are build such that during each processing step the intermediates are sequestered and protected by the appropriate repair enzyme, thereby passing them along like a baton from one enzyme to the next in a coordinated, sequential fashion[18,19]. During BER, the AP site is a vulnerable intermediate, which if unprotected is unstable, mutagenic and cytotoxic. The cellular risks associated with AP site intermediates are accentuated in Tet–Tdg demethylation, where parallel processing of two abasic sites in a homomethylated mCpG dyad could generate

double strand breaks and moreover where demethylation may occur in 5mC tandem arrays in CpG rich islands.

Besides Tdg, the nei endonuclease VIII-like family of DNA glycosylases (Neil1-3) has been implicated in Tet-mediated DNA demethylation. Neils are bifunctional enzymes, which excise the damaged base and introduce a DNA strand break via their AP lyase activity[20,21]. Neil1 and Neil3 were identified as potential binders for oxidized 5mC derivatives[22]. Overexpression experiments suggested that NEILs function as alternative DNA glycosylases to TDG in the excision of 5fC and 5caC[23], apparently consistent with the reported preference of Neils for repairing oxidized bases, including 5-hydroxyuracil, thymine glycol and 8-oxoguanine[20,21,24-29]. However, their requirement for processing of Tet oxidation products and their mode of action in DNA demethylation are unknown.

We conducted a screen to search for novel components of DNA demethylation and identified NEIL1 and NEIL2. Unexpectedly, biochemical analysis reveals that NEIL enzymes neither bind nor process oxidized methylcytosines directly. Instead they cooperate with TDG in AP site processing. NEIL1 and NEIL2 displace TDG from the AP site and cleave the baseless sugar, thereby overcoming TDG product inhibition and accelerating 5fC and 5caC turnover. Knockdown experiments in early *Xenopus* embryos corroborate that Neil2 is required for the removal of genomic 5fC and 5caC and for neural crest development together with Tdg and Tet3. Neils are, hence, involved as AP lyases in the coordinated substrate hand-over during oxidative DNA demethylation.

Results

NEIL1 and NEIL2 are required for removal of 5fC and 5caC

To identify novel components of DNA demethylation, we first analyzed the ability of HeLa cells to demodify oxidized methylcytosines. When HeLa whole cell extracts were incubated with 160 bp oligonucleotides containing a single modified cytosine residue, they replaced 5fC and 5caC efficiently with unmethylated cytosine. In a 'DNA demodification assay' we monitored replacement of cytosine derivatives by unmodified cytosine by gain of HpaII sensitivity, yielding a 79 nt product (Fig. 1a-b). In contrast, oligonucleotides containing 5mC remained unprocessed and 5hmC was only marginally converted. The demodification reaction was sequence-context independent, proceeding also with an oligonucleotide of unrelated sequence (Supplementary Fig. 1a-b). Whole cellular extracts might not mimic the *in vivo* repair scenario. Under these conditions, however, demodification of 5fC and 5caC oligos showed characteristics of short patch BER; i) in the reaction without HpaII digest ('demodification intermediate assay'), it was accompanied by occurrence of 79 and 80 nt products, corresponding to the expected cleaved AP site (79 nt) and incorporated single cytidine with an unligated 3'-OH (80 nt) intermediates, respectively (Fig. 1c), and ii) it was insensitive to the replicative DNA polymerase inhibitor Aphidicolin (Fig. 1d-e).

To test which of the eleven human DNA glycosylases that mediate base excision repair[30] is involved in 5fC and 5caC processing, we downregulated their expression with siRNAs and carried out DNA glycosylase assays (Fig. 2a-b, Supplementary Fig. 1c). Knockdown of *TDG* robustly inhibited 5fC and 5caC removal (Fig. 2c, Supplementary Fig. 2a), consistent with the notion that this DNA glycosylase plays a central role in DNA demethylation[11,12]. In addition, knockdown of the DNA glycosylases NEIL1 and NEIL2 inhibited 5fC and 5caC excision, notably after combined knockdown (Fig. 2d, Supplementary Fig. 2b). NEIL3 was negative in this assay and differs from NEIL1 and NEIL 2 in substrate specificity and structural features[31] as well as by operating mainly as a monofunctional DNA glycosylase[28]. Expectedly, *TDG* siRNA and combined *NEIL1* and *NEIL2* siRNAs also inhibited the demodification of 5fC and 5caC modified oligonucleotides (Fig. 2e, Supplementary Fig. 2c).

Tdg-deficiency in mouse ES cells causes a 5- to 10-fold increase in genomic 5fC and 5caC abundancy[5,13]. If NEIL1 and NEIL2 function in 5fC and 5caC removal, these bases should accumulate when NEILs are depleted. Indeed, in HeLa cells *TDG*, *NEIL1* and *NEIL2* siRNAs increased the genomic levels of TET1-induced 5fC and, except for *NEIL2* depletion, also

5caC (Fig. 2f). Global 5hmC showed a moderate increase, while 5mC levels were unaffected, as expected, because TDG is involved in gene-specific, not global DNA demethylation.

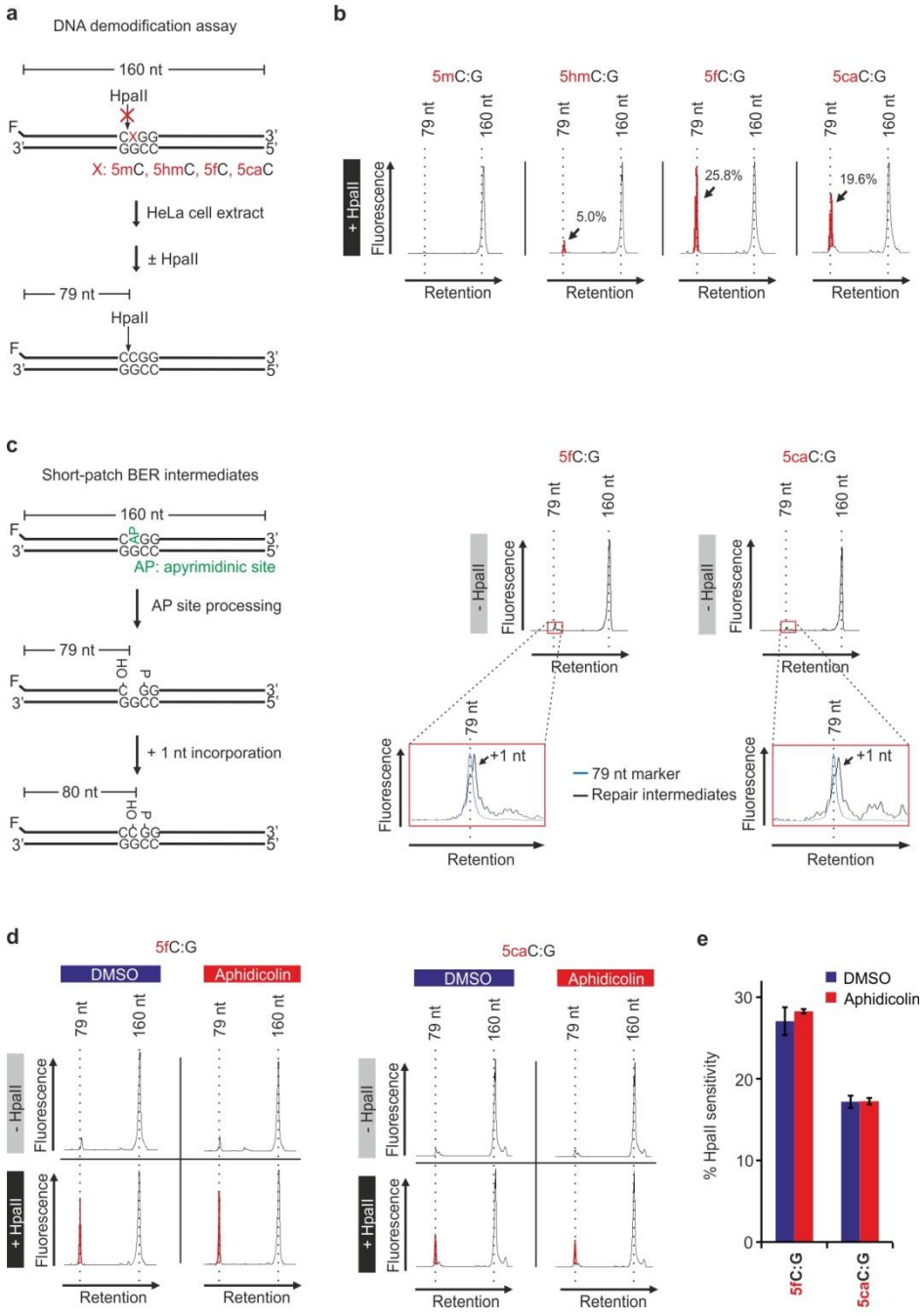

Figure 1: 5fC and 5caC are demodified by short-patch base excision repair in HeLa cell extracts.

(**a**) Scheme of DNA demodification assay. A 160 bp synthetic, fluorescently-labeled oligonucleotide containing the indicated cytosine derivative within a HpaII recognition sequence was incubated with HeLa cell extracts. Replacement of cytosine derivatives by unmodified cytosine was monitored by gain of HpaII sensitivity. Reaction without HpaII

treatment served to monitor repair intermediates, which otherwise would be masked by the HpaII cleavage product. (**b**) Denaturing gel electrophoresis of reaction products from DNA demodification assay (+ HpaII) using 50 µg HeLa extract in a 50 µl reaction on 20 nM 5mC, 5hmC, 5fC and 5caC containing oligonucleotides. Repair efficiencies are represented as integral ratio between HpaII signal peak (red) to the total fluorescent signal per electropherogram. Data are representative of three independent experiments. (**c**) Demodification intermediate assay (– HpaII) on 5fC and 5caC containing oligonucleotides. Left, scheme and expected lengths of short-patch BER intermediates. Right top, denaturing gel electrophoresis of reaction products. Repair intermediates are boxed in red. Right bottom, magnification of intermediates. A 79mer marker oligonucleotide (blue) was overlaid with the reaction products (black). Data are representative of three independent experiments. (**d**) Demodification assay (± HpaII treatment as indicated) as in **b** but in absence (DMSO, carrier) or presence of Aphidicolin. Repair products are highlighted in red. Data are representative of three independent experiments. (**e**) Quantification of HpaII sensitivity (repair products) in absence or presence of Aphidicolin. Error bars, s.d. (n = 3 independent demodification assays).

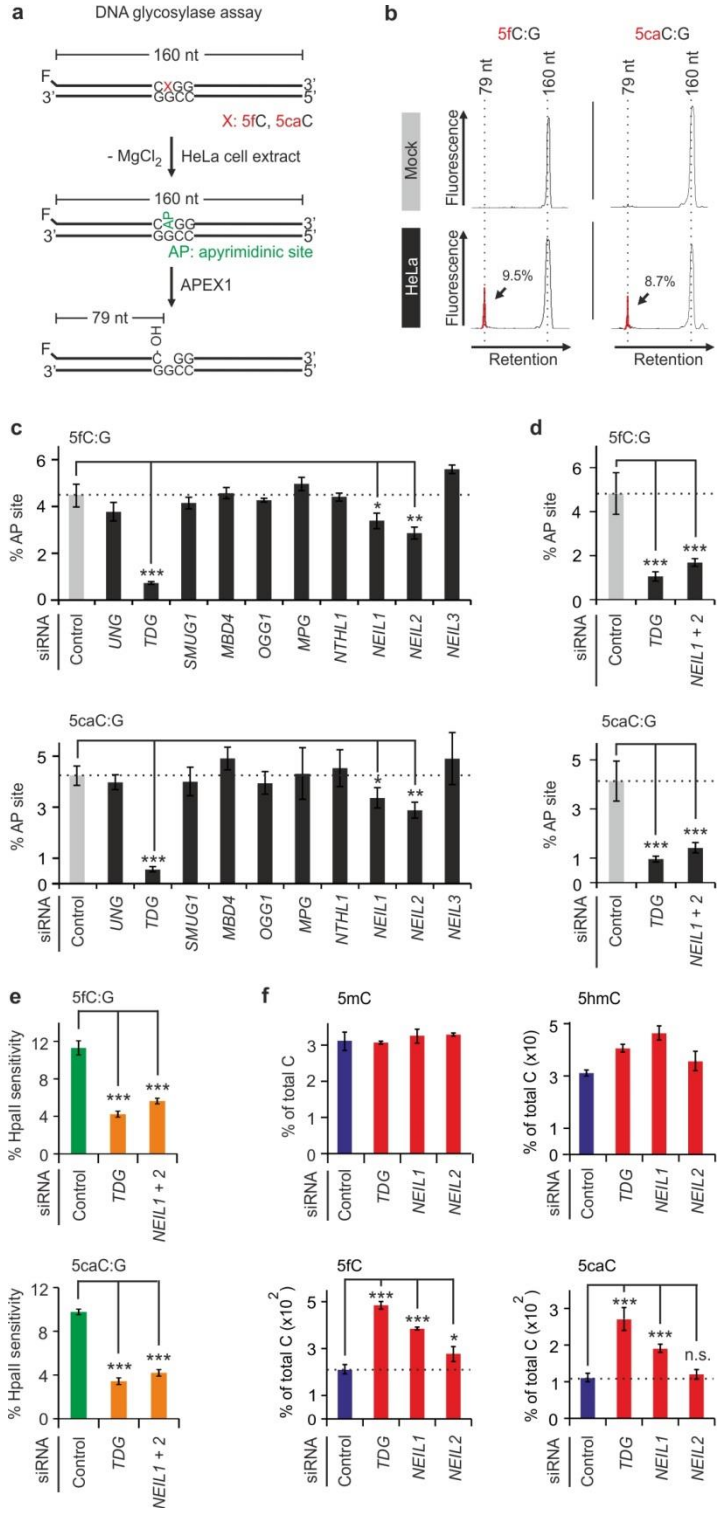

Figure 2: NEIL1 and NEIL2 are required for removal of 5fC and 5caC in HeLa cells.

(**a**) Scheme of DNA glycosylase assay. A 160 bp synthetic, fluorescently-labeled oligonucleotide containing the indicated cytosine derivative was incubated for N-glycosidic bond cleavage by HeLa extract DNA glycosylases in absence of $MgCl_2$. Base excision generates an abasic site, which can be converted into a single-strand break (nucleotide position 79) by recombinant APEX1, and monitored by denaturing PAGE. (**b**) Electropherograms of DNA glycosylase assays. Product peaks of glycosylase activities

(79mers; arrows) are highlighted red with efficiencies shown as % of 79 nt peak integral relative to the total fluorescent signal per electropherogram. Data are representative of three independent experiments. (**c**) siRNA screen for DNA glycosylases required for 5fC and 5caC removal. Data represent percentage of abasic sites (% AP site) generated during the assay as quantified from strand cleavage products (79mer) post APEX1 treatment. (**d**) DNA glycosylase assay using HeLa extracts depleted of *TDG* and *NEIL1 + NEIL2* by siRNAs. (**e**) DNA demodification assay as in Figure 1 b but with HeLa cell extracts depleted as in **d**. (**f**) LC-MS/MS quantification of genomic cytosine modifications from HeLa cells siRNA-depleted of the indicated genes. Cells were transfected with TET1 catalytic domain to elevate levels of rare demethylation intermediates and to facilitate their mass-spectrometric detection.Error bars, s.d. (n = 3 assay repetitions (**c-e**) or cell culture transfections (**f**)). n.s., not significant. **P* < 0.05, ***P* < 0.01, ****P* < 0.005 by two-tailed unpaired Student's t-test.

NEIL2 is required for TCF21 DNA demethylation

Recently, we showed that transcriptional activation of the tumor suppressor *TCF21* is directed by the long non-coding RNA TARID and is accompanied by TET–TDG-mediated DNA demethylation[32]. *TCF21* is silenced and hypermethylated in the cancer cell line HNO387 but can be demethylated and activated by ectopic TARID expression ([32] and Fig. 3b-c). To test if NEIL1 and NEIL2 are required for gene-specific demethylation of the *TCF21* locus we monitored the expression levels and promotor methylation of *TCF21* upon *NEIL1* and *NEIL2* depletion in HNO387 cells. *NEIL2* showed strong expression, while *NEIL1* was hardly expressed in HNO387 cells (Fig. 3a). Interestingly, TARID-triggered *TCF21* expression was blocked by *NEIL2*- but not by *NEIL1* siRNA (Fig. 3b). Moreover, TARID-induced demethylation of the promotor CpGs was impaired when *NEIL2* was downregulated (Fig. 3c). Again, knockdown of *NEIL1* had no effect, as expected from its low expression level. Overexpression of TDG partially reversed the inhibition of *TCF21* induction and promoter hypermethylation by *NEIL2* siRNA (Fig. 3d-e). We conclude that NEIL2 is required for TET–TDG-mediated gene-specific demethylation of *TCF21*.

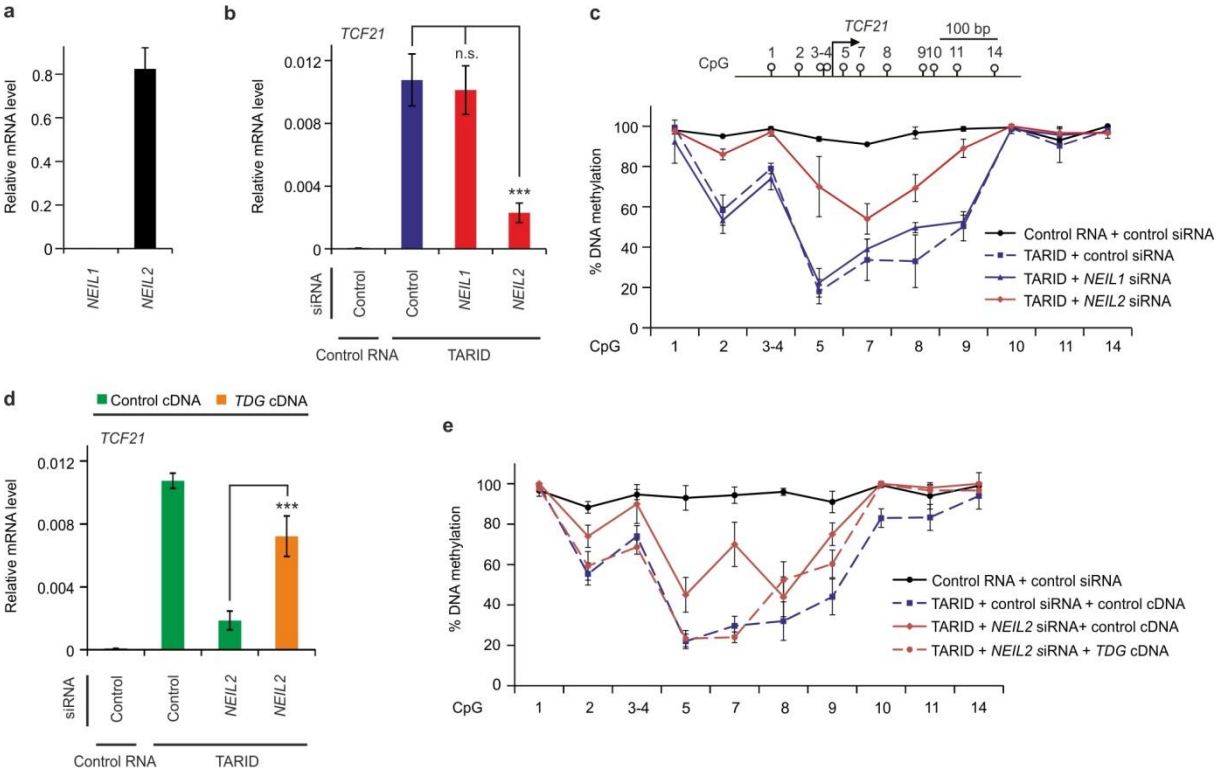

Figure 3: NEIL2 is required for demethylation of *TCF21* in HNO387 cells.

(**a**) qPCR expression analysis of *NEIL1* and *NEIL2* in HNO387 cells relative to *HPRT1* (housekeeping gene). (**b**) qPCR expression analysis of *TCF21* relative to *HPRT1* in HNO387 cells upon transfection with control RNA (Control RNA), TARID and the indicated siRNAs. (**c**) Top, schematic representation of *TCF21* promoter with transcription start site and CpGs analyzed. Bottom, methylation analysis of the *TCF21* promotor by MassARRAY[32] using HNO387 cells transfected as in **b**. (**d**) qPCR expression analysis of *TCF21* as in (b). HNO387 cells were transfected with control RNA, TARID RNA, control siRNA and *NEIL2* siRNA co-transfected with control or *TDG* expression plasmids as indicated. (**e**) Methylation analysis of the *TCF21* promotor as in (**c**) using HNO387 cells transfected as in **d**. Error bars, s.d. (n = 3 cell culture transfections). n.s., not significant. *** $P < 0.005$ by two-tailed unpaired Student's t-test.

NEIL1 and NEIL2 promote TDG-mediated 5fC and 5caC excision

Since NEIL DNA glycosylases excise oxidized bases and were reported to bind 5mC derivatives[22], our findings initially supported a model whereby they act redundantly with TDG as DNA glycosylases, to directly excise 5fC and 5caC from DNA[23]. To test this we purified recombinant TDG, NEIL1 and NEIL2 (Supplementary Fig. 3a) and carried out *in vitro* DNA glycosylase assays. As reported[5,10], TDG but not the catalytically inactive point mutant TDG^{N140A} effectively excised 5fC and 5caC residues from oligonucleotides (Fig. 4a).

Surprisingly, recombinant NEIL1 and NEIL2 showed no excision of 5fC and 5caC from double or single stranded DNA (Fig. 4b). Yet, they exhibited robust glycosylase activity towards their known substrate 5-hydroxyuracil[21] and showed AP lyase activity (Supplementary Fig. 3b-d), indicating that the recombinant enzymes were active.

Furthermore, we carried out DNA binding assays with TDG, NEIL1 and NEIL2 using unmodified and hemi-modified oligonucleotides. TDG bound its substrates 5fC and 5caC, as well as its product, the AP site with several-fold higher affinity than unmodified DNA (Fig. 4c). Low affinity binding of TDG to unmodified DNA was previously interpreted as a lesion scanning mode[33]. In contrast, NEIL1 and NEIL2 did not discriminate between unmodified, 5fC and 5caC containing oligonucleotides (Fig. 4d-e). Interestingly, NEIL1 bound AP site containing oligonucleotides with a 3-fold higher affinity than unmodified DNA, whereas NEIL2 exhibited an overall high DNA binding affinity per se (apparent K_d of 27 nM on unmodified DNA). Binding of NEILs was cooperative towards all ligands, indicative of a switch-like mode of binding and release. We conclude that purified NEIL1 and NEIL2 neither process nor specifically bind 5fC or 5caC.

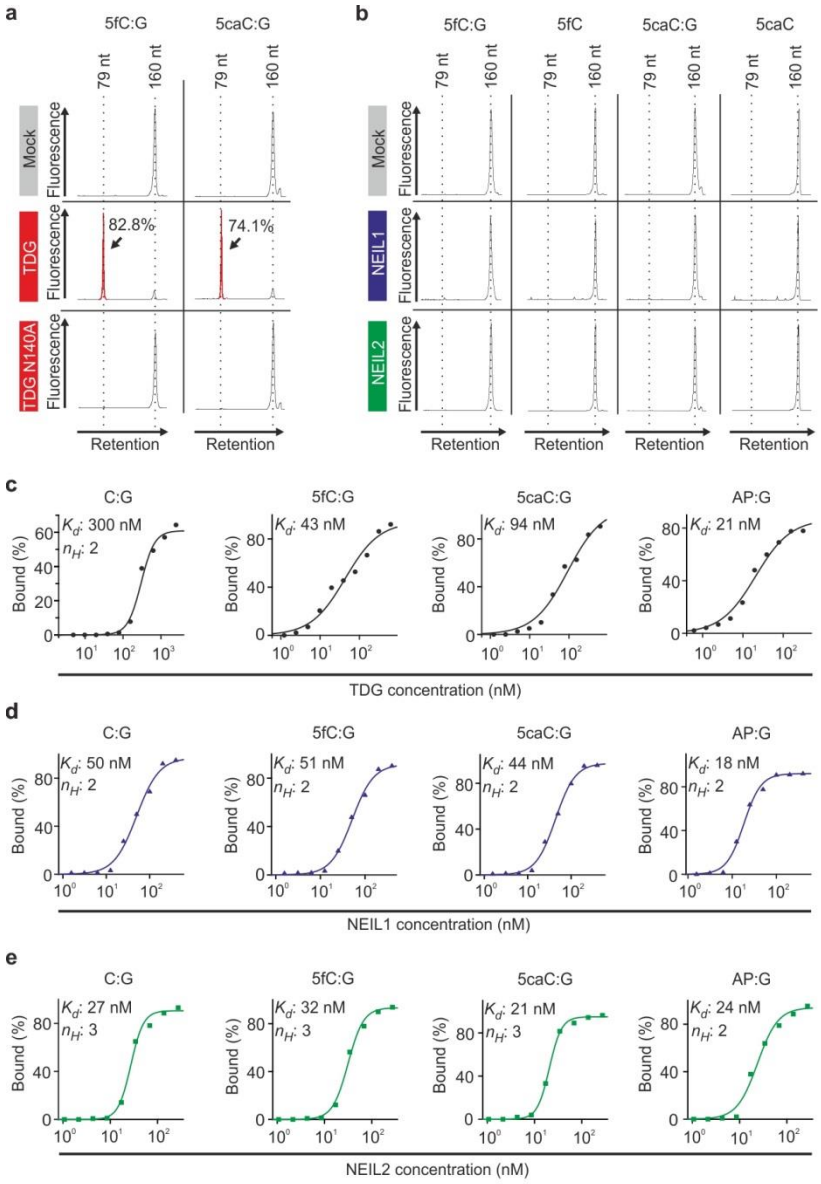

Figure 4: NEIL1 and NEIL2 do not process and bind 5fC and 5caC *in vitro*.

(**a**,**b**) Electropherograms of reaction products from DNA glycosylase assays with 20 nM ds (5fC:G; 5caC:G) and ss (5fC; 5caC) oligonucleotide substrates. Recombinant DNA glycosylase was in 10-fold excess over oligonucleotide substrate (single turnover conditions). (**a**) Human TDG (reaction products highlighted in red with efficiencies shown in %) and catalytically inactive mutant TDG^{N140A}. (**b**) Human NEIL1 and NEIL2. Data are representative of three independent experiments. (**c-e**) DNA binding assays with TDG, NEIL1 and NEIL2. Fitted curves, calculated dissociation constants (K_d) and Hill coefficients (n_H) derived from electrophoretic mobility shift assays towards indicated ds oligonucleotides are shown. Binding assays are representative of two independent experiments with similar outcome.

It seems paradoxical that NEIL DNA glycosylases with their known preference for oxidized lesions do not directly bind or process 5fC or 5caC, neither in double- nor single-stranded DNA. How then do NEILs function in 5fC and 5caC removal? We tested if NEILs cooperate with TDG in DNA glycosylase assays. Intriguingly, addition of NEIL1 or NEIL2 robustly stimulated 5fC and 5caC excision in the presence of wild type TDG but not TDG^{N140A} (Fig. 5a), arguing for a scenario in which NEILs boost base excision of TDG but not *vice versa*. Stimulation of TDG activity by NEILs was specific since recombinant SMUG1, a monofunctional DNA glycosylase, did not enhance TDG base excision (Supplementary Fig. 4a).

In multiple turnover kinetics of 5fC and 5caC excision with TDG alone, the reactions quickly levelled off (Fig. 5b). This rapid plateauing is characteristic for TDG, which is product inhibited after base release, binding and occupying the resulting AP site[34-36]. AP site binding is thought to shield this repair intermediate from further attack until the next general purpose BER enzyme, APEX1, is in place to proceed with strand cleavage. APEX1 is thought to displace TDG from AP sites and thereby enhances TDG turnover[34,37]. Interestingly, NEIL1 and NEIL2 could substitute APEX1 in this context: In the presence of NEIL1 or NEIL2, TDG processed 5fC and 5caC with enhanced steady state turnover, notably towards 5caC (Fig. 5b; Table 1).

Consistent with the ability of NEIL1 and NEIL2 to replace APEX1, TDG stimulation by recombinant APEX1 was slightly lower than for NEIL (Supplementary Fig. 4b; compare to Fig. 5a). Moreover, *APEX1* siRNA did not increase the genomic levels of TET1-induced 5fC and 5caC (Supplementary Fig. 4c), unlike *NEIL1 and NEIL2* siRNAs. Finally, *APEX1* siRNA only marginally inhibited 5fC and 5caC-excision in a glycosylase assay, and 5fC and 5caC processing in a demodification assay (Supplementary Fig. 4d-f).

Recombinant TDG and NEIL proteins directly bound each other and with moderate affinity in microscale thermophoresis assays (apparent K_d's 110-380 nM, Fig. 5c, Supplementary Fig. 5a-b). The affinity of NEIL1 and NEIL2 towards an AP site oligonucleotide was one order of magnitude higher (apparent K_d 18 nM and 24 nM, respectively, Fig 3d-e) and similar to that of TDG towards an AP site (apparent K_d 21 nM, Fig. 4c). The moderate NEIL–TDG interaction in combination with high affinity AP site binding may allow TDG to recruit NEILs, which then displace TDG from the AP site. Indeed, NEIL1 and NEIL2 could effectively displace TDG from an AP site oligonucleotide using near equimolar stoichiometries (Fig. 5d).

Collectively, these results support a model where TDG and NEILs act in the coordinated AP site hand-over during the processing of 5fC or 5caC (Fig. 5e). TDG hydrolyses the modified base and becomes displaced by NEIL1 or NEIL2, whose lyase activity cleaves the DNA backbone, making the displacement irreversible. The resulting single nucleotide gap if bearing 3'- and 5'-phosphate termini is likely processed by polynucleotide kinase, DNA polymerase β and DNA ligase IIIα[38] to yield demethylated cytosine.

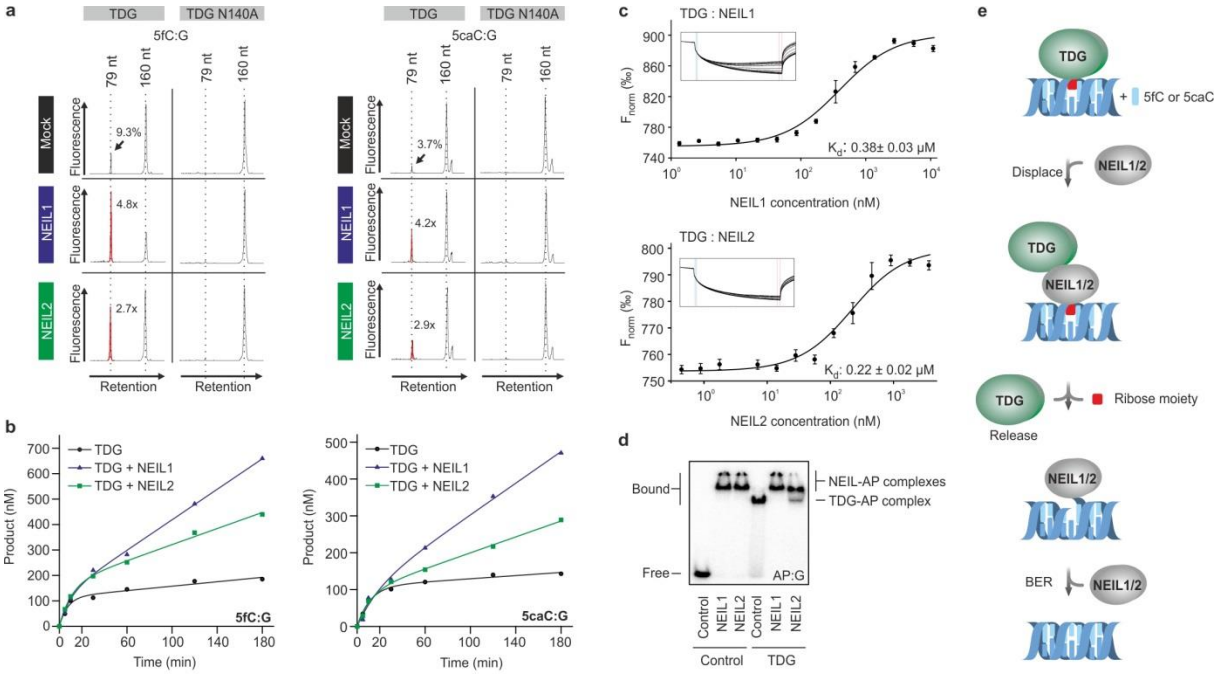

Figure 5: NEIL1 and 2 promote TDG-mediated 5fC and 5caC excision.

(**a**) DNA glycosylase assay with 100 nM oligonucleotide substrates under multiple turnover conditions with TDG and TDG^{N140A} in absence or presence of NEIL1 or NEIL2. Stimulation of base excision in presence of NEIL1 or NEIL2 is highlighted by red peaks with fold changes (left subpanels). Data are representative of three independent experiments. (**b**) TDG base release kinetics under multiple turnover conditions towards 20bp 5fC or 5caC containing oligonucleotides (rate constants are depicted in Table 1). Kinetics are representative of two independent experiments with similar outcome. (**c**) Binding assays of TDG to NEIL1 and NEIL2. Fitted curves for each binding experiment, normalized fluorescence timetraces and calculated K_d-values are shown. Error bars, s.d. (n = 3 binding assays). K_d errors are calculated technical errors derived from curve fittings. F_{norm} (‰), normalized fluorescence per mill. (**d**) AP site binding competition assay. Electrophoretic mobility shift assays with TDG (500 nM), NEIL1 (250 nM) and NEIL2 (750 nM) towards an AP site containing oligonucleotide (20 pM). To probe for TDG displacement the TDG-AP complex was pre-formed prior to NEIL addition. Control, BSA. Experiment was reproduced two times. (**e**) Model for NEIL1 and NEIL2 in TET–TDG-mediated DNA demethylation. TDG is product inhibited and stalls after 5fC and 5caC excision at the resulting AP site (red). NEIL1 or NEIL2 (NEIL1/2) displace TDG from the AP site by transiently contacting TDG and

competing for AP site binding. NEIL1/2 lyase activity generates a strand break and downstream base excision repair (BER) factors mend the lesion.

Neil2 is required for neural crest development in Xenopus

Tet and Tdg are essential for vertebrate embryogenesis[11,12,39,40]. To study the physiological relevance of Neil cooperation with Tdg in this context, we turned to *Xenopus laevis* embryos, where Tet3 functions in early development, notably neural crest specification, as shown by antisense morpholino (MO) oligonucleotide injection[40]. In early *Xenopus* embryos *neil1* expression was low during early development and increased during organogenesis as assessed by qPCR analysis (Supplementary Fig. 5a). Conversely, *neil2* was only expressed during early development, maternally and in neurulae (Supplementary Fig. 6a). Injection of MO oligonucleotides against *neil2*, *tdg* or *tet3*[40] induced a very similar phenotype, with malformed heads, and several neural crest derivatives (pharyngeal pouches, dorsal- and tail fins) reduced or missing (Fig. 6a-b). Control and *neil1* morphants were normal and coinjection of *neil1* MO did not markedly enhance the *neil2* MO phenotype (data not shown). *neil2* morphants showed no enhanced apoptosis or reduced cell proliferation (Supplementary Fig. 6b-c). The *neil2*, *tdg* and *tet3* MO phenotypes were specific because i) they were rescued by mRNA coinjection of the respective human or *X. tropicalis* homologs (Fig. 6a-b); ii) a second MO against a non-overlapping *neil2* sequence (*neil2* MO2) yielded the same neural crest deficiency phenotype as *neil2* MO (Supplementary Fig. 6d); iii) in *neil2* morphants *neil2* expression was over 10-fold induced (Supplementary Fig. 6e), suggesting that a specific cellular mechanism senses Neil2 protein reduction and tries to compensate. Specificity of *tet3* morphants was established previously and we could confirm the phenotype[40].

Consistent with a neural crest defect *neil2*, *tdg* and *tet3* morphants showed down regulation of the neural crest markers *sox10*, *twist* and *slug* on the injected side of unilaterally injected embryos, while *en2* (midbrain) and *krox20* (hindbrain) were unaffected (Fig. 6c-d), with exception of *krox20*, which was reduced by *tet3* MO. The requirement of Neil2, Tdg and Tet3 for neural crest specification was direct and not indirect via inducing mesoderm: Neural crest can be directly formed from *Xenopus* animal caps without mesoderm using combined *noggin* + *wnt8* mRNA injection[41]. In this regime *neil2*, *tdg* and *tet3* MO inhibited *sox10*, *slug* and *twist* expression, but not *N-cam* (pan-neural) (Fig. 6e). We conclude that Neil2, Tdg and Tet3 are required for *Xenopus* neural crest specification.

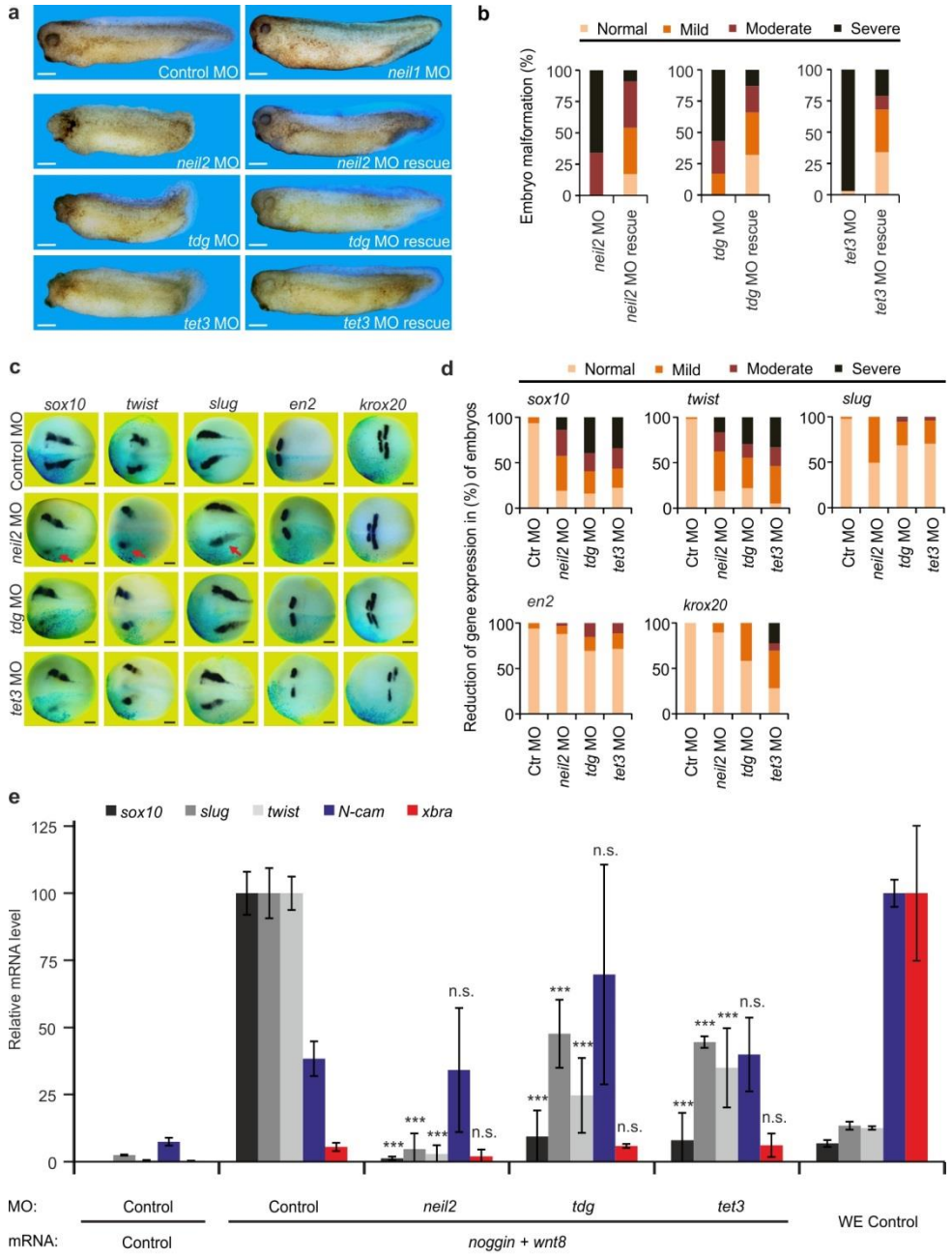

Figure 6: Neil2 is required for neural crest development in *Xenopus laevis.*

(**a**) Phenotypes of stage 34 embryos resulting from *neil1*, *neil2*, *tdg* or *tet3* morpholino (MO) injections (left). Corresponding human (*NEIL2* and *TDG*) and *X. tropicalis* (*tet3*) mRNAs were injected for rescue experiments (right). Scale bars, 200 µm. (**b**) Quantification of embryo malformations shown in **a** (n > 30 embryos per group, for details see source data). (**c**) Expression of neural crest and brain marker genes in *neil2*, *tdg* or *tet3* morphants shown by *in situ* hybridization at stage 15. Embryos were unilaterally co-injected with *lacZ* mRNA as lineage tracer (light blue speckles). Note reduced *sox10*, *twist* and *slug* expression in neural crest after *neil2* MO injection (red arrows). Scale bars, 200 µm. (**d**) Quantification of marker gene expression reduction shown in **c** (n > 30 embryos per group, for details see source data). (**e**) qPCR expression analysis of the indicated marker genes in animal cap explants at stage 16.

Injection with *noggin* and *wnt8* mRNA for neural crest induction and antisense morpholinos was as indicated. Expression of all markers was normalized to *histone h4* and represented as relative expression in percent of the respective control MO sample (*sox10, slug, twist*) or whole embryo (WE) control (*N-cam, xbra)*. Error bars, s.d. (n = 3 explant or embryo batches consisting of 12, 10 and 14 individual explants and 5, 6 and 5 embryos, respectively). n.s., not significant. ***$P < 0.005$ by two-tailed unpaired Student's t-test.

Neil2 is required for 5fC and 5caC removal in Xenopus

We tested if 5fC and 5caC residues accumulate concomitant with a *neil* depletion *in vivo*. We first established quantitative monitoring of genomic 5mC, 5hmC, 5fC and 5caC by LC-MS/MS in *Xenopus* embryos. Tadpole stage embryos had a high genomic level of 5mC (~6%), two-fold higher than HEK293T cells and mouse ES cells (mESCs) (Supplementary Fig. 7a). 5hmC levels were intermediate between HEK293T cells and mouse ES cells, while 5fC and 5caC levels, which are characteristically elevated in mESCs[6], both were even higher in *Xenopus* embryos.

Importantly, the levels of total genomic 5fC and 5caC in *Xenopus* animal caps were elevated by *neil2* MO, further increased by combined *neil1* and *neil2* MOs, and unaffected by *neil1* MO alone (Fig. 7a). The levels of 5mC, 5hmC (Fig. 7a) and the oxidative lesion 8-oxoguanine (8oxoG, Supplementary Fig. 7b) were unaffected, supporting the specificity of the MO effect. Moreover, the increase of 5fC and 5caC levels by *neil2* MO was effectively reduced by *TDG* mRNA coinjection (Fig. 7b). Conversely, knockdown of *tdg* expectedly increased 5fC and 5caC and this could be partially compensated by human *NEIL2* mRNA coinjection, suggesting that residual Tdg activity is enhanced by excess NEIL2. In line with incomplete *tdg* knockdown, combined *tdg* and *neil2* MOs further increased 5fC and 5caC (Fig. 7c). This functional cooperation between *neil2* and *tdg* also manifested phenotypically, where injection of subthreshold MO doses, which by themselves yielded normal embryos, induced malformations when *neil2* was combined with *tdg* or *tet3* MOs (Fig. 7d-e). This experiment is analogous to synthetic lethality in combined mutants, an indicator of functional interaction. In summary, in *Xenopus* embryos Neil2 cooperates with Tdg to process 5fC and 5caC residues and to specify neural crest development together with Tet3. These results, however, do not rule out a function of Tdg and Neil2 in two parallel pathways for 5fC and 5caC processing *in vivo*[23].

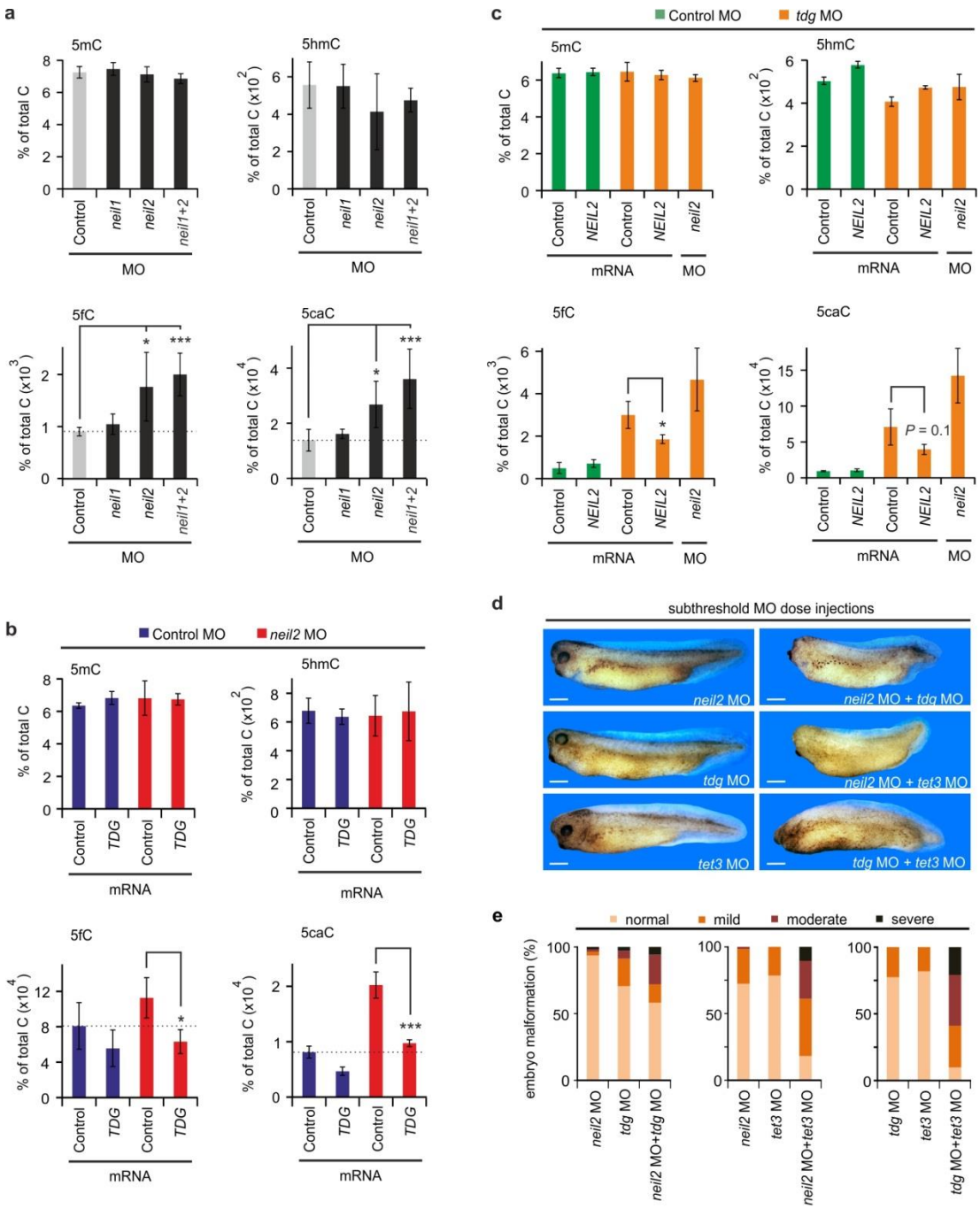

Figure 7: Neil2 is required for 5fC and 5caC removal in *Xenopus* embryos and cooperates with Tet3 and Tdg.

(**a**) LC-MS/MS analysis of genomic 5mC, 5hmC, 5fC and 5caC levels in *neil* morphant animal cap explants at stage 32. Error bars, s.d. (n = 4 explant batches each consisting of 20 animal cap explants). Grey, controls; black, morphants. (**b**) LC-MS/MS analysis as in (a) with Control MO (blue) and *neil2* MO (red) injected animal caps without or with co-injection of human *TDG* mRNA as indicated. Error bars, s.d. (n = 3 explant batches each consisting of 20 animal cap explants). (**c**) LC-MS/MS analysis as in (a), but in Control MO (green) and *tdg* MO (orange) injected animal caps (without or with co-injection of human *NEIL2* mRNA and *neil2* MO as indicated. Error bars, s.d. (n = 3 explant batches each consisting of 20 animal cap

explants). (**d**) Functional cooperation of *neil2, tdg and tet3* in *X. laevis* embryonic development. Subthreshold doses of *neil2, tdg or tet3* morpholinos (10 ng/embryo) were singly injected with Control MO (10 ng/embryo; top) or in combination (bottom) as indicated, to keep total MO dose in all samples constant. Embryos were fixed at st34. Scale bars, 200 µm. (**e**) Quantification of embryo malformations shown in **d** (n > 30 embryos per group, for details see source data). *$P < 0.05$, ***$P < 0.005$ by two-tailed unpaired Student's t-test.

Discussion

Neils function in the coordinated processing of 5fC and 5caC

Propositions of repair-based demethylation mechanisms have been controversial because of the perceived risk of genomic instability, notably for homomethylated mCpGs in tandem arrays. Our study reveals a cooperation of human NEIL1 and NEIL2 with TDG, which functions in the coordinated processing of 5fC and 5caC. TDG is a product inhibited enzyme whose turnover is slow. This may protect against the mutagenic and cytotoxic properties of AP sites, which inhibit certain DNA polymerases, lack base-pairing information during replication, and can lead to strand breaks[42]. APEX1 is thought to cooperate with TDG by stimulating its turnover for a variety of mismatches and lesions[34,37]. Here we show that NEIL1 and NEIL2 can also promote TDG product release. NEIL1 and NEIL2 bind with high affinity to DNA containing AP sites and therefore can compete with TDG for AP site binding. Displacement of TDG by NEIL1 and NEIL2 gains directionality by the NEIL lyase activity. Thus, our study shows that Neil DNA glycosylases act in the coordinated substrate hand-over of the vulnerable AP site intermediate from Tdg. A similar Apex1 bypass reaction was demonstrated in cell free assays where NEIL1 can enhance the activity of OGG1 DNA glycosylase in the removal of 8oxoG[38,43]. Our data do not exclude involvement of Apex1 in Tet–Tdg DNA demethylation, for example Apex1 may process the intermediate of the Neil AP lyase reaction, the 3'-phospho-α,β-unsaturated aldehyde[44].

What may be the relevance of this reaction? Neils may act preferentially on actively transcribed genes together with Tet and Tdg. NEIL2 associates with RNA polymerase II and binds to transcribed but not transcriptionally silent genes[45]. Hence, this preference may not only reflect the involvement of Neils in removing transcription-blocking lesions, but possibly in processing AP sites during Tet–Tdg gene activation. Along this line, NEILs bind to TET proteins[23], consistent with a recruitment of Neils to sites of DNA demethylation. Hence, Neils may act specifically in context of epigenetic gene activation, but not in universal lesion processing by TDG[34,37]. In Arabidopsis, for example, the Apex1 homolog APE1L functions in DNA demethylation downstream of the DNA glycosylases ROS1 and DME[46,47].

TDG stalling at AP sites can also be overcome by sumoylation, which potentiates the stimulatory effect of APEX1 (and presumably also NEIL1 and NEIL2) on TDG[33,36]. Further studies have to explore how these mechanisms are integrated in Tet–Tdg-mediated DNA demethylation.

A role for the Tet–Tdg–Neil module in neural crest formation

Our analysis in *Xenopus* embryos provides evidence that Tet, Tdg and Neil2 interplay is of physiological relevance for neural crest formation during early development. In addition, Tdg and Neil2 are required and cooperate to maintain normal levels of 5fC and 5caC *in vivo*. An unanswered question is if these two biological roles of Tdg and Neil2 - neural crest formation and 5fC and 5caC processing - are linked. It is generally difficult to pinpoint the role of genes with multiple functions and functional redundancies *in vivo*. For example, Tet proteins function not only enzymatically but can also act non-enzymatically in transcriptional regulation[48-50]. Moreover, 5hmC, 5fC and 5caC may not only act as demethylation intermediates but also as epigenetic marks in their own right since they are recognized by specific readers[22]. Thus, it is unclear whether the Tet mutant phenotypes are due to DNA hypermethylation, failure to set oxidized methylcytosine epigenetic marks, or defects in transcription. In addition, *Tet1* and *Tet2* single-mutant mice are viable, while a fraction of *Tet1* and *Tet2* double knockout mice die perinatally with developmental abnormalities[51], indicative of functional redundancy. *Tet3* single mutants die perinatally[52] and triple mutants have not been reported. Similarly, Tdg not only functions in Tet–Tdg demethylation but also as a generic mismatch DNA repair enzyme. Moreover, like Tets, TDG can also act non-enzymatically as a scaffold protein to recruit the transcriptional coactivator CBP/p300 to numerous transcription factors[53]. Thus, while Tdg knock out mice die in utero, the etiology is unclear.

Given similar complexities in *neil2* morphants it is difficult to know whether the observed neural crest defects are due to reduced processing of 5fC and 5caC by Tdg. For example, we cannot exclude that Neil2 functions primarily as a lesion repair DNA glycosylase and that the neural crest may be a particularly sensitive organ in this respect. However, the fact that i) *tet3, tdg* and *neil2* morphants show a similar phenotype affecting the neural crest, ii) that *neil2* morphants did not exhibit significant cell cycle arrest or apoptosis, and iii) that combination of subthreshold MO doses cooperate in producing malformed embryos suggests an at least partially shared role for these enzymes in development, which is related to gene specific 5fC and 5caC processing.

We note that in mouse, *Neil1* and *Neil3* mutants also show neural defects, albeit in adults[54-56], while *Neil2* mutants have not been reported. The observed mouse phenotypes were attributed

to lesion repair deficits. Our results will provide a mechanistic and physiological framework to revisit mouse *Neil* mutants to study the role of the enzymes in the context of DNA demethylation, with its many exciting biological facets, ranging from embryonic stem cell differentiation and reprogramming to cancer.

Acknowledgement

We thank U. Stapf (IMB) for technical assistance, A. Rao (Division of Signaling and Gene Expression, La Jolla Institute for Allergy and Immunology, La Jolla, CA, USA), P. Schär (Department of Biomedicine, University of Basel, Basel, Switzerland), Y. Zheng (New England Biolabs, Ipswich, Massachusetts, USA) for reagents and the IMB core facilities for technical support. This work was supported by an ERC senior investigator grant to C.N. ("DNAdemethylase"). M.U.M was supported by a Natural Sciences and Engineering Research Council of Canada Postdoctoral Fellowship (NSERC-PDF 403829-2011).

Author contributions

L.S. carried out biochemical assays. D.H. conducted *Xenopus* experiments. M.U.M. performed LC-MS/MS measurements. K.A. performed experiments on HNO387 cells. L.S. and S.K. carried out protein-protein interaction assays. All authors analyzed and discussed the data. L.S. and C.N. conceived the study, designed experiments and wrote the paper.

Competing financial interests

The authors declare no competing financial interests.

References

1. Jones, P.A. Functions of DNA methylation: islands, start sites, gene bodies and beyond. *Nat Rev Genet* **13**, 484-92 (2012).
2. Schübeler, D. Function and information content of DNA methylation. *Nature* **517**, 321-6 (2015).
3. Kriaucionis, S. & Heintz, N. The nuclear DNA base 5-hydroxymethylcytosine is present in Purkinje neurons and the brain. *Science* **324**, 929-30 (2009).
4. Tahiliani, M. et al. Conversion of 5-methylcytosine to 5-hydroxymethylcytosine in mammalian DNA by MLL partner TET1. *Science* **324**, 930-5 (2009).
5. He, Y.F. et al. Tet-mediated formation of 5-carboxylcytosine and its excision by TDG in mammalian DNA. *Science* **333**, 1303-7 (2011).
6. Ito, S. et al. Tet proteins can convert 5-methylcytosine to 5-formylcytosine and 5-carboxylcytosine. *Science* **333**, 1300-3 (2011).
7. Pfaffeneder, T. et al. The discovery of 5-formylcytosine in embryonic stem cell DNA. *Angew Chem Int Ed Engl* **50**, 7008-12 (2011).
8. Kohli, R.M. & Zhang, Y. TET enzymes, TDG and the dynamics of DNA demethylation. *Nature* **502**, 472-9 (2013).
9. Wu, S.C. & Zhang, Y. Active DNA demethylation: many roads lead to Rome. *Nat Rev Mol Cell Biol* **11**, 607-20 (2010).
10. Maiti, A. & Drohat, A.C. Thymine DNA glycosylase can rapidly excise 5-formylcytosine and 5-carboxylcytosine: potential implications for active demethylation of CpG sites. *J Biol Chem* **286**, 35334-8 (2011).
11. Cortazar, D. et al. Embryonic lethal phenotype reveals a function of TDG in maintaining epigenetic stability. *Nature* **470**, 419-23 (2011).
12. Cortellino, S. et al. Thymine DNA glycosylase is essential for active DNA demethylation by linked deamination-base excision repair. *Cell* **146**, 67-79 (2011).
13. Shen, L. et al. Genome-wide analysis reveals TET- and TDG-dependent 5-methylcytosine oxidation dynamics. *Cell* **153**, 692-706 (2013).
14. Song, C.X. et al. Genome-wide profiling of 5-formylcytosine reveals its roles in epigenetic priming. *Cell* **153**, 678-91 (2013).
15. Raiber, E.A. et al. Genome-wide distribution of 5-formylcytosine in embryonic stem cells is associated with transcription and depends on thymine DNA glycosylase. *Genome Biol* **13**, R69 (2012).
16. Zhu, B. et al. 5-methylcytosine-DNA glycosylase activity is present in a cloned G/T mismatch DNA glycosylase associated with the chicken embryo DNA demethylation complex. *Proc Natl Acad Sci U S A* **97**, 5135-9 (2000).
17. Fromme, J.C. & Verdine, G.L. Base excision repair. *Adv Protein Chem* **69**, 1-41 (2004).
18. Hosfield, D.J. et al. DNA damage recognition and repair pathway coordination revealed by the structural biochemistry of DNA repair enzymes. *Prog Nucleic Acid Res Mol Biol* **68**, 315-47 (2001).
19. Prasad, R., Shock, D.D., Beard, W.A. & Wilson, S.H. Substrate channeling in mammalian base excision repair pathways: passing the baton. *J Biol Chem* **285**, 40479-88 (2010).
20. Hazra, T.K. et al. Identification and characterization of a human DNA glycosylase for repair of modified bases in oxidatively damaged DNA. *Proc Natl Acad Sci U S A* **99**, 3523-8 (2002).
21. Hazra, T.K. et al. Identification and characterization of a novel human DNA glycosylase for repair of cytosine-derived lesions. *J Biol Chem* **277**, 30417-20 (2002).

22. Spruijt, C.G. et al. Dynamic readers for 5-(hydroxy)methylcytosine and its oxidized derivatives. *Cell* **152**, 1146-59 (2013).
23. Müller, U., Bauer, C., Siegl, M., Rottach, A. & Leonhardt, H. TET-mediated oxidation of methylcytosine causes TDG or NEIL glycosylase dependent gene reactivation. *Nucleic Acids Res* **42**, 8592-604 (2014).
24. Bandaru, V., Sunkara, S., Wallace, S.S. & Bond, J.P. A novel human DNA glycosylase that removes oxidative DNA damage and is homologous to Escherichia coli endonuclease VIII. *DNA Repair (Amst)* **1**, 517-29 (2002).
25. Liu, M. et al. The mouse ortholog of NEIL3 is a functional DNA glycosylase in vitro and in vivo. *Proc Natl Acad Sci U S A* **107**, 4925-30 (2010).
26. Morland, I. et al. Human DNA glycosylases of the bacterial Fpg/MutM superfamily: an alternative pathway for the repair of 8-oxoguanine and other oxidation products in DNA. *Nucleic Acids Res* **30**, 4926-36 (2002).
27. Takao, M. et al. A back-up glycosylase in Nth1 knock-out mice is a functional Nei (endonuclease VIII) homologue. *J Biol Chem* **277**, 42205-13 (2002).
28. Krokeide, S.Z. et al. Human NEIL3 is mainly a monofunctional DNA glycosylase removing spiroimindiohydantoin and guanidinohydantoin. *DNA Repair (Amst)* **12**, 1159-64 (2013).
29. Dou, H., Mitra, S. & Hazra, T.K. Repair of oxidized bases in DNA bubble structures by human DNA glycosylases NEIL1 and NEIL2. *J Biol Chem* **278**, 49679-84 (2003).
30. Krokan, H.E. & Bjoras, M. Base excision repair. *Cold Spring Harb Perspect Biol* **5**, a012583 (2013).
31. Liu, M., Doublie, S. & Wallace, S.S. Neil3, the final frontier for the DNA glycosylases that recognize oxidative damage. *Mutat Res* **743-744**, 4-11 (2013).
32. Arab, K. et al. Long noncoding RNA TARID directs demethylation and activation of the tumor suppressor TCF21 via GADD45A. *Mol Cell* **55**, 604-14 (2014).
33. Steinacher, R. & Schär, P. Functionality of human thymine DNA glycosylase requires SUMO-regulated changes in protein conformation. *Curr Biol* **15**, 616-23 (2005).
34. Waters, T.R., Gallinari, P., Jiricny, J. & Swann, P.F. Human thymine DNA glycosylase binds to apurinic sites in DNA but is displaced by human apurinic endonuclease 1. *J Biol Chem* **274**, 67-74 (1999).
35. Hardeland, U., Bentele, M., Jiricny, J. & Schar, P. Separating substrate recognition from base hydrolysis in human thymine DNA glycosylase by mutational analysis. *J Biol Chem* **275**, 33449-56 (2000).
36. Hardeland, U., Steinacher, R., Jiricny, J. & Schär, P. Modification of the human thymine-DNA glycosylase by ubiquitin-like proteins facilitates enzymatic turnover. *EMBO J* **21**, 1456-64 (2002).
37. Fitzgerald, M.E. & Drohat, A.C. Coordinating the initial steps of base excision repair. Apurinic/apyrimidinic endonuclease 1 actively stimulates thymine DNA glycosylase by disrupting the product complex. *J Biol Chem* **283**, 32680-90 (2008).
38. Wiederhold, L. et al. AP endonuclease-independent DNA base excision repair in human cells. *Mol Cell* **15**, 209-20 (2004).
39. Dawlaty, M.M. et al. Loss of Tet enzymes compromises proper differentiation of embryonic stem cells. *Dev Cell* **29**, 102-11 (2014).
40. Xu, Y. et al. Tet3 CXXC domain and dioxygenase activity cooperatively regulate key genes for Xenopus eye and neural development. *Cell* **151**, 1200-13 (2012).
41. LaBonne, C. & Bronner-Fraser, M. Neural crest induction in Xenopus: evidence for a two-signal model. *Development* **125**, 2403-14 (1998).
42. Wilson, D.M., 3rd & Barsky, D. The major human abasic endonuclease: formation, consequences and repair of abasic lesions in DNA. *Mutat Res* **485**, 283-307 (2001).

43. Mokkapati, S.K., Wiederhold, L., Hazra, T.K. & Mitra, S. Stimulation of DNA glycosylase activity of OGG1 by NEIL1: functional collaboration between two human DNA glycosylases. *Biochemistry* **43**, 11596-604 (2004).
44. Pascucci, B. et al. Reconstitution of the base excision repair pathway for 7,8-dihydro-8-oxoguanine with purified human proteins. *Nucleic Acids Res* **30**, 2124-30 (2002).
45. Banerjee, D. et al. Preferential repair of oxidized base damage in the transcribed genes of mammalian cells. *J Biol Chem* **286**, 6006-16 (2011).
46. Lee, J. et al. AP endonucleases process 5-methylcytosine excision intermediates during active DNA demethylation in Arabidopsis. *Nucleic Acids Res* **42**, 11408-18 (2014).
47. Li, Y. et al. An AP endonuclease functions in active DNA dimethylation and gene imprinting in arabidopsis. *PLoS Genet* **11**, e1004905 (2015).
48. Williams, K., Christensen, J. & Helin, K. DNA methylation: TET proteins-guardians of CpG islands? *EMBO Rep* **13**, 28-35 (2012).
49. Wu, H. et al. Dual functions of Tet1 in transcriptional regulation in mouse embryonic stem cells. *Nature* **473**, 389-93 (2011).
50. Vella, P. et al. Tet proteins connect the O-linked N-acetylglucosamine transferase Ogt to chromatin in embryonic stem cells. *Mol Cell* **49**, 645-56 (2013).
51. Dawlaty, M.M. et al. Combined deficiency of Tet1 and Tet2 causes epigenetic abnormalities but is compatible with postnatal development. *Dev Cell* **24**, 310-23 (2013).
52. Gu, T.P. et al. The role of Tet3 DNA dioxygenase in epigenetic reprogramming by oocytes. *Nature* **477**, 606-10 (2011).
53. Tini, M. et al. Association of CBP/p300 acetylase and thymine DNA glycosylase links DNA repair and transcription. *Mol Cell* **9**, 265-77 (2002).
54. Canugovi, C. et al. Endonuclease VIII-like 1 (NEIL1) promotes short-term spatial memory retention and protects from ischemic stroke-induced brain dysfunction and death in mice. *Proc Natl Acad Sci U S A* **109**, 14948-53 (2012).
55. Regnell, C.E. et al. Hippocampal adult neurogenesis is maintained by Neil3-dependent repair of oxidative DNA lesions in neural progenitor cells. *Cell Rep* **2**, 503-10 (2012).
56. Sejersted, Y. et al. Endonuclease VIII-like 3 (Neil3) DNA glycosylase promotes neurogenesis induced by hypoxia-ischemia. *Proc Natl Acad Sci U S A* **108**, 18802-7 (2011).

Tables

Table 1: Rate constants of TDG in absence or presence of NEIL1 or NEIL2 as calculated from multiple turnover kinetics. Rate constant errors are calculated technical errors derived from the curve fittings (see Figure 5b).

	5fC:G		5caC:G	
	pre-steady state base release	steady state base release	pre-steady state base release	steady state base release
	min^{-1}	min^{-1}	min^{-1}	min^{-1}
TDG	0.14 ± 0.04	0.0038 ± 0.0004	0.09 ± 0.02	0.0020 ± 0.0006
TDG + NEIL1	0.10 ± 0.03	0.0252 ± 0.0011	0.05 ± 0.03	0.0241 ± 0.0022
TDG + NEIL2	0.09 ± 0.02	0.0097 ± 0.0006	0.09 ± 0.02	0.0118 ± 0.0007

Online Methods

Cell culture and transfection

HeLa, HEK293T (ATCC numbers CCL-2 and CRL-11268) and head and neck cancer (HNO387) cells[32] were cultured in Dulbecco's modified Eagle's medium (DMEM, Lonza) supplemented with 10% Fetal Bovine Serum Gold (FBS, PAA), 2 mM L-Glutamine (Lonza), 100 U/ml penicillin-streptomycin (PEN-STREP, Lonza) at 37 °C in 5% CO_2. All cell lines have been tested for mycoplasma contamination and were negative.

Cells have been transiently transfected with siRNAs using Lipofectamine 2000 (Life technologies) and with plasmid DNAs using Turbofect (Thermo Scientific) according to the manufacturer's instructions. siRNA knockdown efficiencies were routinely assessed by qPCR and were at least 60%. Transfection of TDG shown in Figure 3d-e yielded ~10-fold overexpression as tested by qPCR (data not shown).

Mouse E14TG2a (ATCC number CRL-1821) embryonic stem cells (mESCs) were cultured on plates coated with 0.1% Gelatin (Millipore) in DMEM supplemented with 15% PANSera ES FBS (PAN Biotech), 2 mM L-Glutamine, 100 µM non-essential amino acids (NEAA, Gibco), 1 mM sodium pyruvate (Gibco), 100 µM 2-mercaptoethanol (Sigma), 1000 U/ml Leukemia inhibitory factor (LIF, Millipore), 100 U/ml PEN-STREP at 37 °C in 5% CO_2 and 5% O_2.

Reverse transcriptase coupled quantitative real time PCR (RT qPCR)

Total RNA was prepared by RNeasy mini kit (Qiagen) including an on-column DNase digestion according to the manufacturer's instructions. Complementary DNA (cDNA) was synthesized using SuperScript II reverse transcriptase (Life technologies). Quantitative real time PCR was performed on a LightCycler 480 (Roche) in technical duplicates using the Universal ProbeLibrary technology (Roche) including the supplier's LightCycler 480 Probes Master. Quantitative analysis was performed with LightCycler 480 software (Roche). Primer sequences and hydrolysis probe numbers are listed in Supplementary Table 1.

Expression constructs

Human *NEIL1*, *NEIL2* and *APEX1* cDNAs (BC010876.1, BC013964.2 and BC008145.1, respectively) were from the ORFeome clone collection. Human *TDG* and mutant TDG^{N140A} cDNAs (plasmids pRS210 and pRS211, respectively, coding both for N-terminally HA-tagged proteins) were a kind gift from P. Schär, Department of Biomedicine, University of Basel, Basel, Switzerland. *TDG*, TDG^{N140A}, *NEIL1*, *NEIL2* and *APEX1* cDNAs were inserted into pET-24b(+) and/or pET-28a(+) (both from Novagen) encoding C-terminally (TDG, TDG^{N140A}, NEIL1, NEIL2) and N-terminally (NEIL1, NEIL2, APEX1) hexahistidin-tagged proteins for gene expression in *E. coli*. *TDG*, *NEIL1* and *NEIL2* cDNAs were inserted into pCS2FLAG (Addgene plasmid #16331) encoding for N-terminally (TDG) and C-terminally (NEIL1, NEIL2) 2x FLAG-tagged proteins. Additionally, *NEIL1* and *NEIL2* cDNAs were inserted into pCS2HA (Addgene #16330) as C-terminal HA-tag expression constructs. Plasmid pXC1010 containing N-terminally hexahistidin-SUMO-tagged Naegleria gruberi Tet1[57] was a kind gift of Y. Zheng (New England Biolabs, Ipswich, Massachusetts, USA). Human TET1 catalytic domain (aa 1418-2136) was cloned from FH-TET1-pEF[4] containing full length human *TET1* cDNA (kind gift from A. Rao, Division of Signaling and Gene Expression, La Jolla Institute for Allergy and Immunology, La Jolla, CA, USA, Addgene plasmid #49792) into pCS2FLAG as an N-terminal 2x FLAG-tag expression construct. *X. tropicalis tet3* cDNA was from Open Biosystems (MXT1765-99235490).

Protein expression and purification

E. coli BL21-CodonPlus(DE3)-RIL cells (Stratagene) were transformed with the respective expression construct. Cultures were grown at 37 °C to an OD_{600} of 0.6 and induced with 1 mM isopropyl β-D-thiogalactopyranoside (IPTG), followed by cultivation at 16 °C overnight. Pelleted cells were resuspended in lysis buffer (25 mM HEPES-KOH pH 7.6, 0.5 M NaCl, 40 mM Imidazol) and lysed by passage through a Constant Systems LTD cell disrupter (1.8 kbar, constant run). Cell debris were pelleted by centrifugation at 38,400 x g for 30 min and supernatant subjected to a Ni^{2+}-charged chelating sepharose Fast Flow column (GE Healthcare). Bound proteins were eluted by a stepwise gradient of imidazol (60 - 500 mM) in lysis buffer. Fractions containing enriched target proteins were united, desalted with HP buffer (20 mM HEPES-KOH pH 7.6, 5 mM β-mercaptoethanol) and subjected to a HiTrap Heparin HP column (GE Healthcare). Bound proteins were eluted with a linear gradient of 0 - 1.5 M NaCl in HP buffer. Fractions containing pure protein were

concentrated using Vivaspin ultrafiltration devices (GE Healthare). Concentrations of proteins were determined by Bradford assay (Bio-Rad) using BSA as standard.

DNA substrates

160 bp ds oligonucleotides, where one strand contained both, a single modified CpG dinucleotide and a 5'-end fluorescent lable, were individually prepared, purified and annealed. 160 nt ss oligonucleotides were prepared by ligation of three oligonucleotides (73mer, 12mer and 75mer, for sequences see Supplementary Table 1) with T4 DNA ligase (NEB) according to manufacturer's instructions in presence of a complementary splint oligonucleotide. Ligation products were PAGE purified on a 14% denaturing polyacrylamide gel (7 M urea, 1x TBE) followed by ethanol precipitation. Purified DNA strands were hybridized to 160 bp substrates using 500 nM fluorescently-labeled strand and 750 nM complementary strand in 1x SSC. Substrates for multiple turnover kinetics were hybridized using 10 µM fluorescently-labeled 20mer and 15 µM complementary strand in 1x SSC. For oligonucleotide sequences see Supplementary Table 1.

Activity assays

Demodification assay

HeLa whole cell extracts were prepared by lysis in 10 mM HEPES-KOH pH 7.9, 1.5 mM $MgCl_2$, 10 mM KCl, 1% Nonidet P 40 (Sigma) and clearance at 600 x g for 5 min. Concentrations of cell extracts were determined by Bradford assay (Bio-Rad) using BSA as standard. Demodification assays were perfomed in 50 µl containing 50 µg cell extract and 20 nM double stranded 160 bp modified oligonucleotide substrate in 40 mM HEPES-KOH pH 7.8, 70 mM KCl, 5mM $MgCl_2$, 10 µM $ZnCl_2$, 0.5 mM DTT, 2mM ATP, 20 µM dNTPs, 20 mM phosphocreatine, 2.5 µg creatine phosphokinase (Type I, Sigma C3755), 5 µg salmon sperm DNA for 3 h at 37 °C. Reactions were stopped by phenol/chloroform extraction and ethanol precipitation of the DNA. Reaction products were in incubated with 5 units HpaII (Promega) in 7.5 µl for 1h at 37°C, or were mock treated (demodification intermediate assay). Reaction was stopped by adding 2.5 µl loading dye (95% formamide, 20 mM EDTA pH 8.0, 10 mg/ml Dextran-Blue), reaction products were heat denatured and subjected to denaturing 4% PAGE analysis using an Applied Biosystems ABI Prism 377 DNA Sequencer according to

the manufacturer's instructions. Peak areas were quantified using the software GeneScan Analysis (Applied Biosystems).

Small scale siRNA screen

HeLa cells were harvested 48h after siRNA transfection and whole cell extracts were prepared as described above. DNA glycosylase assays were performed with 50 µg cell extract and 20 nM 160 bp DNA substrate in 10 mM HEPES-KOH pH 7.4, 100 mM KCl, 10 mM EDTA, 0.5 mM DTT in a total volume of 50 µl for 60 min at 37 °C. Reactions were stopped and DNA was isolated as described above. To generate strand breaks at AP sites reaction products were incubated with 5 u recombinant APEX1 (M0282, NEB) for 30 min at 37 °C in a total volume of 10 µl. Enzymatic strand cleavage by APEX1 instead of alkali treatment of the reaction products[10] proved necessary since DNA substrates containing 5-formyl- or 5-carboxylcytidine residues showed significant strand cleavage after boiling in 150 mM NaOH even in absence of any prior enzymatic incubation (data not shown). After strand cleavage, 2.5 µl loading dye were added, reaction products heat denatured and subjected to electrophoresis as described above. Reactions were stopped by adding 2.5 µl loading dye, reaction products heat denatured and subjected to gel electrophoresis as described above.

Glycosylase assays with purified proteins

Single turnover reactions with TDG, NEIL1 and NEIL2 were performed with 200 nM enzyme and 20 nM 160 bp substrate in glycosylase buffer (10 mM HEPES-KOH pH 7.4, 1 M trimethylamine-N-oxide[21], 100 mM KCl, 10 mM EDTA, 0.5 mM DTT, 100 µg/ml BSA) for 20 min at 37 °C. Stimulation of TDG excision was carried out with 6 nM TDG alone or in combination with 30 nM NEIL1 or NEIL2 and 100 nM of 160 bp substrate in glycosylase buffer for 2h at 37 °C. Control reactions with mutant TDG^{N140A}, SMUG1 and APEX1 were performed essentially as depicted above. Multiple turnover kinetics were conducted with 150 nM TDG alone or in combination with 20 nM NEIL1 or 75 nM NEIL2 and 1 µM 20 bp DNA substrate (sequences see Supplementary Table 1) in glycosylase buffer at 37 °C for up to 3h. For stimulation assays the active enzyme fraction was determined and used. TDG active fraction was derived from multiple turnover kinetics[43] and NEIL1 and NEIL2 active fractions were determined by AP trapping assay using cyanoborohydride[28] (data not shown). Based on this assay only a minor fraction of NEIL1 and NEIL2 protein appeared active and some contribution of the 'inactive' Neil fraction in the TDG stimulation assay cannot be ruled out. Downstream processing of reaction products and analysis was essentially as described above.

Data for multiple turnover kinetics were fitted by non-linear regression to the following equation[43] using GraFit 7 (Erithacus Software):

$$A_t = A_\infty(1-e^{-kt}) + vt$$

A_∞, amplitude of the burst; *k*, 1st order rate constant; *t*, time; *v*, reaction rate in the linear phase.

AP lyase assay

To test NEIL1 and NEIL2 for their ability to incise at AP sites 20 nM of a 160 bp substrate bearing a single T:G mismatch was incubated with 200 nM TDG in glycosylase buffer for 20 min at 37 °C followed by phenol/chloroform extraction and ethanol precipitation of the DNA. After resuspension DNA was incubated with 200 nM NEIL1 or NEIL2 (C- or N-terminally hexahistidin tagged) or 20 nM APEX1 in a total volume of 10 µl for 20 min at 37 °C. Reactions were stopped by adding 2.5 µl loading dye, reaction products heat denatured and subjected to gel electrophoresis as described above.

Electrophoretic mobility shift assays (EMSAs)

End-labeling of DNA was performed with 200 nM unmodified 20mer oligonucleotide using [γ-^{32}P] ATP (Perkin Elmer) and T4 polynucleotide kinase (NEB) according to manufacturer's instructions. 100 nM labeled DNA was hybridized in SSC buffer (150 mM NaCl, 15 mM trisodium citrate) with 100 nM complementary oligonucleotides bearing either no modification or a single 5fC, 5caC, or a tetrahydrofuran (AP site), respectively (sequences see Supplementary Table 1). Unincorporated [γ-^{32}P] ATP was removed by G-25 Quick Spin Columns (Roche). EMSAs were performed with 20 pM duplex DNA and different amounts of enzyme in binding buffer (20 mM Tris-HCl pH 7.6, 100 mM NaCl, 1mM EDTA, 1 mM DTT, 10% glycerol, 100 µg/ml BSA) for 20 min at 4 °C or at room temperature. AP site binding competition assay was performed with 20 pM of an AP site containing double stranded oligonucleotide, preincubated with 50 µg/ml BSA (Control) or 500 nM TDG in binding buffer for 10 min at room temperature before adding 500 µg/ml BSA (Control), 250 nM NEIL1 or 750 nM NEIL2 for another 10 min. PAGE was done as described previously[58] but with 10% native polyacrylamide gels. Phosphorimaging was done on a Typhoon FLA 9500 (GE Healthcare) and quantification using ImageQuant TL software (GE Healthcare).

Determination of dissociation constants (K_d's) was performed by fitting data for bound duplex (%) over log [enzyme] with non-linear regression to the equations for 1-site (TDG on modified DNA) or cooperative ligand binding (TDG on unmodified DNA, NEIL1 and NEIL2 throughout) using GraFit7 (Erithacus Software). For K_d calculation and AP site competition the active enzyme fractions were used (see above).

Microscale thermophoresis

For protein/protein interactions purified TDG, NEIL1 or NEIL2 were labeled using Monolith NT Protein labeling Kit RED-NHS (NanoTemper technologies) essentially as described by the manufacturer. Binding reactions were composed of 50 nM labeled protein and increasing amounts of unlabeled recombinant NEIL1, NEIL2, TDG or SMUG1 (NEB) in MST buffer (50 mM Tris/HCl pH 7.6, 150 mM NaCl, 10 mM MgCl2, 0.05% TWEEN® 20) and incubated for 5 min at room temperature (RT). Binding was monitored in hydrophilic capillaries on a Monolith NT.115 (NanoTemper technologies) using 80% Led power, 60% MST power, 30 sec laser-on time and 5 sec laser-off time. To test microscale thermophoresis for high affinity binding 30 nM purified EGFP (STA-201, Cell Biolabs) was incubated with increasing amounts of αGFP antibody (DLN-07227, Dianova, validated for specificity prior to microscale thermophoresis) in MST buffer for 5 min at RT. Binding was conducted as described above with the exception of using standard treated capillaries and 100% Led power (Supplementary Fig 4b). Curve fittings and calculation of the dissociation constants (Kd Fit) were performed with NT Analysis software (NanoTemper technologies).

***X. laevis* embryo manipulation and staining**

Animal experiments with *X. laevis* were approved by state authorities (Landesuntersuchungsamt Rheinland-Pfalz). No blinding or randomization was performed. No statistical method was used to predetermine sample size. Embryos were obtained by *in vitro* fertilization as described[59]. Human and *X. tropicalis* expression constructs as depicted above were used as templates to generate mRNAs with the MEGAscript SP6 Transcription kit (Life technologies) according to the manufacturer's instructions. Morpholino antisense oligonucleotides (sequences are depicted in Supplementary Table 1) were designed to target the start codon of the respective gene. Morpholinos and mRNAs were injected 4 times into

animal blastomeres at 2-4 cell stage with a total volume of 10 nl per embryo. Total amounts of single morpholinos injected per embryo were as follows: *neil1* MO, 60ng; *neil2* MO and *neil2* MO2, 40ng; *tdg* MO, 20ng and *tet3* MO, 60ng (30 ng per isoform-specific MO). The synergy experiment was performed with reduced doses of morpholinos per embryo: *neil2* MO, 10ng; *tdg* MO, 10ng and *tet3* MO, 20ng. For *neil1* and *neil2* double knockdown, embryos were injected with a mixture of 20ng *neil1* MO and 40ng *neil2* MO. Control mRNA used for injections was *preprolactin*. Animal cap assays were performed as described[60]. In brief, the indicated MOs or mRNAs were animally injected in both blastomeres of two-cell stage embryos, the animal caps were dissected from the embryos at stage 8.5, cultivated further and harvested at the equivalent of stage 16 for qPCR analysis or stage 32 for mass spectrometry analysis. Whole mount *in situ* hybridization was performed as described[61]. *In situ* hybridization probes were generated from cDNAs for *X. laevis* neuronal marker genes using the Dig RNA labeling kit (Roche). For lineage tracing, *lacZ* mRNA was co-injected (250 pg/blastomere) and β-gal staining was performed as described[62] using X-gal as substrate. TUNEL assay and whole mount immunostaining of phospho-histone H3 were carried out as described[63,64].

Mass spectrometry analysis of genomic DNA

Generation and purification of ^{15}N-labeled 5hmC, 5fC and 5caC

Stable isotope labeling of DNA modifications was performed by a series of enzymatic -reactions. Firstly, a DNA strand of 83 bp length was PCR amplified using ^{15}N-labeled dCTP (Silantes) instead of unlabeled dCTP in the reaction mixture. Forward primer: CTCCTCTGACTGTAACCACG, reverse primer: AGGCTTCTGGACTACCTATGC, template: CTCCTCTGACTGTAACCACGCCGGTACGTTACGATACGATTACGTAATACGATTTCGAACCGGCATAGGTAGTCCAGAAGCCT. Purified PCR product was MspI (NEB) digested to remove unlabeled primer sequences and PAGE purified on a non-denaturing 20% polyacrylamide gel. Subsequently, DNA was *in vitro* methylated with M.SssI (NEB), phenol/chloroform-purified and incubated with purified NgTet1 for 30 min as described previously[57]. Finally, DNA was degraded to nucleosides with nuclease P1 (Roche), snake venom phosphodiesterase (Worthington) and alkaline phosphatase (Fermentas) essentially as described[65]. Individual nucleosides were separated on an Agilent 1290 Infinity Binary LC

system (Agilent technologies) using a ReproSil 100 C18 column (Jasco). Isotopically labeled 5hmC, 5fC and 5caC were identified by analytical HPLC in tandem with triple quadruple mass spectrometry (Agilent 6490, Agilent Technologies) and purified by preparative HPLC. An aliquot was mixed with known concentrations of corresponding unlabeled 5hmC, 5fC and 5caC nucleosides (Berry & Associates) and the concentrations of ^{15}N-labeled nucleosides were determined after LC-MS/MS by comparing the areas of the labeled and unlabeled compounds.

Genomic DNA preparation and LC-MS/MS analysis.

Genomic DNA was isolated after RNase A (Fermentas) treatment of lysed cells by DNeasy blood & tissue kit (Qiagen) according to the manufacturer's instructions followed by ethanol precipitation using ammonium acetate as salt. For the assessment of genomic 8oxoG levels DNA was isolated in the presence of desferrioxamine essentially as described[66]. About 1 µg of DNA was degraded to nucleosides with nuclease P1 (Roche), snake venom phosphodiesterase (Worthington) and alkaline phosphatase (Fermentas)[65]. An equal volume of isotopic standard mixture ($^{15}N_3$-C (Silantes), $^{2}H_3$-5mC (TRC) and self-synthesized $^{15}N_3$-5hmC, $^{15}N_3$-5fC and $^{15}N_3$-5caC, (see above) was added to the DNA and about 100 ng of total DNA was injected for LC-MS/MS analysis. Quantitative analysis was performed on an Agilent 1290 Infinity Binary LC system (Agilent technologies) using a ReproSil 100 C18 column (Jasco) coupled to an Agilent 6490 triple quadrupole mass spectrometer (Agilent technologies). Running buffers were 5 mM ammonium acetate pH 6.9 (A) and Acetonitrile (B). Separations were performed at a flow rate of 0.5 ml/min using the following gradient: 0% of solvent B from 0 min to 8 min, linear increase to 15% solvent B for the next 16 min. Washing and reconditioning of the column was performed with a flow rate of 1.0 ml/min with 15% solvent B for one minute and 100% buffer A for additional 5 min. During the last minute the flow rate was linearly decreased to the initial value of 0.5 ml/min. The detailed mass spectrometer settings as well as the multiple reaction monitoring (MRM) transitions are listed in Supplementary Table 2.

Quantification of highly abundant C and 5mC was performed using 100x diluted samples. The data were analyzed with the ***Agilent*** MassHunter Quantitative ***Analysis software version B.05.02*** (Agilent technologies) using isotopic standards to confirm the peak identity. Areas of the integrated peaks were exported into Microsoft Excel with which the areas were normalized to the area of the corresponding isotopic standard. Absolute values for the nucleosides were calculated using linear interpolation from a standard curve. Linear

interpolation was performed using the two closely matching data points from the standard curve. Standards were spiked into the mixture of isotopic standards to normalize for ionization variability. The standard curve for every nucleoside was prepared to cover the amount of the corresponding nucleoside in the DNA sample analyzed. The linearity of standard curves over each region was monitored after every run and confirmed to be between 1-0.996 (R^2-values) within a concentration range of at least two orders of magnitude. The technical standard deviation was < 7%. Standard curves were newly prepared with every new dataset.

Supplementary Table 1 Oligonucleotides used in the study**.**

siRNA sequences (siGENOME SMARTpool, human, Dharmacon)

Name	**Target sequence**
Control siRNA	1: UAGCGACUAAACACAUCAA 2: UAAGGCUAUGAAGAGAUAC 3: AUGUAUUGGCCUGUAUUAG 4: AUGAACGUGAAUUGCUCAA
UNG siRNA	1: CUACAGACAUAGAGGAUUU 2: GAACUCGAAUGGCCUUGUU 3: GCAGUGCCAUUGAUAGGAA 4: CAAGCCAACUCUCAUAAGG
TDG siRNA	1: GGAAGUAUGGUAUUGGAUU 2: AGGAGGACGUAUUCUAGUA 3: CCACGAAUAGCAGUGUUUA 4: GGACGUAUUCUAGUACAGA
SMUG1 siRNA	1: GCAACUACGUGACUCGCUA 2: CCAAGAGCAUCCUAAACGA 3: UCUACAAUCCCGUGGAGUA 4: UUUCGGAGCCUGUGGGCAU
MBD4 siRNA	1: CAACGACUCUUACCGAAUU 2: CAAAGAAGAUGUUGCUAUG 3: GAAAGAAGAUGAGGGUGUU 4: CCACGAACACAGAUAGAAA
OGG1 siRNA	1: GAUCAAGUAUGGACACUGA

	2: AGAGGUGGCUCAGAAAUUC 3: GGUUCUGCCUUCUGGACAA 4: GGAGCAAAGUCCUGCACAC
MPG siRNA	1: GAAGCAGCGACCAGCUAGA 2: ACAUCAUUUACGGCAUGUA 3: GGCCCAUACCGCAGCAUCU 4: GGUCAGUGUGGUCGACAGA
NTHL1 siRNA	1: GGAGCAAGGUGAAAUACAU 2: GGACCAAGAAGGCAACCAA 3: CUGAUGCUCUCCAGCCAAA 4: GGAUGCACCUGUGGACCAU
NEIL1 siRNA	1: GACCAGAGGUUCUUCAAUG 2: GGACCAAGCUGCAGAAUCC 3: GAGCUGCGCCUGAUACUGA 4: UACGAAACCUAGCGGAUAA
NEIL2 siRNA	1: GGGCUAGGGAACAUCAUUA 2: GCGAGGAUGAUUCUGAGUA 3: GCUAUACACUGCUGGACCA 4: GGGCAGCAGUAAGAAGCUA
NEIL3 siRNA	1: GAUGCUAGGUGAUGUGCUA 2: GCAAGCUACCGACUAGAAA 3: UUAAUGAAGUACCCGUGUA 4: GGACCUGUGUGGUGUGUAC
MUTYH siRNA*	1: UAUAUGGGCUGGCCUUGGA 2: GAUCAACUACUAUACCGGA 3: CAGAGCAGCUUCAGCGCAA 4: CCAUCUAUUCAGAGACGUA

Stealth siRNA sequences (Invitrogen)

Name	**Sequence (5'→3')**
MUTYH siRNA*	CAGUCCUGACGUGGAGGAGUGUGCU

* Note: A sufficient knockdown of *MUTYH* could not be achieved by neither of the two different siRNAs tested.

Morpholino antisense oligonucleotides (MO, Gene Tools)

Name	**Sequence (5'→3')**
Control MO	CCTCTTACCTCAGTTACAATTTATA
neil1 MO	GAAGCTCCGGACCCTCAGGCATAGC
neil2 MO	GTCTGACTGTGGGACCTTCCGGCAT
neil2 MO2	CATGTCTGCGGCCTTCATCAGAGGA
tdg MO	GCCTCCATTCTGCTGTTCGATATTA
tet3 isoform1 MO	CTGAGTCTCCATCATGTTTCAGCCA
tet3 isoform2 MO	GATGTGGGCTGAGTCTCCATCATAG

Oligonucleotides used for generation of 160 bp substrates (Sigma)

Orientation of oligonucleotides for ligation.

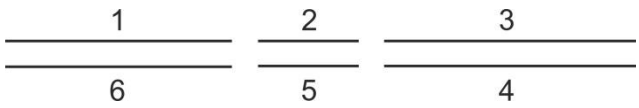

Name	**Sequence (5'→3')**
1	[CRh6G]GAACCCCACGACATCACTCATTCAAGATAACCAGCCACCTTGATCTGCCTTGTAGGTGGAGAGTCTCCCCGCT CRh6G: Carboxyrhodamine 6G
2_T	[Phos]AGGATCTGGCCC
2_5mC	[Phos]AGGATC[5mC]GGCCC 5mC: 5-methylcytosine
2_5hmC	[[Phos]AGGATC[5hmC]GGCCC 5hmC: 5-hydroxymethylcytosine
2_5fC	[Phos]AGGATC[5fC]GGCCC 5fC: 5-formylcytosine
2_5caC	[Phos]AGGATC[5caC]GGCCC 5caC: 5-carboxylcytosine
2_5hU	[Phos]AGGATC[5hU]GGCCC 5hU: 5-hydroxyuracil
2_5mC_context 2	[Phos]TCAGAC[5mC]GGATG 5mC: 5-methylcytosine
2_5hmC_context 2	[Phos]TCAGAC[5hmC]GGATG 5mC: 5-methylcytosine
2_5fC_context 2	[Phos]TCAGAC[5fC]GGATG 5mC: 5-methylcytosine
2_5caC_context 2	[Phos]TCAGAC[5caC]GGATG 5mC: 5-methylcytosine
3	[Phos]CGCCCAGCGTCTTGTCATTGGCGAATTCGAACACGCAGATGCAGTCGGGGCGGCGCGGTCCGAGGTCCACTTCGC

Splint_1+2+3	CGAATTCGCCAATGACAAGACGCTGGGCGGGGCCGGAT CcTAGCGGGGAGACTCTCCACCTACAAGGCAG
Splint_1+2+3_context 2	CGAATTCGCCAATGACAAGACGCTGGGCGCATCCGGTC TGAAGCGGGGAGACTCTCCACCTACAAGGCAG
4	GCGAAGTGGACCTCGGACCGCGCCGCCCCGACTGCATC TGCGTGTTCGAATTCGCCAATGACAAGACGCTGGGCG
5	[Phos]GGGCCGGATCCT
5_context 2	[Phos]CATCCGGTCTGA
6	[Phos]AGCGGGGAGACTCTCCACCTACAAGGCAGATCAA GGTGGCTGGTTATCTTGAATGAGTGATGTCGTGGGGTTC
Splint_4+5+6	CTGCCTTGTAGGTGGAGAGTCTCCCCGCTAGGATCCGGC CCCGCCCAGCGTCTTGTCATTGGCGAATTCG
Splint_4+5+6_context 2	CTGCCTTGTAGGTGGAGAGTCTCCCCGCTTCAGACCGGA TGCGCCCAGCGTCTTGTCATTGGCGAATTCG

Phos: 5'-phosphate

Oligonucleotides for multiple turnover kinetics (Sigma)

Name	**Sequence (5'→3')**
R6G_5fC	[CRh6G]CGCTAGGATC[5fC]GGCCCCGCC CRh6G: Carboxyrhodamine 6G , 5fC: 5-formylcytosine
R6G_5caC	[CRh6G]CGCTAGGATC[5caC]GGCCCCGCC CRh6G: Carboxyrhodamine 6G, 5caC: 5-carboxylcytosine
20mer_complementary	GGCGGGGCCGGATCCTAGCG

Oligonucleotides used for EMSAs (Sigma)

Name	**Sequence (5'→3')**
20mer_dC	CGCTAGGATCCGGCCCCGCC
20mer_AP	CGCTAGGATC[THF]GGCCCCGCC THF: tetrahydrofuran
20mer_5fC	CGCTAGGATC[5fC]GGCCCCGCC 5fC: 5-formylcytosine

20mer_5caC	CGCTAGGATC[5caC]GGCCCCGCC 5caC: 5-carboxylcytosine
20mer_complementary	GGCGGGGCCGGATCCTAGCG

Quantitative RT-PCR primers (Sigma) and UPL probe numbers (Roche)

Gene	**Direction**	**Sequence (5'→3')**	**UPL probe**
human TBP	Forward Reverse	GAACATCATGGATCAGAACAACA ATAGGGATTCCGGGAGTCAT	87
human HPRT1	Forward Reverse	TGACACTGGCAAAACAATGCA GGTCCTTTTCACCAGCAAGCT	73
human UNG	Forward Reverse	CTCGAATGGCCTTGTTTTCT GAGGGATGAGCCGTCTGTAG	45
human TDG	Forward Reverse	TGGAGTAAAGGTTAAGAACTTGGA A TGCACTGGATGATGGCATA	41
human SMUG1	Forward Reverse	TTTTTGGATTTCTTCCTCATCAA GCAGGCTCATGGATGGAC	18
human MBD4	Forward Reverse	GGGCAAAAACCATTGTCAAG TCGGTAAGAGTCGTTGCCATA	86
human OGG1	Forward Reverse	CTCCACTCCTGCCCTGTG CAGTGTGCAGGACTTTGCTC	58
human MPG	Forward Reverse	TTTACGGCATGTACTTCTGCAT ATGGTCTCCAGACCTTCCAG	19
human NTHL1	Forward Reverse	GACAGCATCCTGCAGACAGA GGTCTGCTTGATGTATTTCACCT	25
human NEIL1	Forward Reverse	CCAGGCAGTGGGAAGTCA AGGGAGGGTGGCAGAGTC	10
human NEIL2	Forward Reverse	GGGGCAGCAGTAAGAAGCTA GGAATAATTTCTTTCCATGGACCT	1
human NEIL3	Forward Reverse	CTACCTAGAGAAGCACAATGTGGA CCATTGTTAGGTCCAATCTTCAA	31
human MUTYH	Forward Reverse	ATGACACCGCTCGTCTCC GCTTCTGCCTCCCTTCCT	27
human TCF21	Forward Reverse	CATTCACCCGGTCAACCT TCAGGTCACTCTCGGGTTTC	49
X. laevis histone H4	Forward Reverse	GCGGGATAACATTCAGGGTA GCTTGACTCCCCCTCTCC	70

X. laevis sox10	Forward Reverse	AGCTCTAGCAGCTGGTCCAT TCTGCCACAGTTTGAGAGTGTT	117
X. laevis slug	Forward Reverse	GGCTACTACAAGGGCACA TCC CGAATGCTCTGTTGCAGTGT	47
X. laevis twist	Forward Reverse	ACTGGCCTCCAGATACATCG GAGTCCAGCTCGTCGCTCT	53
X. laevis ncam	Forward Reverse	AAGGCAAAGACATCGAGGAG GCACCTCTACAATGGGCTCT	8
X. laevis xbra	Forward Reverse	CCTGTCTCTTTTAGCAAAGTCAAA CTTGTGCAAAGAGTTTAACATAAT CTG	22

Supplementary Table 2 LC-MS/MS settings used for the study.

Agilent 6490 triple quadruple mass spectrometer settings

Source parameters	
Ion Mode	positive
Gas temperature	110 °C
Gas flow	19 L/min
Nebuliser	25 psi
Sheath gas temperature	375 °C
Sheath gas flow	11 L/min
Capillary voltage	3000 V
Nozzle voltage	0 V
iFunnel parameters	
High pressure RF	70 V
Low pressure RF	80 V

To avoid the fragmentation of nucleosides at the source, the fragmentor voltage was decreased to 300 V.

MRM transitions

Nucleoside	**Precursor ion**	**Fragment ion (m/z)**	**Collision energy**	**Cell accelerator**

	(m/z)			**voltage**
C* (natural isotopologe +1)**	229	113	5	8
5mC	241.9	126	6	8
5hmC	257.9	142	8	7
5fC	256.1	140	6	8
5caC	272	156	6	8
8oxoG	283.9	168	10	8
$^{15}N_3$-C	231	115	5	8
$^{2}H_3$-5mC	244.9	129	6	8
$^{15}N_3$-5hmC	260.9	145	8	7
$^{15}N_3$-5fC	259.1	143	6	8
$^{15}N_3$-5caC	275	159	6	8
$^{13}C^{15}N_2$-8oxoG	286.9	171	10	8

*MS 1 and 2 resolutions were set to unit for all ions except C and G where MS1 resolution was set to enhanced

detection of natural isotopomers increases the dynamic range of the method as described (Tsuji, M. et al. *J Chromatogr B Analyt Technol Biomed Life Sci* **953-954, 38-47, 2014).

Supplementary Figures

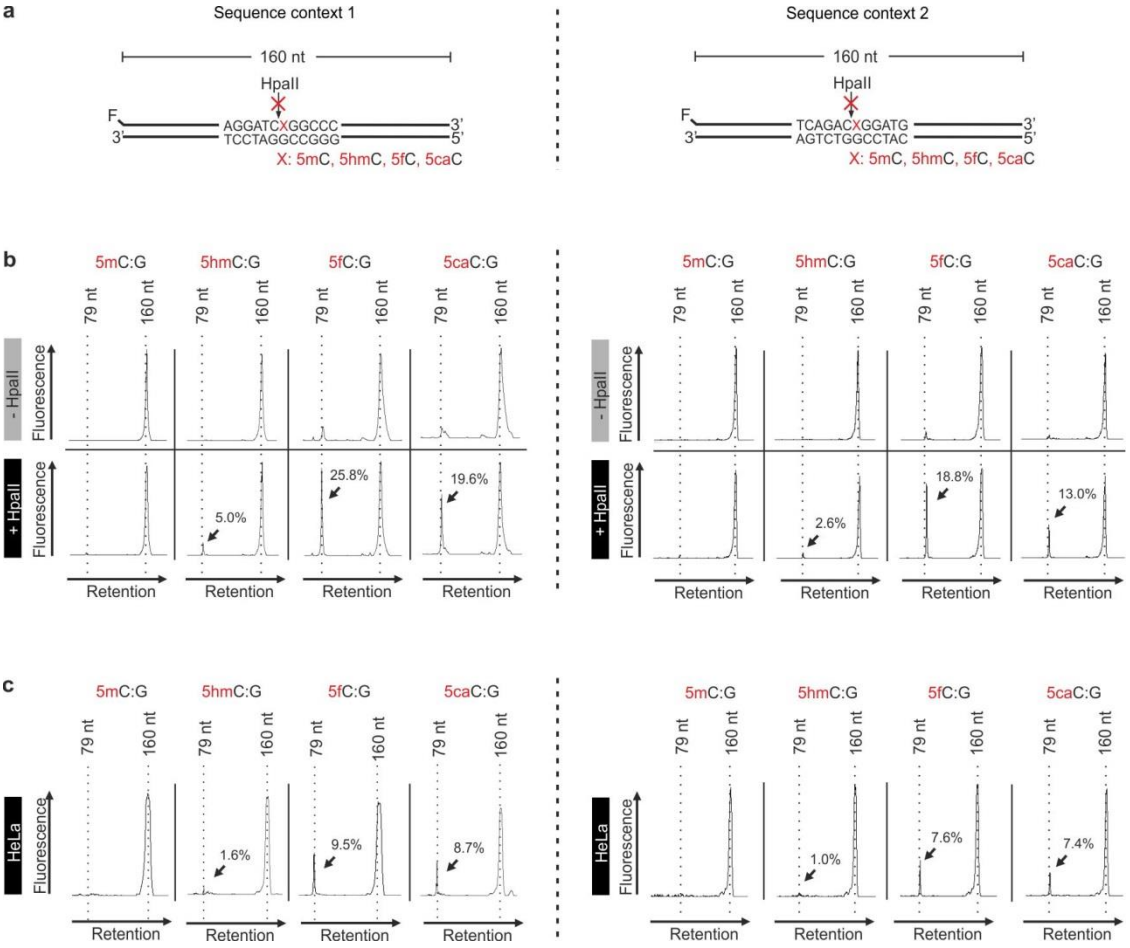

Supplementary Figure 1: DNA demodification and glycosylase activities are sequence-context independent.

(a) Scheme of the substrates used for the assays. Left, sequence context 1, right, sequence context 2. The sequence context difference flanking the HpaII recognition site is shown. (b, c) DNA demodification assay (b) and DNA glycosylase assay (c) using HeLa cell extract (50 µg in a 50 µl assay) and 20 nM 5mC, 5hmC, 5fC and 5caC containing 160 bp dsDNA of the respective sequence context (compare also Figure 1b and Figure 2b). Product peaks of demodification- (+ HpaII treatment) and glycosylase activities (79mers; arrows) are shown with efficiencies in % of 79 nt peak integral relative to the total fluorescent signal per electropherogram. Note the similar glycosylase and demodification activities of the extract towards both oligos.

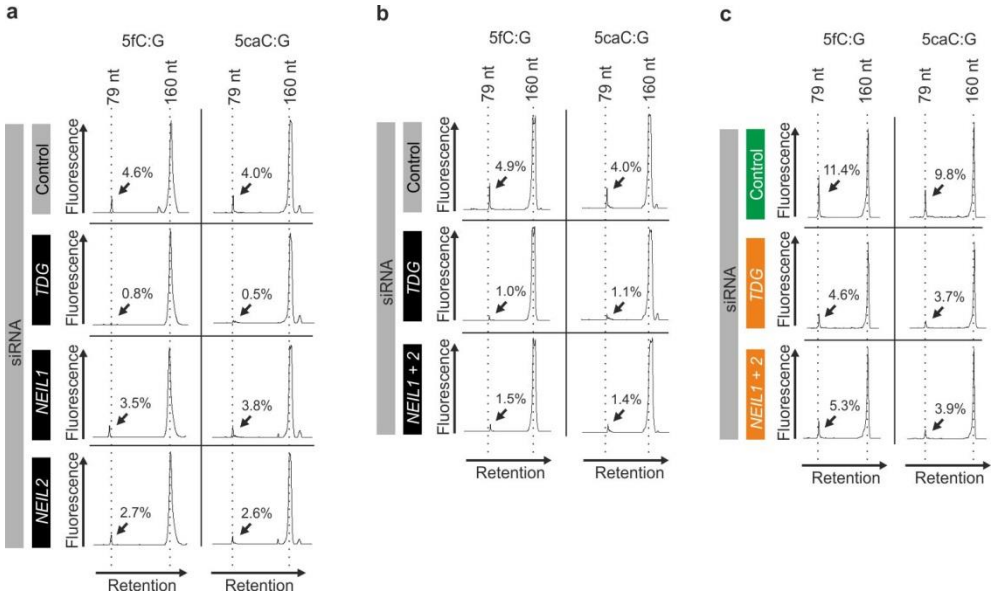

Supplementary Figure 2: Representative electropherograms of DNA glycosylase and DNA demodification assays.

(a,b) Primary data electropherograms from DNA glycosylase assays from (a) Figure 2c and (b) Figure 2d. Arrows indicate cleavage products (79 nt) with amounts of products shown as percentages above. (c) Primary data electropherograms from DNA demodification assay of Figure 2e. Arrows indicate HpaII cleavage products (79 nt) with amounts of products shown as percentages (arrow).

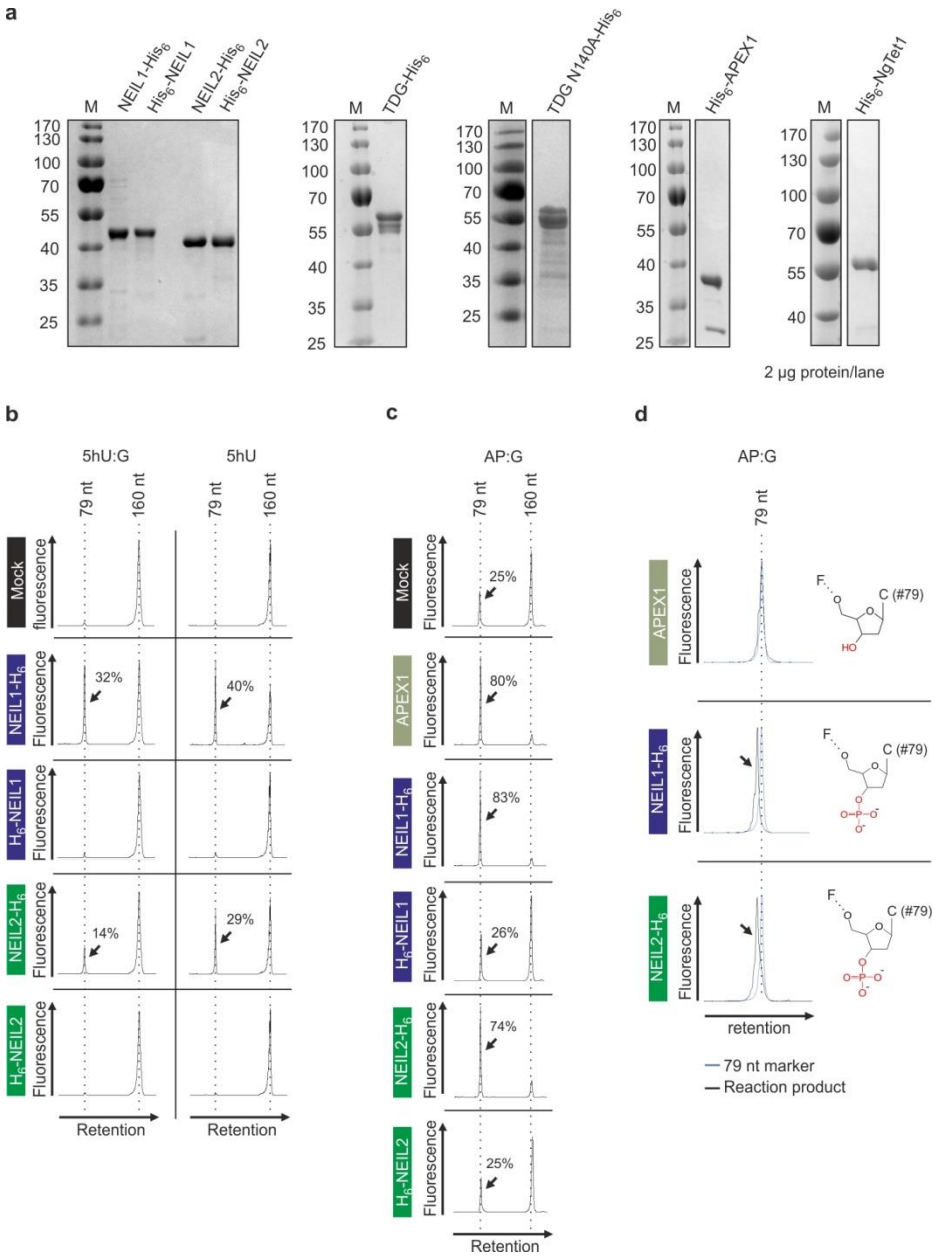
a
M
NEIL1-His6
His6-NEIL1
NEIL2-His6
His6-NEIL2
TDG-His6
TDG N140A-His6
His6-APEX1
His6-NgTet1
170
130
100
70
55
40
35
25
2 µg protein/lane
b
5hU:G
5hU
79 nt
160 nt
Mock
NEIL1-H6
H6-NEIL1
NEIL2-H6
H6-NEIL2
Fluorescence
32%
40%
14%
29%
Retention
c
AP:G
25%
80%
83%
26%
74%
25%
d
APEX1
F.
C (#79)
HO
retention
79 nt marker
Reaction product

Supplementary Figure 3: Recombinant NEIL1 and NEIL2 possess 5hU glycosylase and AP lyase activity.

(a) Coomassie-stained SDS-PAGE of the indicated purified recombinant proteins used in this study. NgTet1: Naegleria gruberi Tet1. His6: N- or C-terminal hexahistidin tag. Relative molecular weights of marker proteins (M) [x103] are indicated on the left. (b-d) Electropherograms of reaction products from DNA glycosylase assays with ds (5hU:G; AP:G) and ss (5hU) oligonucleotide substrates. (b) NEIL1 and NEIL2 process ds and ssDNA containing 5-hydroxyuracil. Arrows indicate reaction products with efficiencies (%). Note: N-terminally hexahistidin-tagged NEIL1 or NEIL2 (H6-NEIL1, H6-NEIL2) are inactive and serve as negative controls. (c) NEIL1 and NEIL2 process AP sites. Arrows indicate reaction products with efficiencies (%). Note that spontaneous AP site hydrolysis under mock conditions is 25% (background). Synthesis of AP site containing oligonucleotides is described in 'Online Methods' section. (d) Recombinant NEIL1 and NEIL2 harbor AP lyase activity. A 79mer marker oligonucleotide was mixed with cleavage products shown in (c). The APEX1 cleavage product containing a 3'-hydroxyl co-migrated with the 79mer marker (blue peak). The cleavage products of NEIL1 or NEIL2 migrate slightly faster (arrows), indicative of a 3'-phosphate residue (containing two additional negative charges) after AP lyase reaction (β,δ-elimination).

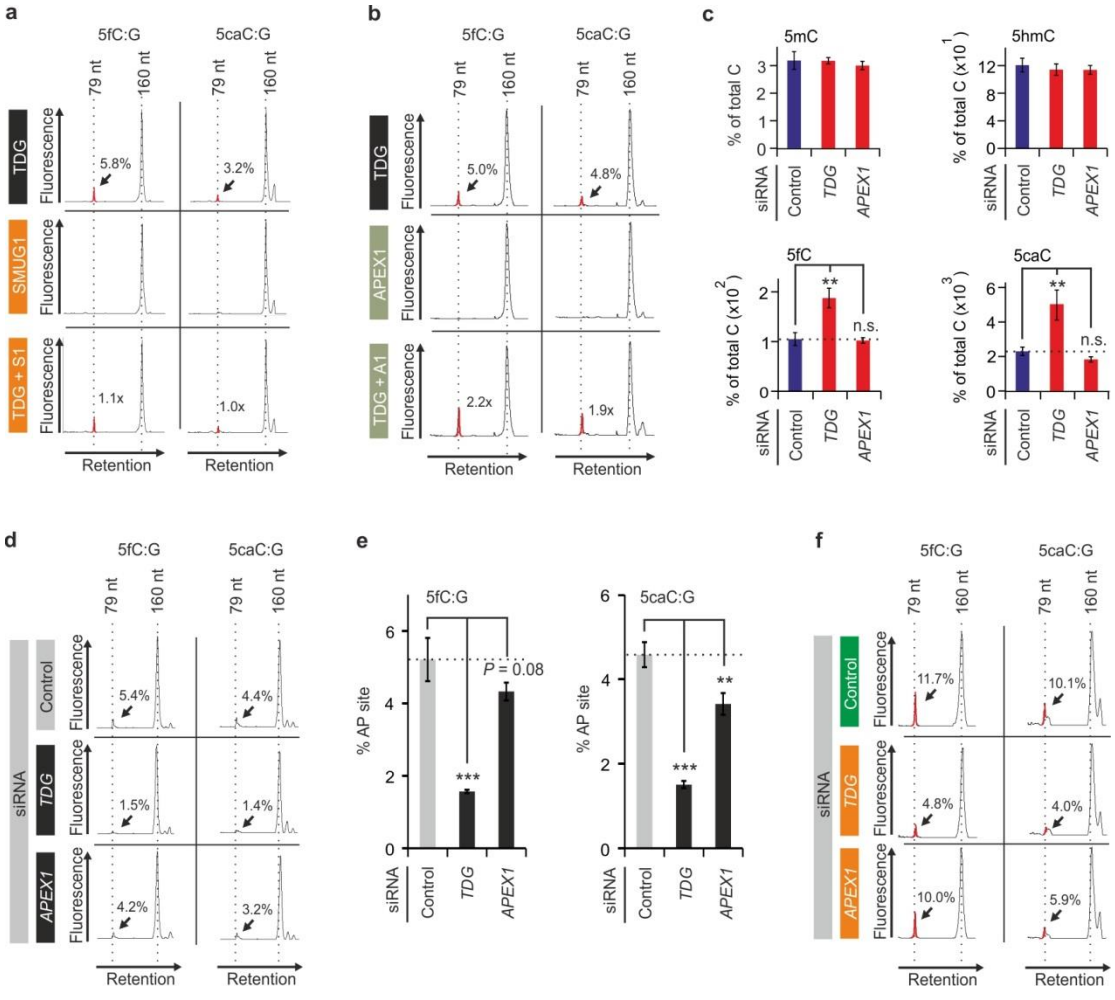

Supplementary Figure 4: TDG stimulation controls with SMUG1/APEX1 and effects of APEX1 on 5fC and 5caC processing in HeLa cells.

(a) DNA glycosylase assay of TDG and SMUG1 alone or in combination (100-fold molar excess SMUG1 (total protein) over TDG) on 5fC and 5caC containing ds oligonucleotides. Product peaks of glycosylase activities (79mers) are highlighted in red with efficiencies shown in % and -fold stimulations. Note: SMUG1 had no detectable glycosylase activity towards 5fC and 5caC substrates and was not able to stimulate base excision of TDG. S1, SMUG1. (b) DNA glycosylase assay as in (a) but with purified APEX1 instead of SMUG1 using a 5-fold molar excess (total protein) over TDG. A1, APEX1. (c) LC-MS/MS quantification of genomic cytosine modifications as in Figure 2f from HeLa cells siRNA depleted of the indicated genes. (d) DNA glycosylase assay on 5fC and 5caC containing oligonucleotides using HeLa extracts as in c. (e) Quantification of DNA glycosylase activities shown in d. Error bars, s.d. (n = 3 assay repetitions). **P < 0.01, ***P < 0.005 by two-tailed unpaired Student's t-test. (f) Demodification assay on 5fC and 5caC containing oligonucleotides using HeLa extracts siRNA depleted of the indicated genes. Repair efficiencies are shown as %.

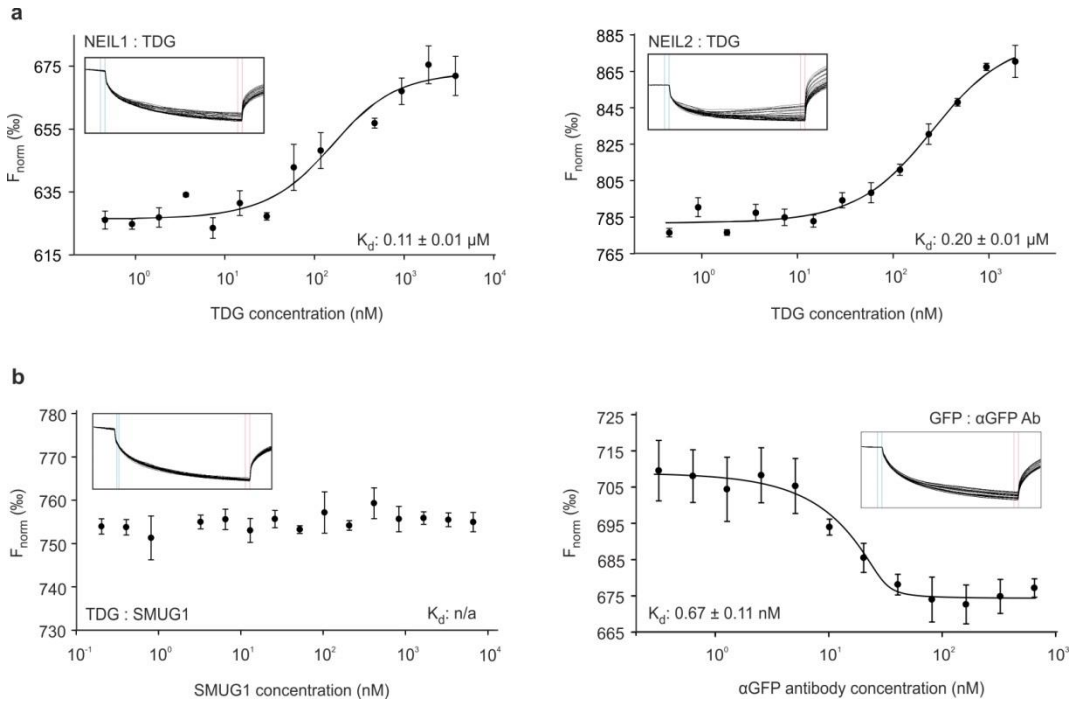

Supplementary Figure 5:NEIL1 and NEIL2 interact with TDG.

(a,b) Microscale thermophoresis binding assays. (a) Binding of fluorescently-labeled NEIL1 and NEIL2 to non-labeled TDG (reverse labeling as compared to binding assay shown in Figure 5c). (b) Left: Fluorescently-labeled TDG and SMUG1 do not interact in vitro. Right, positive control: High affinity binding of GFP to αGFP antibody. Fitted curves for each binding experiment (n = 3 binding assays), normalized fluorescence timetraces and calculated Kd-values are shown. Kd errors are calculated technical errors derived from the curve fittings. Fnorm (‰), normalized fluorescence per mill.

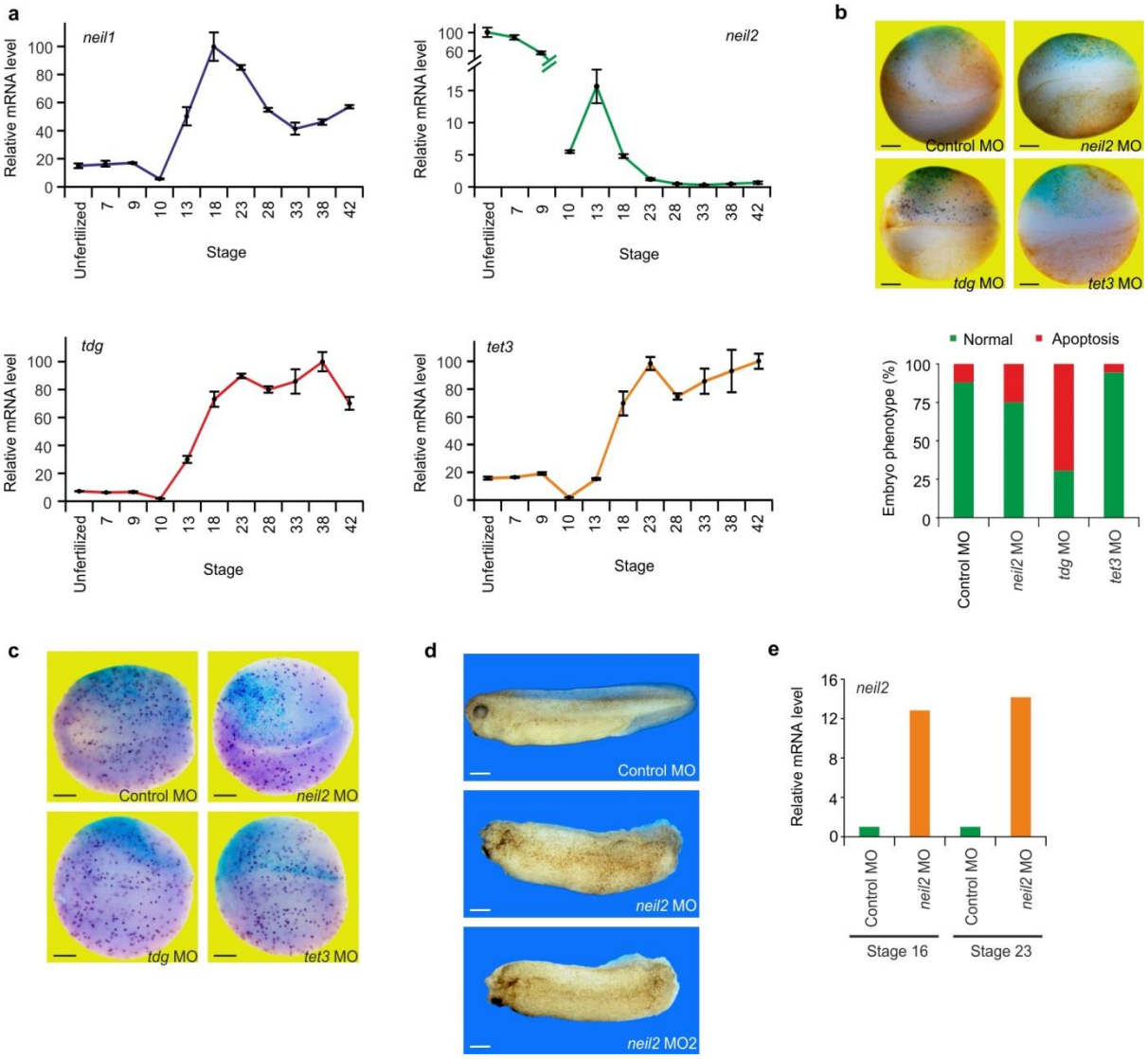

Supplementary Figure 6: Characterization of neil1, neil2, tdg and tet3 in X. laevis embryogenesis.

(a) qPCR expression profiles of neil1, neil2, tdg and tet3 during different stages of X. laevis development. Highest expression values per profiled gene were arbitrarily set to 100. Error bars, s.d. (n = 3 embryo batches each consisting of at least 5 embryos). (b) TUNEL (apoptosis) assay of unilaterally morpholino injected embryos (lineage traced by lacZ, light blue speckles) and quantification of TUNEL signal (dark blue speckles; n = 25, 32, 36, 36 embryos from left to right). Note that only tdg MO induces substantive apoptosis. (c) Phospho-histone H3 (cell proliferation) assay of unilaterally morpholino injected embryos as in (b). Note: No obvious differences in proliferation were detected (n >30 embryos each). (d) Phenotype of stage 34 embryos resulting from neil2 MO and neil2 MO2 injections. Note: Both morpholinos induced the same phenotype. (e), Relative expression levels of neil2 (normalized to h4) in control MO and neil2 MO injected embryos at stage 16 and stage 23. Scale bars, 200 µm.

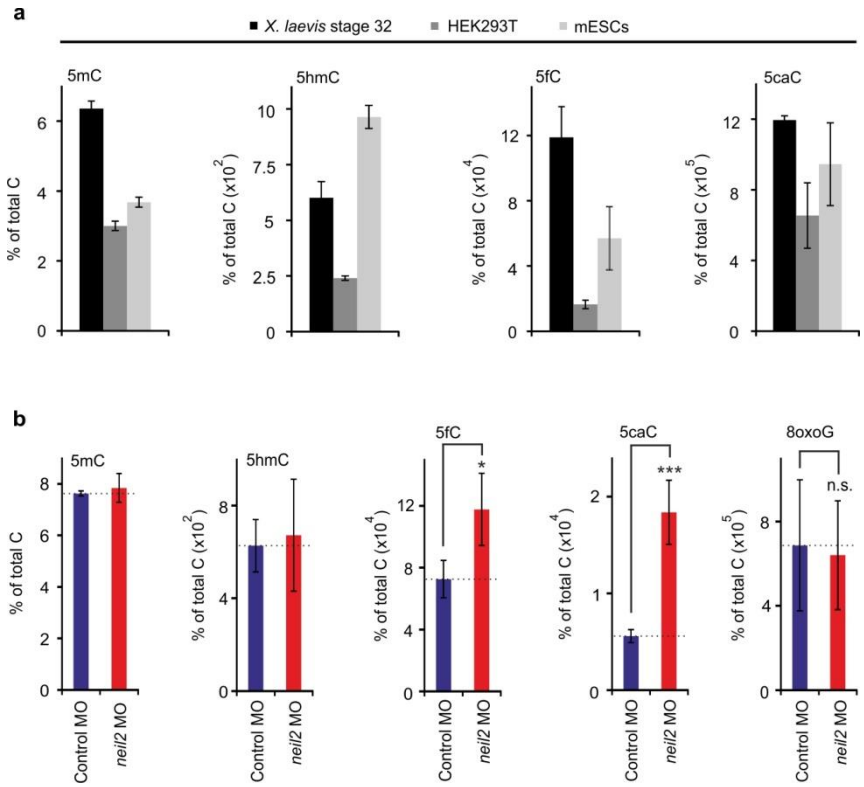

Supplementary Figure 7: Relative abundance of X. laevis genomic DNA modifications.

(a) Quantification of total genomic 5mC, 5hmC, 5fC and 5caC levels in X. laevis whole embryos at stage 32, human HEK293T cells and mouse ES cells (mESCs) by LC-MS/MS. Error bars, s.d. (n = 3 X. laevis embryo batches consisting each of at least 5 embryos and 3 cell cultures of HEK293T and mESCs, respectively). (b) LC-MS/MS quantification as in (a) but in control and neil2 morphant Xenopus animal cap explants including measurements of 8oxoG. Error bars, s.d. (n = 3 explant batches each consisting of 20 animal cap explants). n.s., not significant. *P < 0.05, ***P < 0.005 by two-tailed unpaired Student's t-test.

Online Methods References

57. Hashimoto, H. et al. Structure of a Naegleria Tet-like dioxygenase in complex with 5-methylcytosine DNA. *Nature* **506**, 391-5 (2014).
58. Onizuka, K., Yeo, J., David, S.S. & Beal, P.A. NEIL1 binding to DNA containing 2'-fluorothymidine glycol stereoisomers and the effect of editing. *Chembiochem* **13**, 1338-48 (2012).
59. Gawantka, V., Delius, H., Hirschfeld, K., Blumenstock, C. & Niehrs, C. Antagonizing the Spemann organizer: role of the homeobox gene Xvent-1. *EMBO J* **14**, 6268-79 (1995).
60. Villanueva, S., Glavic, A., Ruiz, P. & Mayor, R. Posteriorization by FGF, Wnt, and retinoic acid is required for neural crest induction. *Dev Biol* **241**, 289-301 (2002).
61. Bradley, L., Wainstock, D. & Sive, H. Positive and negative signals modulate formation of the Xenopus cement gland. *Development* **122**, 2739-50 (1996).
62. Sive, H.L., Grainiger, R.M. & Harland, R.M. Early Development of Xenopus laevis: A Laboratory Manual. *Cold Spring Harbor Laboratory Press, New York* (2000).
63. Saka, Y. & Smith, J.C. Spatial and temporal patterns of cell division during early Xenopus embryogenesis. *Dev Biol* **229**, 307-18 (2001).

64. Hensey, C. & Gautier, J. Programmed cell death during Xenopus development: a spatio-temporal analysis. *Dev Biol* **203**, 36-48 (1998).
65. Kellner, S. et al. Absolute and relative quantification of RNA modifications via biosynthetic isotopomers. *Nucleic Acids Res* **42**, e142 (2015).
66. Ravanat, J.L. et al. Cellular background level of 8-oxo-7,8-dihydro-2'-deoxyguanosine: an isotope based method to evaluate artefactual oxidation of DNA during its extraction and subsequent work-up. *Carcinogenesis* **23**, 1911-8 (2002).

4.2 Chapter 2. Neil DNA glycosylase deficiency elicits neural crest defects mimicking Treacher-Collins-Syndrome

4.2.1 Introduction

In Chapter 1, I discovered that Neil2 deficiency induces NCC defects and microcephaly in *Xenopus* embryos. This raises the question of the underlying mechanism. So in Chapter 2, I aimed to answer this question.

During early *Xenopus* embryogenesis, fertilized embryos undergo rapid cell divisions in the absence of cell growth and gap phases. It is hypothesized that embryos developing in external environments without parental protection have evolved a fast cell cycle to ensure they hatch as quickly as possible in adaptation to a dangerous environment [237, 238]. Amongst other specializations, inactivation of the cellular surveillance system, i.e. DNA damage checkpoints, facilitates rapid cell division. Only after the mid-blastula transition (MBT), when zygotic genome activation (ZGA) takes place, are DNA damage checkpoints activated [239]. This applies to both Tp53 dependent and independent checkpoints. The Tp53 dependent checkpoints require ZGA to transcriptionally activate the expression of *p21* [155, 156]. Tp53 independent checkpoints require Chk1, which although maternally provided, is only activated after MBT [240, 241]. Coinciding with the activation of DNA damage checkpoints at the onset of MBT, cells gain the ability to undergo apoptosis, which eliminates irreparable damaged cells accumulated before MBT [242–244].

Even if cell cycle arrest, DNA repair and apoptosis cannot be triggered pre-MBT, constituents of the Chk1 checkpoint and apoptotic pathways are already present at this stage, albeit inactivated [240–243, 245]. This maternal provision of DDR enzymes could allow the fastest possible repair of DNA damage accumulated before MBT as it enables DNA repair already to occur while zygotic DNA repair enzymes are still being synthesized.

As shown in Chapter 1, Supplementary Figure 6, *neil2* mRNA was maternally provided. Its expression level decreased drastically after MBT (st8.5), indicating it might be specifically involved in repairing damaged DNA accumulated pre-MBT. Neil2 is a bifunctional DNA glycosylase, which preferentially repairs ROS-generated oxidized cytosine derivatives [35, 246, 247]. Neil2 knockout mouse embryos fail to repair oxidative DNA damage and are susceptible to innate inflammation [44], while Neil2 knockdown *Xenopus* embryos display NCC defects and microcephaly (4.1 Chapter 1, Figures 6A and 6C). Why and how does a

deficiency of the same DNA glycosylase lead to these diverse and tissue specific phenotypes? To address these questions, in the 2nd half of my PhD project, I mainly focused on elucidating the underlying molecular mechanism leading to NCC defects and the microcephaly of Neil2 knockdown *Xenopus* embryos.

4.2.2 Results

4.2.2.1 Neil2 deficiency induces a Tp53-dependent DDR in *Xenopus* embryos

To gain insights into the underlying molecular mechanism leading to NCC defects and microcephaly in *neil2* MO injected *Xenopus* embryos, I performed whole transcriptome analysis of control MO and *neil2* MO injected embryos. Gene ontology (GO) enrichment analysis of upregulated genes in Neil2 knockdown embryos indicated that the top hits are transcriptionally regulated by Tp53 (Figure 4.2.1A). Upregulation of Tp53 target genes was validated via RT-qPCR expression analysis in neural plate explants (Figure 4.2.1B). Among the upregulated Tp53 target genes, *aen* [248, 249] and *eda2r* [250, 251] are involved in inducing cell apoptosis, *ccng1*, *LIF*, and *mdm2* [252, 253] in feedback regulation, *rad51* [254]in DNA repair, *rfc3* [255] in promoting cell cycle progression, *riok3* [256]in innate inflammation response, and *ulk* [257] in cell autophagy. Expression of *tp53* itself was also upregulated. These results indicate a Tp53-dependent DDR in Neil2 knockdown embryos.

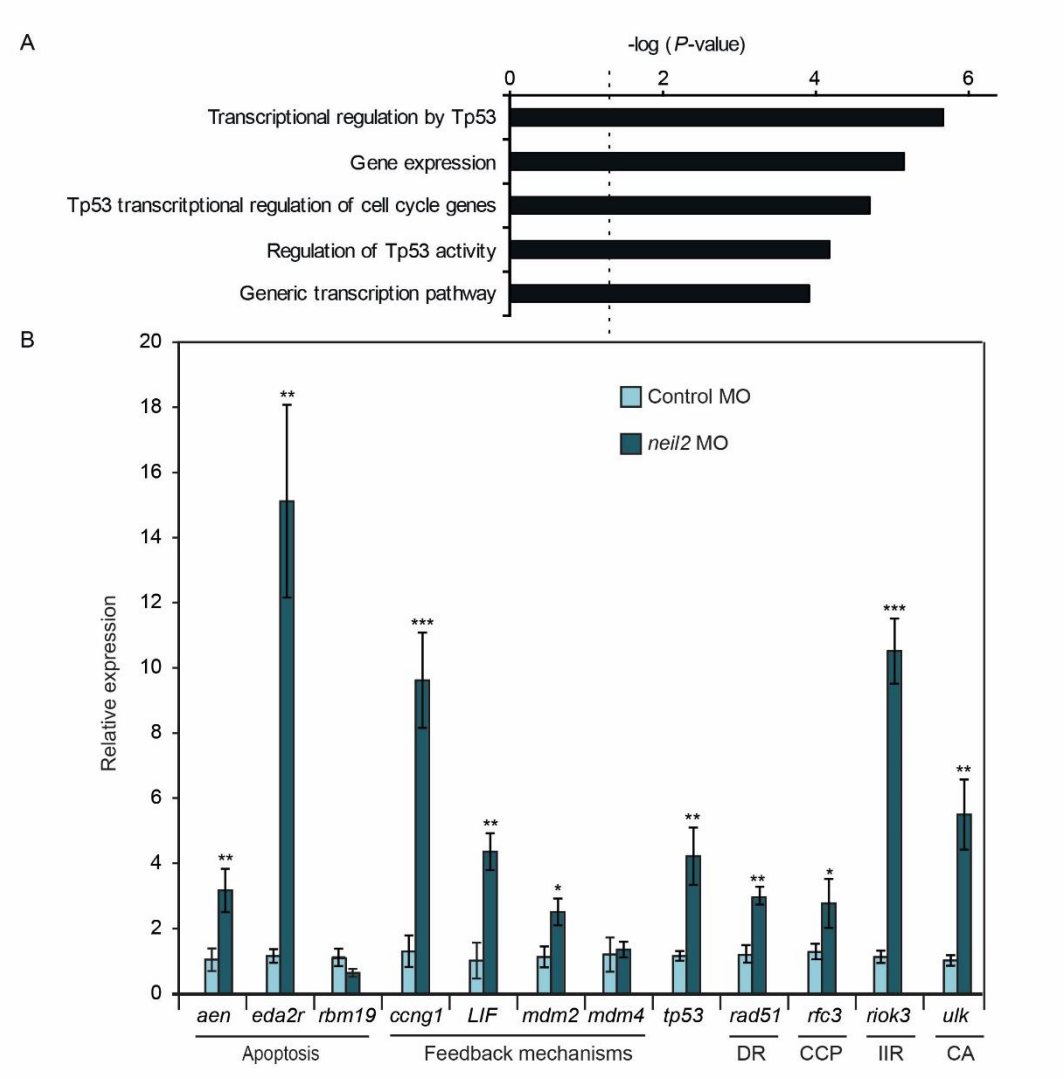

Figure 4.2.1 Induction of Tp53 target genes in Neil2 knockdown *Xenopus* embryos

A. Gene ontology pathway analysis of *neil2* MO upregulated genes at st23. Dashed line indicates the significance threshold p =0.05. **B**. qPCR expression analysis of direct Tp53 target genes in neural plate explants from control and *neil2* MO injected embryos at st14. Expression of target genes was normalized to *h4* expression and is presented as relative mRNA level of control MO injected embryos. (n=3, each 'n' contained ≈10 neural plate explants). DR, DNA repair; CCP, cell cycle progression; IIR, innate inflammation response; CA, cell autophagy. Data presented as mean ± s.d., *p<0.05, **p<0.01, ***p<0.001 (t test).

Both maternally and zygotically, two *neil2* isoforms are expressed in *Xenopus laevis*. In previous experiments, a *neil2* MO targeting both isoforms was employed. To distinguish which isoform is responsible for induction of the Tp53 dependent DDR, and whether there is a difference between the maternal and the zygotic contribution, different MOs were designed: Two MOs targeting each isoform separately were designed to block translation of both maternally and zygotically transcribed *neil2* mRNA (Figure 4.2.2A), as well as a *neil2_splicing* MO to block mRNA splicing of both *neil2* isoforms after the start of ZGA (Figure 4.4.2B). Phenotypically, only injection of *neil2 isoform 1* MO (*neil2X1* MO) induced

microcephaly, while injection of *neil2 isoform 2* MO (*neil2X2* MO), or *neil2_splicing* MO led to no obvious developmental defects (Figure 4.4.2C). Consistent with the microcephaly phenotype observed in *neil2X1* morphants, Tp53 protein levels were only elevated in *neil2X1*, but not in *neil2X2* and *neil2_splicing* morphants (Figure 4.4.2D). In *Xenopus tropicalis*, there is only one isoform of *neil2*. A guide RNA (gRNA) targeting *tropicalis neil2* was designed and co-injected with cas9 mRNA, inducing a reading frame shift in injected embryos. However, those embryos developed normally and there was no upregulation of Tp53 in knockout F0 embryos (Data not shown). This is in line with the results obtained in *Xenopus laevis*, as maternally provided *neil2* in CRISPR injected *Xenopus tropicalis* might be sufficient to prevent the phenotype from occurring. To eliminate maternally provided *neil2* mRNA, *neil2* knockout F1 would have to be generated. Thus, the results indicated that zygotic *neil2* has little to no contribution to the microcephaly phenotype, and that in *Xenopus laevis*, only maternal *neil2X1* is responsible for it.

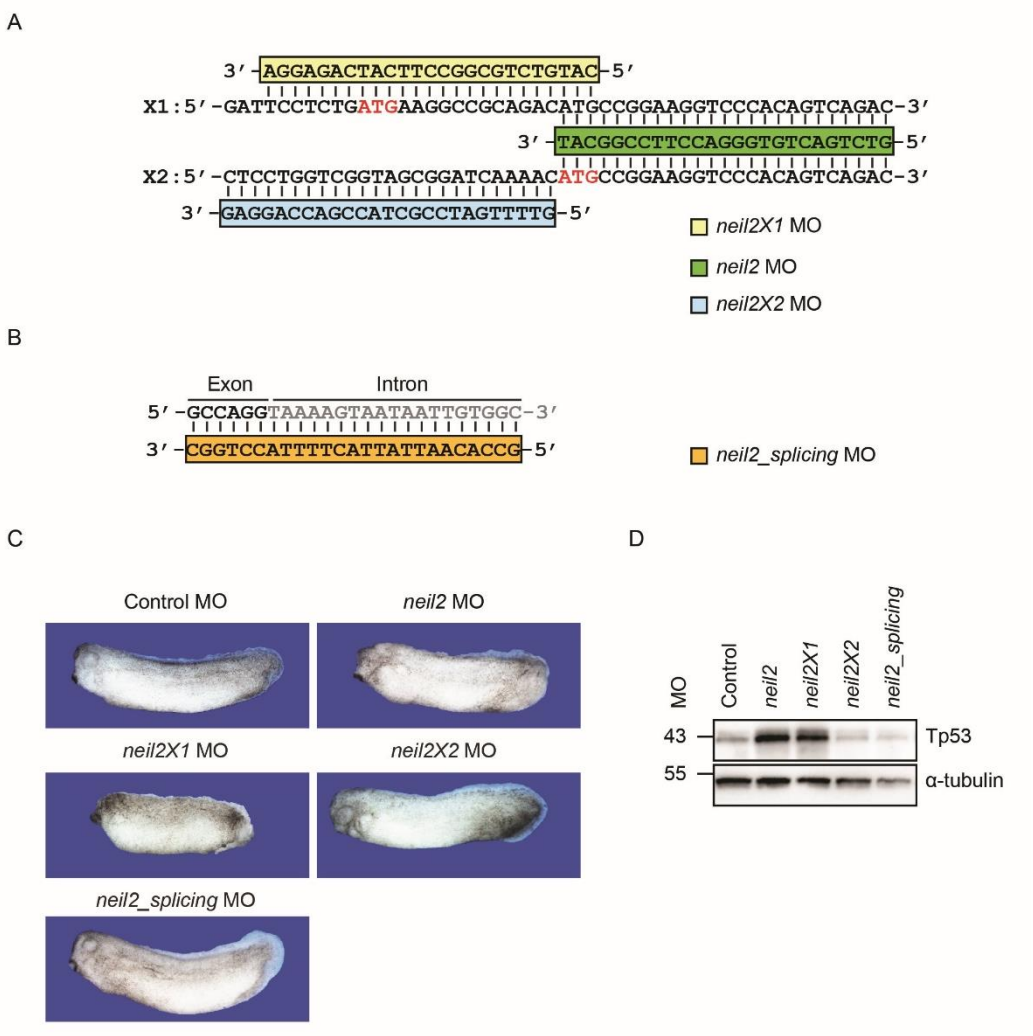

Figure 4.2.2 Accumulation of Tp53 in Neil2X1 knockdown *Xenopus* embryos

A. Illustration of antisense MO oligomers targeting *neil2 isoform 1* (*neil2X1*), *neil2 isoform 2* (*neil2X2*), and the consensus sequence of both isoforms (*neil2*). These MOs block translation of targeted transcripts, both maternally and zygotically transcribed. *neil2X1* MO, yellow; *neil2X2* MO, light blue; and *neil2* MO, green. ATG is labeled in red to indicate the start codon for both isoforms. **B**. Illustration of the antisense MO oligomer targeting an exon-intron boundary of both isoforms and thus blocking zygotic mRNA splicing. The intron is indicated in grey. **C**. Representative embryo malformations in MO injected embryos at st32. D. Representative Western Blot of Tp53 protein levels in indicated MO injected *Xenopus* embryos at st23. α-tubulin used as loading control. Reproduced in 4 independent experiments.

I showed that Neil2 is required for NCC development in *Xenopus laevis* (Chapter 1, Figure 6). During *Xenopus laevis* embryonic development, NCC differentiation initiates at the neural plate border at the end of gastrulation, around st12.5 [50]. Expression of *tp53* was mainly restricted to the neural plate (Figure 4.2.3A), also upon knockdown of Neil2 (data not shown). One Tp53 target gene, *ccng1*, was highly upregulated specifically in the neural plate after *neil2* MO injection even though the injection was performed in the entire half of the embryo, as indicated by the light blue lineage tracer lacZ (Figure 4.2.3B). The spatial expression pattern of *tp53* and upregulation of Tp53 target gene *ccng1* in the neural plate indicated that activation of Tp53 and its target genes might play a role during NCC differentiation, and that their increased expression and activation upon *neil2* MO injection might in turn perturb NCC differentiation.

To better understand the molecular mechanism leading to NCC differentiation defects in Neil2 deficient embryos, I analyzed pS345 Chk1 and Tp53 protein levels in neural plates of control and *neil2* MO injected embryos during early NCC differentiation. Chk1 gets phosphorylated on S345 in response to genotoxic stress. Subsequently, pS345 Chk1 activates DNA damage checkpoints to ensure that cells have adequate time to repair the lesions [258–261]. In Neil2 deficient neural plates, pS345 Chk1 was strongly upregulated transiently at st14, while at st15, pS345 Chk1 levels were again indistinguishable between control and Neil2 morphants (Figure 4.2.3C). The difference in Tp53 levels between Neil2 deficient neural plates and control MO injected neural plates started to become observable at late st14, and further increased at st15 (Figure 4.2.3C). Levels of Tp53 in Neil2 deficient embryos increased as embryos developed, to the point that it was even detectable in protein lysates prepared from whole embryos at st23 (Figure 4.2.2D).

The results suggest that in Neil2 deficient embryos, during early NCC differentiation, cells in neural plates transiently activated DNA damage checkpoints to repair damaged DNA that was accumulated due to the lack of repair enzyme Neil2.

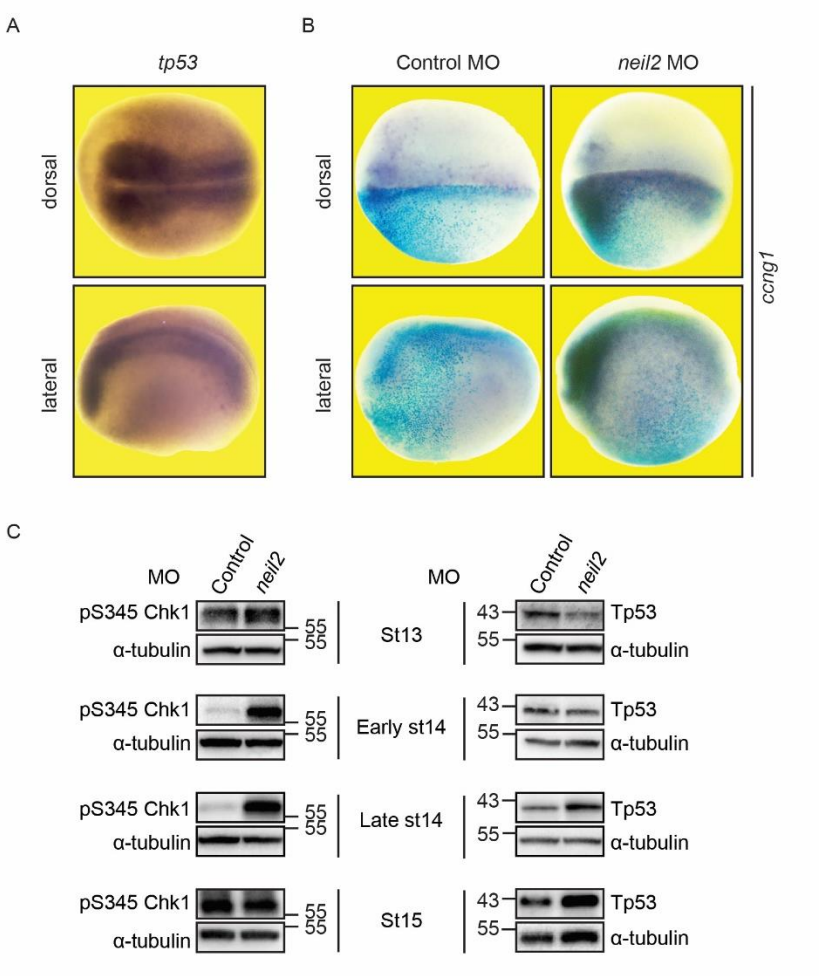

Figure 4.2.3 Accumulation of pS345 Chk1 and Tp53 in Neil2 deficient neural plates

A. Expression of *tp53* shown by *in situ* hybridization at st16 in dorsal and lateral view. Anterior to the left. **B**. Expression of *ccng1* shown by *in situ* hybridization in control and *neil2* MO unilaterally injected embryos. 250pg/embryo X-gal mRNA was co-injected with MO as lineage tracer (visible as light blue speckles). Anterior to the left. **C**. Representative Western Blot of pS345 Chk1 and Tp53 protein levels in neural plate explants from control and *neil2* MO injected embryos during early NCC differentiation. α-tubulin was used as loading control. Reproducible from 4 independent experiments.

The rather transient activation of DNA damage checkpoints in Neil2 deficient neural plates might also explain why there was no obvious delay of cell proliferation in *neil2* MO injected embryos (Chapter 1, Supplementary Figure 6C). Western blot analysis of phosphorylated histone H3, which is a cell proliferation marker, in Neil2 deficient neural plates also showed no difference compared to neural plates dissected from control MO injected embryos (data not shown). Elevation of Tp53 protein levels in Neil2 deficient neural plates indicated that cell apoptosis might take place in those cells. However, I only observed a small amount of apoptotic cells in Neil2 deficient embryos through TUNEL staining (Chapter 1, Supplementary Figure 6B). To detect ongoing cell apoptosis using another method, I performed Western Blot analysis of caspase-3 in Neil2 deficient neural plates (Figure 4.2.4).

The active form of caspase-3, cleaved caspase-3 was strongly induced in Neil2 deficient neural plates, and this induction was rescued by co-injection of human *NEIL2* mRNA. Notably, ectopic expression of human *NEIL2* mRNA in control MO injected neural plates also reduced cleaved caspase-3, indicating that NEIL2 protected cells from undergoing apoptosis, which might be a result of an improved removal of oxidative DNA damage accumulated before MBT.

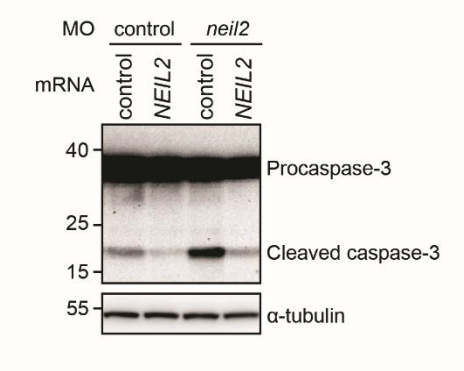

Figure 4.2.4 Activation of cell apoptosis in Neil2 deficient neural plates

Western Blot of caspase-3 levels in neural plate explants from control and *neil2* MO injected embryos. Human *NEIL2* co-injected for rescue. α-tubulin used as loading control. n=1.

4.2.2.2 High Tp53 levels impair cranial NCC differentiation in *Xenopus*

All results pointed to the direction that increased Tp53 levels in Neil2 deficient embryos were the cause of NCC differentiation defects, which eventually led to a microcephaly phenotype. To further confirm this, I overexpressed *tp53* mRNA in *Xenopus* embryos. As shown in Figure 4.2.5, the NCC marker *slug* was equally expressed on both sides in control mRNA injected embryos, while in *tp53* mRNA injected embryos, expression of *slug* decreased on the injected side, indicated in light blue. Additionally, embryos injected with *tp53* mRNA developed microcephaly presumably due to the failure in NCC differentiation (Figure 4.2.5B).

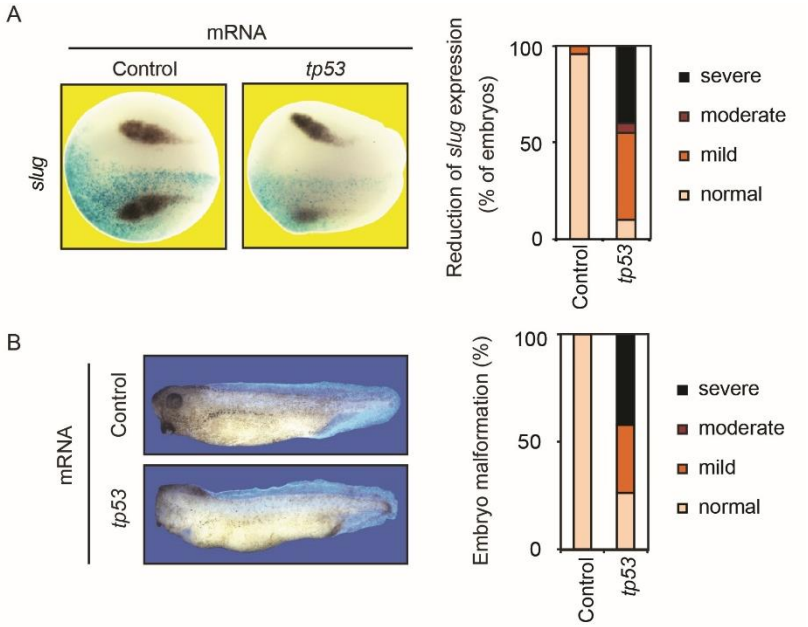

Figure 4.2.5 Ectopic expression of *tp53* induces NCC defects and microcephaly in *Xenopus*

A. Expression of *slug* shown by *in situ* hybridization in control and *tp53* mRNA injected embryos. 250pg/embryo X-gal mRNA was co-injected with control (bovine preprolactin) and *tp53* mRNA as a lineage tracer (visible as light blue speckles). Dorsal view, and anterior to the left. Quantification of reduction of *slug* expression was obtained from ≥20 embryos/ group. **B**. Embryo morphology in control and *tp53* mRNA injected embryos. Quantification of embryo malformation was obtained from ≥19 embryos/group.

To confirm if elevated Tp53 was the cause of microcephaly in Neil2 morphants, Tp53 was knocked down in Neil2 morphants through co-injection of *tp53* MO and *neil2* MO. Increased expression of Tp53 target genes *aen*, *ccng1*, *eda2r*, and *riok3* in Neil2 morphants was rescued to control levels (Figure 4.2.6A).

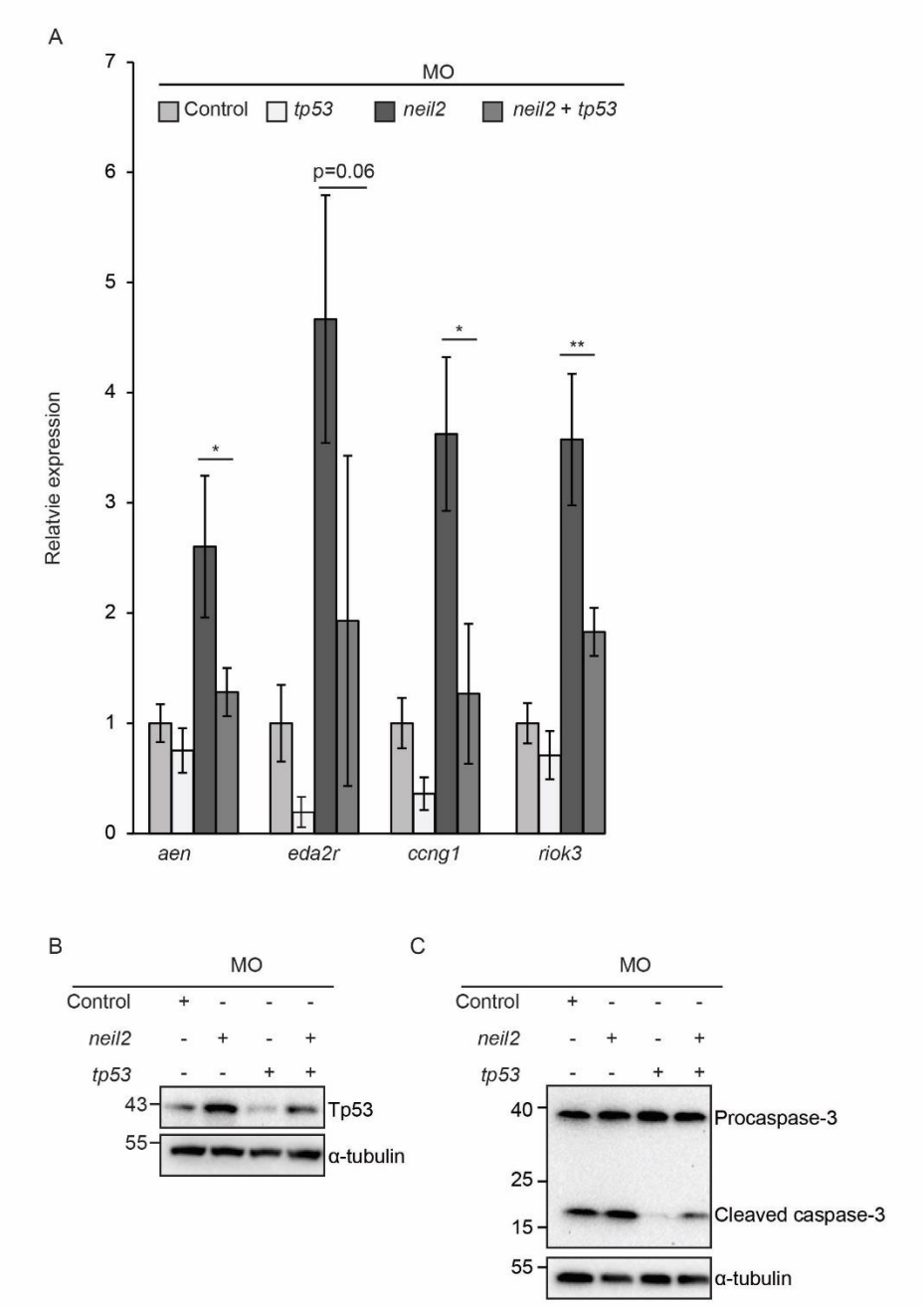

Figure 4.2.6 Knockdown of Tp53 protects Neil2 deficient embryos from undergoing cell apoptosis

A. qPCR expression analysis of direct Tp53 target genes in control MO, *tp53* MO, *neil2* MO single-injected, and *neil2* MO and *tp53* MO co-injected embryos. Error bars obtained from biological triplicates, each batch contained 6 embryos. **B**. Western Blot analysis of Tp53 protein levels in neural plates dissected from control MO, *tp53* MO, *neil2* MO single-injected, or *neil2* MO and *tp53* MO co-injected embryos. **C**. Western Blot analysis of caspase-3 protein levels in neural plates dissected from control MO, *tp53* MO, *neil2* MO single-injected, or *neil2* MO and *tp53* MO co-injected embryos. α-tubulin was used as loading control. n=1.

Western Blot analysis showed that Tp53 protein levels were strongly decreased in *tp53* MO injected embryos. In addition, *tp53* MO was able to reduce accumulation of Tp53 protein in Neil2 deficient neural plates (Figure 4.2.6B). Consistent with Tp53 protein levels, active

caspase-3 protein levels were drastically decreased in *tp53* MO injected embryos, and Tp53 MO was also able to rescue induction of active caspase-3 protein in Neil2 deficient neural plates (Figure 4.2.6C). A reduction of this cell apoptosis marker in *neil2* MO and *tp53* MO co-injected embryos raised the possibility that *tp53* MO might rescue the microcephaly phenotype induced by a knockdown of Neil2.

Injection of *tp53* MO indeed partially rescued the microcephaly phenotype of Neil2 deficient embryos. Notably, *tp53* MO itself also induced a moderate microcephaly phenotype, which was consistent with previous observations from other studies [225] (Figure 4.2.7).

Taken together, the results show that increased Tp53 protein levels in Neil2 deficient embryos triggered cell apoptosis in neural plates. Reducing Tp53 levels inhibited cell apoptosis and partially rescued the microcephaly phenotype caused by Neil2 deficiency.

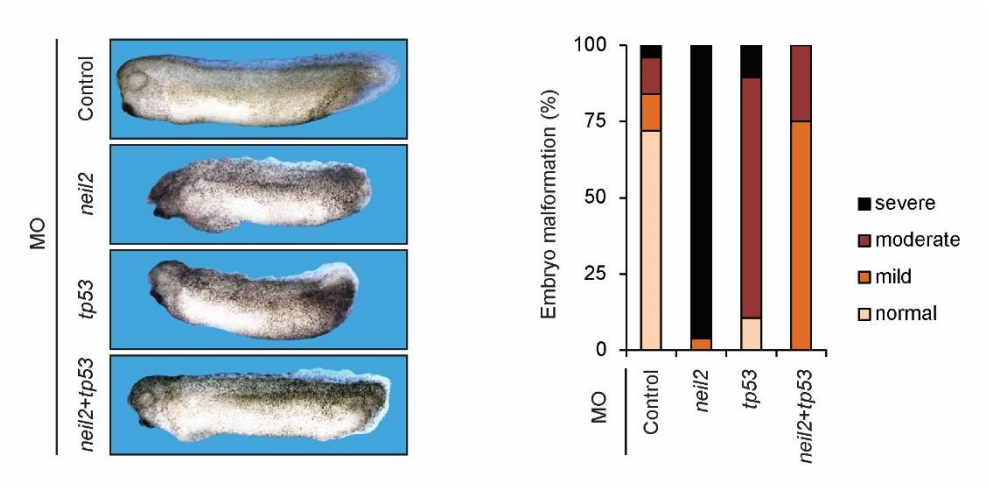

Figure 4.2.7 Knockdown of Tp53 rescues the microcephaly phenotype of Neil2 deficient embryos

Embryo morphology in control MO, *tp53* MO, *neil2* MO single-injected, or *neil2* MO and *tp53* MO co-injected embryos. Quantification of embryo malformation was obtained from ≥19 embryos/ group.

4.2.2.3 ROS inducer pyocyanin phenocopies cranial NCC defects and microcephaly phenotypes of Neil2 morphants

As mentioned above, the Tp53-induced DDR in Neil2 deficient embryos was probably triggered by a failure to efficiently remove oxidative DNA lesions accumulated before MBT. This raised the question: Could excessive amounts of oxidative DNA lesions introduced to *Xenopus* embryos via chemical treatment phenocopy the cranial NCC defects and microcephaly phenotypes of Neil2 morphants? The ROS inducer pyocyanin is a redox active toxin produced by *Pseudomonas aeruginosa*. Pyocyanin generates ROS and thereby induces

oxidative stress in cells [262, 263]. Hence, embryos were treated with pyocyanin to increase the amount of oxidative DNA lesions in cells. At st14, which is the crucial stage for NCC differentiation, expression of *tp53* and Tp53 target genes *aen, eda2r, ccng1, riok3,* and *ulk* was upregulated in pyocyanin treated embryos (Figure 4.2.8A). Elevated expression of the Tp53 target gene *ccng1* was mainly restricted to neural plates (Figure 4.2.8B) from pyocyanin treated embryos and resembled the *ccng1* expression pattern in Neil2 deficient embryos (Figure 4.2.3B).

In addition, pS345 Chk1 levels were strongly increased in pyocyanin treated embryos, while they were barely detectable in DMSO treated embryos (Figure 4.2.8C). For Tp53, not only the total levels were upregulated, but also a small shifted band appeared in pyocyanin treated embryos, indicating that some Tp53 was modified post-translationally (Figure 4.2.8C).

On a molecular level, pyocyanin treatment mimicked what was observed in Neil2 deficient embryos. This posed the question whether pyocyanin treated embryos would also develop cranial NCC defects and microcephaly.

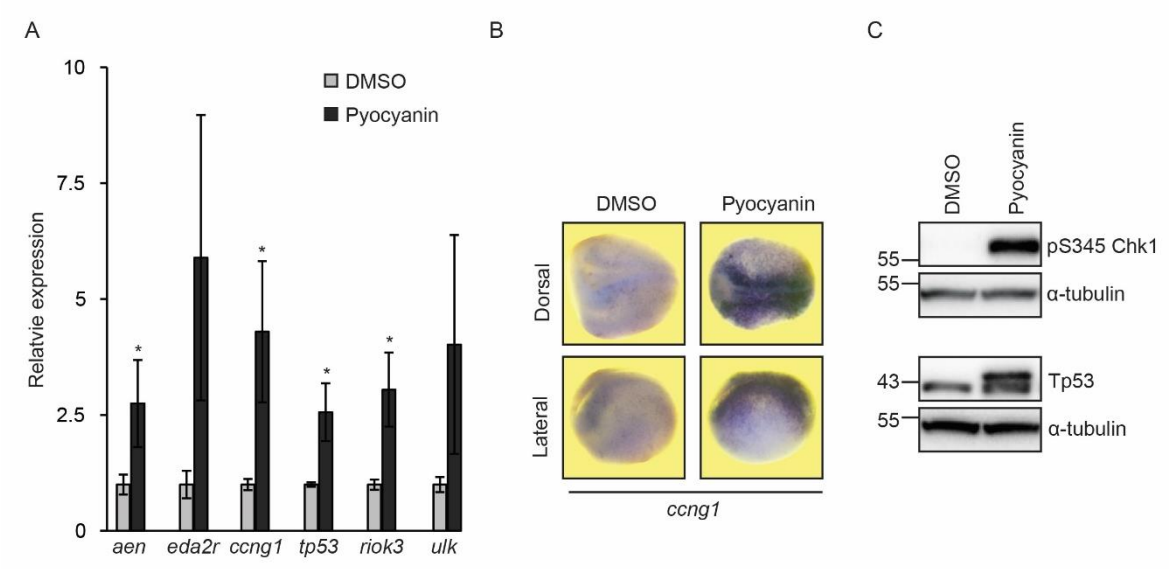

Figure 4.2.8 Treatment with ROS inducer pyocyanin induces a Tp53 DDR in *Xenopus* embryos

A. qPCR expression analysis of *tp53* and Tp53 target genes in pyocyanin treated embryos. Relative expression normalized to histone *h4*. Error bars obtained from biological triplicates, each batch contained 6 embryos. * $p<0.05$ (t test). **B**. Expression pattern analysis of Tp53 target gene *ccng1* in pyocyanin treated embryos via *in situ* hybridization. Head to the left. **C**. Western blot analysis of pS345 Chk1 and Tp53 protein levels in pyocyanin treated embryos. α-tubulin was used as a loading control.

To analyze whether pyocyanin treatment leads to cranial NCC defects, I performed *in situ* hybridizations using NCC markers *slug*, *sox10*, and *twist;* brain markers *en2* and *krox20*; and eye marker *rx1* in both DMSO and pyocyanin treated embryos at st16. Expression of all NCC

markers and especially *sox10* and *twist* was decreased in pyocyanin treated embryos, and in severe cases, their expression was barely detectable. While pyocyanin treatment also decreased expression of the hindbrain marker *krox20*, it had no effect on expression of *en2* or *rx1*, highlighting that pyocyanin did not disrupt embryogenesis in general, but elicited tissue specific effects (Figure 4.2.9A). Later in embryonic development, pyocyanin treated embryos developed microcephaly phenotypes similar to those observed in Neil2 deficient embryos (Figure 4.2.9B, Figure 4.2.7). Notably, only embryos treated with low doses of pyocyanin showed NCC specific defects, while higher doses of pyocyanin treatment abolished development of the entire head, which resembled the phenotype observed after a high dose of *neil2* MO injection (data not shown).

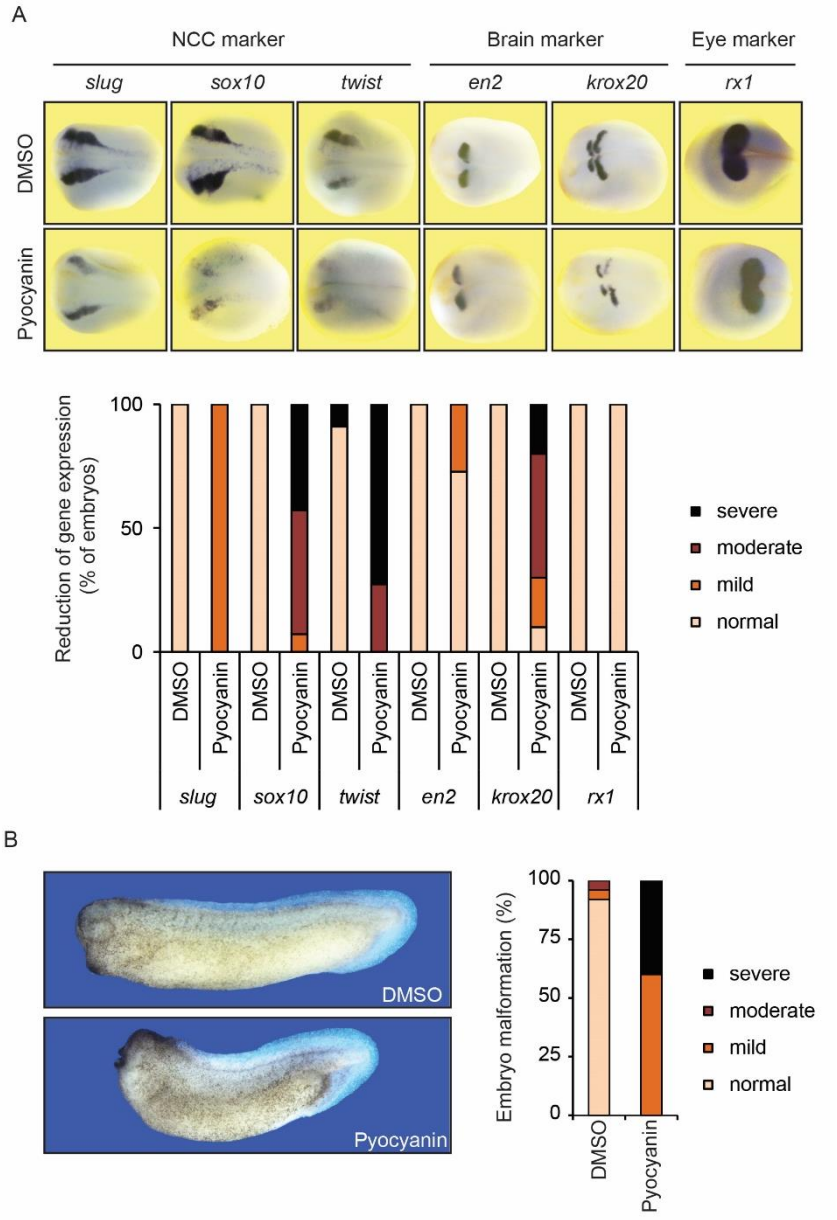

Figure 4.2.9 Pyocyanin treatment induces cranial NCC defects and microcephaly phenotypes

A. Expression pattern analysis by *in situ* hybridization in either DMSO or pyocyanin treated embryos at st16. NCC markers: *slug, sox10, twist*. Brain markers: *en2, krox20*. Eye marker: *rx1*. For quantification, n≥10 for each batch, except for pyocyanin treated embryos probed with *slug*, where n=7. Dorsal view and anterior to the left, except for *rx1*, which shows front views, with ventral parts of embryos to the left. **B**. Embryo morphology of DMSO and pyocyanin treated embryos. Quantification was obtained from≥15 embryos/ batch.

Accumulation of oxidative DNA lesions can be achieved by either increasing their cause (ROS inducer), or by decreasing their removal (knockdown of DNA glycosylase). To further validate whether the microcephaly phenotypes observed in Neil2 morphants were caused by accumulated oxidative DNA damage, embryos were injected with subthreshold doses of *neil2* MO (decreasing lesion removal) and further treated with a subthreshold dose of pyocyanin (increasing lesion formation). Although some control MO injected embryos developed microcephaly phenotypes when treated with subthreshold doses of pyocyanin, *neil2* MO injected embryos developed a more severe malformation of the head when treated with subthreshold dose of pyocyanin, demonstrating a synergistic effect of *neil2* MO and pyocyanin in inducing microcephaly phenotypes in *Xenopus* embryos (Figure 4.2.10).

Increasing oxidative stress by treating embryos with ROS inducer pyocyanin mimicked the Tp53 DDR in Neil2 deficient embryos, which led to NCC defects and microcephaly phenotypes. Further, the synergistic effect of *neil2* MO and pyocyanin treatment in inducing microcephaly phenotypes in *Xenopus* embryos indicated that accumulation of oxidative DNA lesions was possibly the cause of the Tp53 DDR in Neil2 morphants.

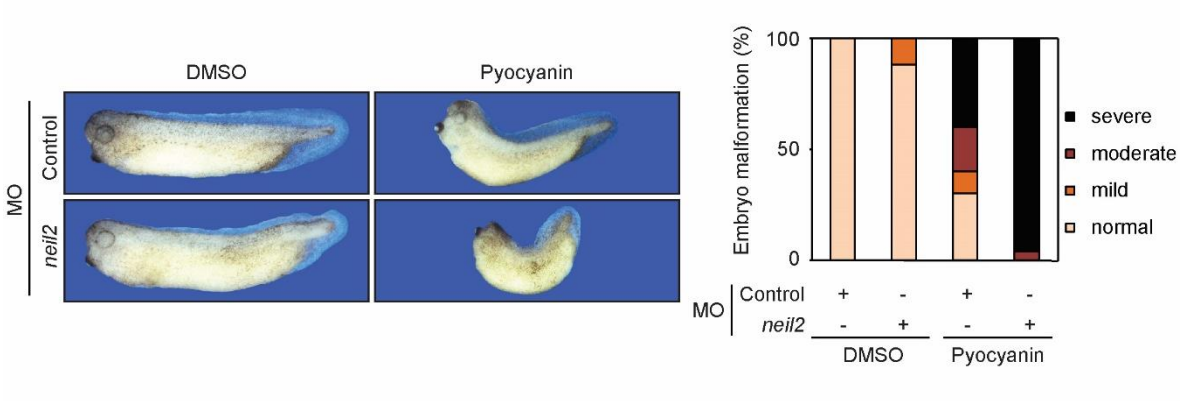

Figure 4.2.10 Synergistic effect of *neil2* MO and pyocyanin treatment in inducing microcephaly phenotypes

Embryo morphology and quantification of embryos injected with subthreshold doses of MO and pyocyanin treated embryos. Quantification was obtained from⩾10 embryos/ batch.

4.2.2.4 Neil2 deficiency induces craniofacial abnormalities mimicking Treacher-Collins-Syndrome

Craniofacial cartilages are derived from cranial NCCs. A failure of NCC differentiation leads to malformation of craniofacial cartilages, resulting in various syndromes including TCS. Upon *Tcof1* knockdown, mouse embryos develop a TCS-like phenotype with hypoplastic craniofacial cartilages. The size of all structures illustrated in Figure 4.2.11A is reduced in Tcof1 deficient embryos, leading to a deformation of craniofacial cartilage [264].

Embryos injected with 40ng *neil2* MO developed NCC defects, but died prior to cranial cartilage differentiation. Therefore, a reduced dose of *neil2* MO (20ng) was injected to allow cultivation to st45, when cartilage staining could be performed. Lower doses of *neil2* MO induced hypoplasia of craniofacial cartilages. Although all craniofacial elements were present, their size was reduced. The cavities in the BR were not as visible as they were in control morphants. Moreover, Neil2 deficient embryos developed severe edema. All abnormalities in *neil2* MO injected embryos were rescued by overexpression of human *NEIL2* mRNA, validating the specificity of *neil2* MO (Figure 4.2.11B).

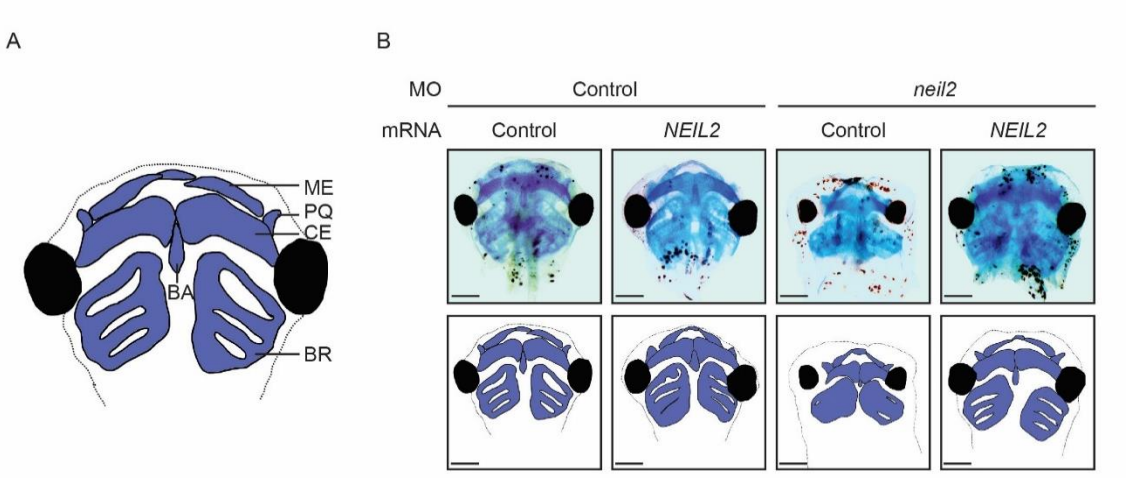

Figure 4.2.11 Neil2 deficiency induces craniofacial cartilage abnormalities

A. Illustration of craniofacial cartilage: Meckel's cartilage (ME), palatoquadrate cartilage (PQ), ceratohyal cartilage (CE), branchial cartilage (BR), basihyal cartilage (BA). **B**. Cartilage staining of control MO and *neil2* MO injected embryos at st45. Control mRNA or human *NEIL2* was co-injected to rescue the cartilage malformation. MO, 20ng/embryo; mRNA, 2ng/embryo. Illustrations on the lower panels were drawn based on the staining from corresponding upper panels. Dashed lines indicate outlines of heads. Scale bar=500µm.

4.2.3 Discussion

TCS is a congenital craniofacial disorder, which affects newborns with an incidence of 1/50,000 [76]. Patients are diagnosed with a series of anomalies in facial structures. Mutations in three genes (TCOF1, POLR1C, and POLR1D) have been shown to be functionally related to the pathology of TCS. During mouse embryonic development, *Tcof1* is strongly and dynamically expressed in neuroepithelium and NCCs [87], while *Polr1c* and *Polr1d* are expressed in the eyes and the central nervous system [81]. All three genes are functionally involved in ribosome biogenesis [77, 78]. Deficiency of Tcof1, Polr1c, or Polr1d disrupts proper ribosome biogenesis, induces nucleolar instability, triggers a Tp53 dependent DDR, and eventually causes NCC defects, leading to the craniofacial anomalies seen in TCS [74].

In addition to its function in ribosome biogenesis, Tcof1 also protects the neuroepithelium from undergoing apoptosis induced by high levels of ROS. Tcof1 deficiency leads to accumulation of DNA damage and cell apoptosis in the neuroepithelium. Antioxidant treatment of Tcof1 deficient embryos reduces cell apoptosis and rescues craniofacial anomalies, indicating that Tcof1 plays important roles in protecting neuroepithelial cells from oxidative stress induced DNA damage. However, antioxidants are not capable of rescuing the disruption in ribosome biogenesis. It is unclear whether there is a causative correlation between ribosome biogenesis and oxidative DNA damage repair in Tcof1 mutants. However, both processes converge on the activation of Tp53 induced cell apoptosis. Inhibition of Tp53 rescues cell apoptosis and craniofacial anomalies in Tcof1 deficient embryos, but it also cannot restore ribosome biogenesis [92, 224].

ROS have long been considered deleterious by-products of cell metabolism, but recent studies indicated that they also regulate signaling pathways involved in cell proliferation, regeneration, immune response, and cell death [265–267]. Thus, keeping a certain amount of ROS around is important. However, ROS levels have to be precisely regulated to avoid cell damage. Both too high and too low levels of ROS induce developmental defects during embryonic development [224]. ROS levels are generally high in the neuroepithelium, so increasing them further makes the neuroepithelium particularly susceptible to defects.

In *Xenopus* embryos, ROS levels increase immediately after fertilization to stimulate cell proliferation before MBT [268]. At the same time, ROS production might cause oxidative DNA damage to the genome. Given that DNA damage checkpoints are inactivated before MBT, it is puzzling how embryos cope with DNA lesions accumulated before MBT. One

hypothesis is that embryos initiate cell apoptosis at the onset of MBT to remove cells with high amounts of irreparable DNA lesions. My results provided another possible explanation, namely that embryos are equipped with maternally supplied DNA repair enzymes, such as Neil2, which initiate DNA repair once the DNA damage checkpoints are activated. Two types of MOs are frequently employed to study gene function during *Xenopus* early embryonic development: translation blocking MO and pre-mRNA splicing modifying MO. Application of these two types of *neil2* MOs clarified that only knockdown of maternally provided Neil2 triggered the Tp53 dependent DDR and induced microcephaly. Injection of pre-mRNA splice modifying *neil2* MO that inhibited *neil2* mRNA maturation after ZGA did not cause any Tp53 accumulation or embryonic malformation.

During *Xenopus* embryonic development, maternally provided mRNAs are destabilized right after MBT, coinciding with ZGA when corresponding zygotic transcripts take over. The expression pattern of Neil2 under physiological conditions – strongly maternally provided, and then rapidly decreased upon ZGA – fits the hypothesis of Neil2 in protecting genomic stability from ROS-induced oxidative DNA lesions accumulated before MBT.

Oxidative DNA lesions accumulate in transcribed regions of the genome in Neil2 deficient mice. However, those mouse embryos do not show any obvious phenotype[44], and this contrasts with microcephaly phenotypes observed in Neil2 morphants in *Xenopus*. It is puzzling where the difference between mice and frogs comes from. Compared to *Xenopus* embryos, mouse embryos develop inside the womb where they are exposed to much lower levels of oxygen. Given that ROS production is highly correlated with environmental oxygen levels, Neil2 deficient mouse embryos developing *in vivo* are less threatened by ROS-induced oxidative DNA lesions. In fact, when cultured *in vitro*, where oxygen levels are much higher, Neil2 deficient mouse ESCs failed to differentiate into NCCs (unpublished data from Lars Schomacher). Thus, it would be interesting to re-analyze the phenotype of Neil2 deficient mice under high ROS conditions, which could be achieved by e.g. feeding mice with a high fat diet [43].

Another difference between *Xenopus* and mouse early embryonic development is that during evolution, mouse embryonic development has abandoned rapid cell cleavages in the absence of genomic surveillance. ZGA takes place as early as 2-cell stage in mouse embryogenesis, while in *Xenopus*, ZGA is initiated after 12 cell divisions [269, 270], which suggests that maternally provided Neil2, which protects *Xenopus* embryos from early oxidative lesions, has probably lost its role in mammalian embryonic development. In *Xenopus tropicalis*, CRISPR

knockout Neil2 F0 developed normally. If CRISPR knockout Neil2 F0 would be grown to adulthood, they might be susceptible to innate inflammation, recapitulating phenotypes in Neil2 knockout mice [44].

Why are predominantly NCCs affected in Neil2 deficient embryos? In other words, why are NCCs so sensitive to the Tp53 dependent DDR induced by Neil2 deficiency? By using *Xenopus* as a model system, I hypothesized that both timing and location of a Tp53-dependent DDR are essential for the induction of NCC defects. Neil2 morphants attempted to arrest cell cycle to repair the DNA lesions, as shown by the transient induction of pS345 Chk1 (Figure 4.2.3C). However, the amount of DNA lesions in Neil2 deficient embryos seemed to exceed the threshold that other repair factors could repair. Therefore, damaged cells were destined for apoptosis, evidenced by Western Blot analysis of cleaved caspase-3. Temporally, all those events occurred when NCC differentiation was taking place. Spatially, the final consequence of Tp53 dependent DDR, cell apoptosis, took place in the neural plate from which NCC originate. In conclusion, cell apoptosis eliminated NCC progenitors in Neil2 deficient embryos, which eventually led to microcephaly and defects in craniofacial structures.

Why does DDR induced cell apoptosis mainly take place in neural plates? One reason could be that Tp53 target genes and *tp53* itself are mainly expressed in neural plates [225,227–229,271]. Tp53 mediates cell fate decisions via its downstream gene regulatory network. The restricted expression pattern of *tp53* and its target genes sensitizes neural plates to a Tp53 dependent DDR. Notably, *tp53* and most of its target genes are also weakly expressed outside neural plates [227], implying that when DNA damage exceeds a certain threshold, cells outside the neural plates would also be affected by a DDR. Slightly higher doses of *neil2* MO or pyocyanin were lethal to *Xenopus* embryos (data not shown), confirming that cells outside of neural plates were also responsive to DDR, but to a lesser degree. To ensure proper embryogenesis and especially NCC differentiation, ROS production must be controlled within the safe range to reduce unnecessary introduction of oxidative DNA lesions.

Pyocyanin treatment, which induces ROS production [258, 259], mimics Neil2 deficiency. Similar to Neil2 morphants, pyocyanin treated embryos displayed pS345 Chk1 and Tp53 upregulation, increased expression of Tp53 target genes (Figure 4.2.8), a downregulation of NCC markers and microcephaly (Figure 4.2.9). The difference between pyocyanin treatment and *neil2* MO injection is that pyocyanin treatment elevates ROS levels in embryos, which introduces oxidative lesions to all cellular components and causes various types of oxidative DNA lesions [272], while Neil2 deficiency only leads to accumulation of certain types of

DNA lesions (Table 3.1) [25]. Unfortunately, it was technically challenging to measure levels of those DNA lesions in Neil2 deficient embryos. Therefore, the type and amount of DNA lesions in Neil2 deficient vs. pyocyanin treated embryos remains to be determined.

One minor finding was that expression levels of nitric oxide synthase 1 (NOS1) were significantly reduced in *neil2* MO injected embryos, and that they could not be rescued by knockdown of *tp53* (data not shown). Deficiency of Nos1 causes craniofacial defects in *Xenopus* [273], indicating that there might also be a Tp53 independent molecular mechanism involved in regulating NCC differentiation and craniofacial structure formation in Neil2 deficient embryos. This hypothesis is further supported by the fact that knockdown of *tp53* only partially rescued microcephaly in Neil2 deficient embryos. Moreover, NOS1 generates NO, which together with its oxidative product peroxynitrite affects apoptosis [274, 275], indicating there might be NO-induced, Tp53-independent cell apoptosis taking place in Neil2 deficient embryos. This was supported by the fact that knockdown of *tp53* was not able to reduce cleaved caspase-3 levels at later developmental stages (data not shown).

5. General discussion

As a bifunctional DNA glycosylase, Neil2 preferentially removes oxidized cytosine derivatives to protect genomic integrity. My study provided *in vivo* evidence supporting a novel role of Neil2 in promoting substrate turnover of Tdg in Tet mediated active DNA demethylation. In *Xenopus* embryos, knockdown of Tet3, Tdg and Neil2 led to similar defects in NCC differentiation. A synergistic effect on embryo malformation was observed in embryos injected with combinations of subthreshold MO doses. This might suggest a partially shared role for these enzymes in development, which is related to 5fC and 5caC processing in active DNA demethylation. Given that Tet3, Tdg and Neil2 are genes with multiple functions, the similarity of NCC defects and synergistic effects in embryo malformation might also be caused by their unique functions that are not related to active DNA demethylation.

Three Tet family members (*Tet1*, *Tet 2* and *Tet3*) are characterized in mammals, but only *tet2* and *tet3* are annotated in *Xenopus*. Consistent with what I showed in the first chapter of the results, Xu et al. reported defects of eye and neural development in Tet3 morphants. They further demonstrated that Tet3 binds to its target gene promoters and modulates 5mC/5hmC status to regulate gene expression, especially for genes involved in regulating eye and neural development, such as *rx* and *pax6* [276]. However, it was mechanistically unclear how 5mC/5hmC levels affect gene expression. Does 5hmC act as a demethylation intermediate, with reduced 5hmC levels indicating an impaired demethylation in Tet3 morphants? Or does 5hmC acts as an epigenetic mark on its own, with reduced 5hmC levels in Tet3 morphants leading to a decreased recruitment of relevant co-factors to the target gene promoters?

Meanwhile, recent studies proved that Tet enzymes take part in DDR. 5hmC co-localizes with DNA damage marks, such as 53BP1 and γH2AX, indicating that there might be cross-talk between active DNA demethylation and DDR [276–279]. How Tet mediated active DNA demethylation relates to DDR is disputed. Some favor a direct model in which 5hmC functions as a signal to recruit DNA damage repair factors [279],while others proposed that a lack of Tet enzymes might impair DNA demethylation of DNA repair genes, repressing expression of repair genes [280]. Another study reported that ATR targets Tet3 directly to increase its expression [281], which might be a link between ATR-dependent DDR and Tet3 mediated DNA demethylation. Deficiency of Tet3 leads to accumulation of DNA damage, reflected by an increase in DNA damage mark γH2AX [281]. Therefore, eye and neural developmental defects of Tet3 morphants might be partially caused by accumulation of DNA

damage. Consistent with this hypothesis, a stabilization of Tp53 was seen by Western Blot analysis in Tet3 morphants (data not shown).

Tdg knockout is lethal in mouse embryos, as mutant embryos develop internal hemorrhages [282, 283]. In *Xenopus*, injection of a reduced dose of *tdg* MO allowed embryos to survive through early embryogenesis. Tdg morphants showed NCC defects and microcephaly phenotypes. In mice, Tdg deficiency downregulates retinoic acid (RA)-dependent gene expression [283, 284]. RA plays critical roles in NCC differentiation and migration, especially in cranial NCCs [285–287]. Tdg is a multifunctional protein. Most studies favor the model that its interaction with transcription factors and histone acetyltransferases to demethylate developmental gene promoters plays more essential roles during embryogenesis, compared to its function in DNA repair and active DNA demethylation [282–284, 288]. Western Blot analysis of Tp53 showed that there was also an accumulation of Tp53 in Tdg morphants (Data not shown). However, it is yet unknown if the activation of Tp53 in Tdg morphants was induced by reduced recruitment of active transcription factors to repair gene promoters, or by a failure to remove mismatch mutations.

Concerning Neil2, as discussed, NCC defects in Neil2 morphants might be caused by inefficient removal of oxidative DNA damage accumulated pre-MBT. Additionally, Neil2 also possesses AP lyase activity, which allows Neil2 to further process AP sites generated by Tdg after excision of 5fC and 5caC in active DNA demethylation [35]. Therefore, Neil2 knockdown might lead to an AP site accumulation which may induce mutations and stall DNA replication forks [289, 290]. Genome instability triggers Tp53 dependent DDR. Thus, involvement of Neil2 in both DNA repair and active DNA demethylation might account for Tp53 activation in Neil2 morphants.

DNA repair factors, especially BER factors such as Tdg and Neil2 play indispensable roles also in active DNA demethylation. Meanwhile, the critical factors of active DNA demethylation, Tet enzymes, are also involved in DDR. These multifunctional properties of Tet3, Tdg, and Neil2 make it difficult to distinguish whether their involvement in active DNA demethylation or in DNA damage repair is more important for NCC differentiation. However, irrespective of the exact mechanism, Tp53 accumulation seems to be the key downstream mediator of the observed MO phenotypes. Tp53 activation was observed in Tet3, Tdg, and Neil2 morphants (data not shown). This provides a possible explanation for the synergistic effects of combinations of subthreshold MO doses of *Tet3*, *Tdg* and *Neil2* in inducing NCC defects and microcephaly.

In conclusion, my thesis provided *in vivo* evidence to support that Neil DNA glycosylases promote substrate turnover of Tdg during DNA demethylation. Neil2 knockdown induced a Tp53 dependent DDR accounting for NCC defects and craniofacial abnormalities in *Xenopus* embryos, mimicking TCS. Although strong evidence indicated that the Tp53 dependent DDR might be induced by accumulation of oxidative DNA damage in Neil2 morphants, it could not be excluded that there might also be accumulation of AP site and β-elimination products in Neil2 morphants, which is capable of triggering a Tp53 dependent DDR. To determine the causes of the Tp53 dependent DDR, the amounts of AP sites, β-elimination products and oxidative DNA lesions should be quantified in Neil2 morphant neural plate explants. Human NEIL2 reduced cell apoptosis in *Xenopus* embryos. Therefore, overexpression of human *NEIL2* mRNA might rescue apoptotic NCC death and craniofacial abnormalities in Tcof1 morphants. In addition, appropriate supplementation of antioxidants to reduce accumulation of oxidative DNA damage in Neil2 morphants might rescue NCC defects. Further studies to answer these questions would help us better understand the etiology of craniofacial abnormalities and might shed light on their prevention and treatment.

6. Material and Methods

6.1 Equipment and materials

6.1.1 Equipment

-80°C freezer (Sanyo); 1ml syringe (Neolab); agarose gel chambers (BioRad); bacterial incubators (Thermo Scientific); bacterial shaker (Infors); balances (Sartorius, Kern); Bioanalyzer (Agilent); blotting apparatus (BioRad); calibration slide (AmScope); capillary (Promega); centrifuges (Heraeus); concentrator Plus Speedvac (Eppendorf); E-Gel electrophoresis system (Invitrogen); embryo incubators (Aqua lytic and Sanyo); forceps dumont #5 (Sigma-Aldrich); heating blocks (Eppendorf); HiSeq 2500 sequencing system (Illumina); hybridization water bath (Julabo); LightCycler 480 (Roche); magnetic stirrer (Heidolph); MassSpec (Agilent); microinjector (Warner Instruments); microloader (Eppendorf); micromanipulator (Singer Instruments); Mineral oil (Sigma-Aldrich); microcentrifuges (Heraeus); microscope (Leica); microwave oven (Sharp); multidispenser pipette (Eppendorf); Nanodrop 2000 spectrophotometer (Thermo Scientific); needle puller (Sutter instrument); orbital shaker (Neolab); PAGE minigel chambers (BioRad); PCR thermocyclers (Biometra); pH meter (Mettler Toledo); pipet boy (Integra); pipettes (Eppendorf); power supplies (BioRad); Qubit (Thermo Fisher); rotator (Neolab); stereomicroscope (Leica); transferpipette (Neolab); ultrapure water purification system (Millipore); UV photodocumentation system (BioRad); vortexer (Scientific industries).

6.1.2 Chemicals and pre-made buffers

100x Penicillin/Streptomycin (Lonza); 1,1,2-Trichloro-1,2,2-trifluoroethane (Sigma-Aldrich); 1x complete™ (Roche); 12% Criterion™ XT Bis-Tris Protein Gel (BioRad); agarose (Biozym); ammonium acetate (Sigma-Aldrich); ampicillin (Sigma-Aldrich); aqua ad iniectabilia plastic (Besamex); bactotryptone (Sigma-Aldrich); BCIP (Roche); bicinchoninic acid (Sigma-Aldrich); Böhringer blocking reagent (Roche); boric acid(Sigma-Aldrich); bovine serum albumin (Sigma-Aldrich); bromphenol blue (Sigma-Aldrich); Calcium chloride (Sigma-Aldrich); Calcium nitrate tetrahydrate (Sigma-Aldrich); CHAPS (Sigma-Aldrich); chloroform (Roth); citric acid (Sigma-Aldrich); copper(II) sulfate solution (Sigma-Aldrich); deionised formamide (Millipore); dimethylsulfoxide (Sigma-Aldrich); disodium hydrogen phosphate (Sigma-Aldrich); dithiothreitol (Sigma-Aldrich); dNTPs (Thermo Scientific); EDTA (Sigma-Aldrich); EGTA(Sigma-Aldrich); ethanol (Sigma-Aldrich); ethidium bromide

(Roth); fetal bovine serum (Lonza); Ficoll 400 (Sigma-Aldrich); formaldehyde (37%, Roth); formamid (deionized, AppliChem); glycerol (Sigma-Aldrich); glycine (Sigma-Aldrich); Glycogen (Fermentas); goat serum (Invitrogen); heparin sodium salt (Sigma-Aldrich); HEPES (Sigma-Aldrich); horse Serum (Invitrogen); human chorionic gonadotrophin (hCG) (genaxxon bioscience); hydrochloric acid (Sigma-Aldrich); Hydrogen peroxide solution (Sigma-Aldrich); isopropanol (Sigma-Aldrich); L-Cysteine hydrochloride monohydrate (Sigma-Aldrich); leibovitz's L-15 Medium, no phenol red (Gibco); m7G(5')ppp(5')G RNA Cap Structure Analog (NEB); magnesium chloride (Sigma-Aldrich); magnesium sulfate (Sigma-Aldrich); maleic acid (Sigma-Aldrich); ß-mercaptoethanol (Sigma-Aldrich); methanol (Sigma-Aldrich); MOPS (Thermo Scientific); MS 222, Ethyl 3-aminobenzoate methanesulfonate salt (Sigma-Aldrich); NBT (Roche); N-Ethylmaleimide (Sigma-Aldrich); nuclease-free water (Qiagen); NuPAGE 4-12% Bis-Tris Midi Protein Gels (Thermo); phenol (Roth); potassium chloride (Sigma-Aldrich); PhosStop™ (Roche); Potassium dihydrogen phosphate (Sigma-Aldrich); Potassium ferricyanide (Sigma-Aldrich); Potassium ferrocyanide (Sigma-Aldrich); potassium hydroxide (Sigma-Aldrich); protease inhibitor cocktail tablets (Roche); PVP40 (Thermo Scientific); pyocyanin (Sigma-Aldrich); Qiazol (Qiagen); Random primers (Invitrogen); restore™ Western Blot Stripping Buffer (Thermo); Roticlear (Roth); skim milk powder (Sigma-Aldrich); Sodium bicarbonate (Sigma-Aldrich); sodium chloride (Sigma-Aldrich); sodium dodecyl sulfate (Sigma-Aldrich); sodium hydroxide (Sigma-Aldrich); sucrose (Sigma-Aldrich); triethanolamine (Sigma-Aldrich); Tris base (Sigma-Aldrich); Tris HCl (Sigma-Aldrich); Triton X-100 (Sigma-Aldrich); Tween-20 (Sigma-Aldrich); xylene cyanole (Sigma-Aldrich); yeast extract (Sigma-Aldrich); yeast RNA (Roche).

6.1.3 Kits and enzymes

BamHI (NEB); ClaI (NEB); DIG RNA Labeling Mix 10x conc (Roche); DNAse I (Roche); DNeasy Blood & Tissue kit (Qiagen); EcoRI (NEB); miRNeasy mini kit (Qiagen); NotI (NEB); pGEM_T-easy (Promega); Proteinase K (Roche); PCR purification kit (Qiagen); Qiaprep Midiprep kit (Qiagen); Qiaprep Miniprep kit (Qiagen); Qiaquick Gel extraction kit (Qiagen); QIAquick® PCR Purification Kit (Qiagen); RNAse A (Ambion); RNeasy Mini Kit (Qiagen); SfiI (NEB); SP6 RNA polymerase (Ambion); Superscript II Reverse Transcriptase (Invitrogen); SuperSignal West Pico/Femto (Thermo Scientific); T3 RNA polymerase (Ambion); T7 RNA polymerase (Ambion); XbaI (NEB); XhoI (NEB).

6.1.4 Buffers and embryo culture media

6.1.4.1 General molecular biology buffers

Name	Recipe
10X TBE	1M Tris base, 1M boric acid, 20 mM EDTA, autoclaved
20X TBS	3M NaCl, 5.36 mM KCl, 1M Tris-HCl pH 7.4, autoclaved
4X Lämmli	60 mM Tris-HCl pH 6.8, 2% sodium dodecyl sulfate, 10% glycerol, 5% β- mercaptoethanol, 0.01% bromophenol blue
6X DNA loading buffer	60% (w/v) sucrose, 0.25% xylene cyanole, 0.25% bromphenol blue
dNTP mix	5 mM dATP, 5mM dCTP, 5mM dGTP, 5mM dTTP
Luria broth (LB)	10g bactotryptone, 5g yeast extract, 10g NaCl in 1l water, pH7.5, autoclaved
PBS	9.0 g/l NaCl, 144 mg/l KH_2PO_4, 795 mg/l Na_2HPO_4
TE buffer	10 mM Tris pH8.0, 1mM EDTA

6.1.4.2 *in situ* hybridization buffers, β-gal staining buffer, and alcian blue staining solution

Name	Recipe
0.5M $K_3Fe(CN)_6$	16.5g $K_3Fe(CN)_6$ in 100ml 1X PBS, stored at 4°C
0.5M $K_4Fe(CN)_6$	21.1g $K_4Fe(CN)_6$ in 100ml 1X PBS, stored at 4°C
10X MEM	1M MOPS, 20mM EGTA, 10mM $MgSO_4$. Sterilized by filtration. Stored in dark. pH 7.4
20X SSC	3M NaCl, 0.3M sodium citrate, pH 7.0.
4 % formaldehyde	4 % formaldehyde in 1XPTw, prepared freshly
5X MAB	500 mM Maleic acid, 750mM NaCl, pH 7.5
Alcian Blue staining solution	20 mg Alcian Blue,15 ml Acetic Acid, 35 ml 100% Ethanol
APB	100mM Tris-HCl, 50mM $MgCl_2$, 100mM NaCl, 0.1% Tween-20, prepared freshly
APB + NBT/BCIP	1 µl NBT/ml APB; 3.5 µl BCIP/ml APB

Bleaching solution	50% formamide, 1% H_2O_2 in 5X MAB
Boehringer Block (BMB)	10% BMB in 1X MAB, autoclaved and stored at -20°C
Denhart's 100X solution	2% BSA, 2%PVP, 2% Ficoll 400, stored at -20°C
Hybridization buffer	50% deionised formamid, 5X SSC, 1mg/ml Torula RNA, 100µg/ml Heparin, 1X Denhart's, 0.1% Tween-20, 0.1% CHAPS, 10mM EDTA in DEPC H_2O. stored at -20°C
MEMFA	4% formaldehyde in 1XMEM, prepared freshly
PTw	1X PBS, 0.1% Tween-20
PTw/Proteinase K solution	10mg/ml Proteinase K in PTw
Triethanolamine	0.747g in 50ml H_2O, pH 7.5, prepared freshly
β-gal staining buffer	0.24mM X-gal, 0.05M $K_3Fe(CN)_6$, 0.05M $K_4Fe(CN)_6$, 1mM $MgCl_2$ in 1X PBS, prepared freshly

6.1.4.3 Embryo preparation and culture media

Name	Recipe
10X Barths'	889 mM NaCl, 10 mM KCl, 24 mM $NaHCO_3$, 100 mM Hepes, 8 mM $MgSO_4$.7H2O, 3.3 mM $Ca(NO_3)_2.4H_2O$, 4.1 mM $CaCl_2.2H_2O$, pH 7.6, autoclaved
10X Ringers Solution	67.8g NaCl, 2.16g KCl, 2.65g $CaCl_2.2H_2O$, 11.9g Hepes in 1L H2O, pH 7.2, autoclaved
2% L-Cysteine	2% L-Cysteine, pH7.8-8.0, prepared freshly
66% L-15	66% L-15, 1X Penicillin/Streptomycin in dH2O, stored at 4°C
MS222	1.5g MS222, 1.4g $NaHCO_3$ in 1L tap water, prepared freshly
NOP	2% NP40, 20mM Tris pH7.5, 150mM NaCl, pH 7.5. Stored at 4°C
NOP+	NOP, 1x PhosStop™, 1x complete™, 2mM DTT, 5mM NEM (N-Ethylmaleimide). Prepared freshly and kept on ice

6.1.5 Antibodies

Target protein	Host species	Conjugate	Company	Order number
Caspase-3	Rabbit		Cell Signaling	9662
Digoxigenin	Sheep	Akaline phosphatase	Roche	11093274910
Histone H3	Rabbit		Abcam	ab1791
Mouse IgG	Goat	Horse radish peroxidase	Dianova	115-035-146
phospho-Chk1 (S345)	Rabbit		NEB	2341S
phospho-Histone H3 (S10)	Rabbit		Roche	06-570
Rabbit IgG	Goat	Horse radish peroxidase	Dianova	111-035-144
Tp53	Mouse		Thermo	MA1-12549
α-Tubulin	Mouse		Sigma	T5186

6.1.6 Plasmids

6.1.6.1 Plasmids obtained from company/ non-profit organization

Designation	Origin	Company	Order number
pCMVsport6-**ccng1**	*Xenopus laevis*	Thermo Scientific	MXL1736-202776388

6.1.6.2 Plasmids obtained from AG Niehrs, Heidelberg

Designation	Origin	Sense RNA	Antisense RNA	Clone chart
p33-**en2**	*Xenopus laevis*	XhoI/T7	XbaI/T3	Undefined
pBS.EP400/**krox20**	*Xenopus laevis*	HindIII/T7	EcoRI/T3	# P62
pGEMT-X**Sox10**	*Xenopus laevis*	NotI/T7	NcoI/SP6	# P1367
pMX363*X**Slug**	*Xenopus laevis*		ClaI/SP6	# P1369
pRN **PPL**		Sfi I/T3		# P66
psp46TNLS**LacZ**		XbaI/SP6		# P83
pSP73-X**twiT**18	*Xenopus laevis*		BamHI or EcoRI/T7	# P93

6.1.6.3 Plasmids obtained from other labs

Designation	Origin	Antisense RNA	Obtained from
pCS^{2+} Cas9		NotI/ SP6	Dr. Yonglong Chen lab
pGEM2-**rx1**	*Xenopus laevis*	XhoI/ SP6	Dr. Thomas Hollemann lab

6.1.7 Primers

6.1.7.1 Primers for RT-qPCR

Primer name	Forward primer	Reverse primer	UPL probe
aen	tttgccagctgaactcactc	caatcaaacgtaaaccacaagc	33
ccng1	tttgccagctgaactcactc	caatcaaacgtaaaccacaagc	11
eda2r	cccatggtttgatatgattgg	tcaatctcaaaatgtagtgtgtgc	63
LIF	tcaatctcaaaatgtagtgtgtgc	ttcaagaattcaggaaatgtagttgt	27
mdm2	gcttctgactcaaaaccatgc	tgcaggatgatcgactgaag	6
mdm4	cacaaatttaattcaccagtaaaacg	gaaagtccagataccagtctttgc	3
rad51	cgactgcgctctacaggac	atgcatctgacgtgctgaaa	14
rbm19	tgcagaagtggatggacaga	gcagcagatggcaaaaca	89
rfc3	cagctgaaagctgatgttgc	atagctttgctgccgagttg	46
riok3	aaacatgacgaggtggtgtg	ctggaattctggggcaaa	4
tp53	agtcacctgatgcgagtgg	cccgctatttacatcctcca	80
ulk	ggaacagatccgaactggaa	tcagcttcttcaccacttgc	25

6.1.7.2 Primers for gRNA assembly

Xenopus	Target gene	gRNA primer sequence
tropicalis	*neil2*	5′-GCAGCTAATACGACTCACTATAG **GAATTTACCACAAAGGCAGT** GTTTTAGAGCTAGAAATA-3′
laevis	*neil2**	5′-GCAGCTAATACGACTCACTATAG **CGTTGCTTTTGATTTACCTG** GTTTTAGAGCTAGAAATA-3′

**Xenopus laevis neil2* gRNA used as negative control

6.1.8 Morpholinos

MO name	MO sequence
neil2X1 MO	CATGTCTGCGGCCTTCATCAGAGGA
neil2X2 MO	GTTTTGATCCGCTACCGACCAGGAG
neil2 MO	GTCTGACTGTGGGACCTTCCGGCAT
neil2_splicing MO	GCCACAATTATTACTTTTACCTGGC

6.2 Methods

Preparation of chemically competent XL1-blue *Escherichia coli* bacteria, plasmid amplification in *Escherichia coli*, spectrophotometric quantification of DNA and RNA, restriction digests, DNA ligations, PCR, and agarose gel electrophoresis were carried out as described [291]. All primers were synthesized by Sigma Aldrich. Plasmid DNA was sequenced by Eurofins GATC Biotech.

6.2.1 Amplification and purification of plasmids

For plasmid amplification, plasmids were transformed into *Escherichia coli* XL-1 blue chemically competent bacteria by a 30-60s heatshock at 42°C, 5 min incubation on ice and subsequent incubation in LB containing an appropriate selection antibiotic overnight at 37°C. Plasmid DNA was purified from bacteria using Qiagen Miniprep or Midiprep kits according to the manufacturer's recommendation. DNA amount and purity were estimated on a Nanodrop 2000 spectrophotometer.

6.2.2 *in vitro* fertilization of *Xenopus laevis*

Female frogs were primed approximately 16h before the first collection of eggs. For this, 500 units of re-suspended hCG were injected into the dorsal lymph sac. The primed frogs were kept in tap water in an 18°C incubator. After 16h, the female frogs were squeezed and their eggs were collected into a glass petri dish. Male frogs were anesthetized in freshly prepared MS222 solution for 10min and subsequently sacrificed by decapitation. Testes were dissected and kept in 66% L-15 at 4°C. Half of a testis was transferred into 500µl 1X Ringers. The testis was minced with forceps, and then was pipetted through a 1ml pipet tip until no significant resistance was observed. Half a testis was sufficient to fertilize approximate 500 eggs. Therefore, the proportion of testis and volume of 1X Ringers had to be adjusted according to the amount of eggs obtained. The testis suspension was added to the eggs and mixed with a 1ml pipet tip into a monolayer. After 3 minutes incubation, 0.1X Barth's was added to cover the eggs. After 10 minutes incubation, 0.1X Barth's was removed and fertilized embryos were treated with 2% L-Cysteine, pH 7.6-8.0 on a horizontal shaker (80rpm) for 10min at RT to remove the jelly coat outside of the embryos. Then the L-Cysteine was removed and embryos were washed with tap water for at least 3 times. Subsequently, 0.1X Barth's was added for a short wash. For microinjection, embryos were incubated in 0.3X Barth's. For chemical treatment, embryos were kept in 0.1 X Barth's.

6.2.3 mRNA *in vitro* transcription

For mRNA preparation, 10µg plasmid DNA was linearized with 100U of appropriate restriction enzyme for 2 hours at 37°C. Linearized plasmid was purified using a PCR purification kit (Qiagen) according to the manufacturer's instructions. mRNA was transcribed from 5.85µl linearized plasmid (0.1-1µg) using 2µl SP6, T3, or T7 RNA polymerase (Ambion) in presence of 6.4µl dNTP mix, 3.75µl RNA cap structure analog and 2 µl of the corresponding buffer for 2 hours at 37°C. After DNAseI digestion (1µl, Ambion) for 15 minutes at 37°C, probes were purified using the RNeasy mini kit (Qiagen) according to the manufacturer's instructions. mRNA quantity was estimated on a Nanodrop 2000 spectrophotometer and quality was examined on a 2% agarose gel.

6.2.4 Needle calibration and microinjection

A needle puller (Model P-97) was set to the following parameters: heat, 545; pull, 80; vel, 180; and time, 80, and was used according to the manufacturer's instructions. The pulled needle was introduced into the micromanipulator and fixed. A #5 forceps was used to clip the needle near the tip. Then the microinjector and the pressure valve were switched on. A drop of RNase free water was introduced to a piece of parafilm. The needle was filled with the prepared RNase free water by pressing the fill button on the microinjector. For calibration, the pressure was set to 8-12 psi. Mineral oil was dropped onto the black circle of the calibration slide to better visualize the micro-ruler. Injection time was adjusted to obtain a drop with the diameter of 0.2mm, which corresponded to approximately 5nL. The needle was then filled with mRNA or MO. For each embryo, 10nl mRNA or MO were injected. The microinjection was carried out in 0.3X Barth's. Two hours after microinjection, embryos were switched into 0.1 X Barth's for cultivation.

6.2.5 Embryo fixation

Embryos that have reached their desired developmental stage [292] were fixed in freshly prepared MEMFA for 10min, then the MEMFA was exchanged and embryos were incubated for another 1h at room temperature (RT), or 4°C overnight (O/N). After fixation, embryos were washed twice in 100% ethanol at RT for 5min and stored in 100% ethanol at -20°C.

6.2.6 β-gal staining

Embryos that have reached their desired developmental stage [292] were fixed in freshly prepared MEMFA for 20min. After washing them 5 times in 1X PBS at RT for 10min, embryos were stained in β-gal staining buffer for 0.5~6h until color intensity was satisfactory. Then embryos were washed twice in 1X PBS at RT for 10min and fixed in MEMFA at RT for 1h. After fixation, embryos were washed twice in 100% ethanol at RT for 5min and stored in 100% ethanol at -20°C.

6.2.7 *in situ* hybridization

6.2.7.1 Probe transcription

For probe transcription, plasmid DNA was linearized and purified as described in 6.2.3. RNA was transcribed from 2µg linearized plasmid using 4µl SP6, T3, or T7 RNA polymerase (Ambion) in presence of 5µl DIG-labeled NTPs (Roche), 2µl RNAse inhibitor and the corresponding buffer for 2 hours at 37°C. After DNAseI digestion (2µl, Roche) for 15 minutes at 37°C, probes were purified using the RNeasy mini kit (Qiagen) according to the manufacturer's instructions. Probe quantity and quality was afterwards examined on a 2% agarose gel.

6.2.7.2 Rehydration of embryos

Embryos of various stages, prefixed in MEMFA, were rehydrated as shown in the table below:

Step	Ethanol (%)	Buffer (%)	Incubation (min)	No. of times
1	Ethanol 100%		5	1 x @
2	Ethanol 75%	dH_2O 25%	5	1 x @
3	Ethanol 50%	dH_2O 50%	5	1 x @
4	Ethanol 25%	PTw 75%	5	1 x @
5		PTw 100%	5	4 x @

@ = Overhead shaking

6.2.7.3 Proteinase K treatment

Up to this step, embryos of the same stage were kept together in one tube. Each batch was kept in 1 ml PTw containing 10μg/ml Proteinase K. Embryos of gastrula, neurula and tail bud stages were incubated at room temperature, and tadpole stage embryos were incubated at 37°C.

st12-14: RT, 6min; st32: RT, 15min; st34-36: RT, 17min; st40: RT, 25min; st42: RT, 35min or 37°C, 30min; st43:37°C, 35min; st44:37°C, 37min; st48: 37°C, 45min.

6.2.7.4 Refixing embryos

Proteinase K activity was stopped by treatment with acetanhydride and the embryos were refixed with PTw and formaldehyde. The steps are shown below:

Step	Buffer	Other components	Incubation (min)	No. of times
1	0.1 M Triethanolamine pH 7.5		5	2 x @
2*	0.1 M Triethanolamine	10 μl acetanhydride	5	1 x @
3*		5 μl acetanhydride	5	2 x @
4	PTw		0	1 x @
5	PTw + 4 % formaldehyde		20	1 x @
6	PTw		5	5 x @

*At step 2 & 3 without changing buffer, 10 μl acetanhydride was added, 5 min later 5 μl acetanhydride was added twice, every time for 5 min.

6.2.7.5 Hybridization

The embryos were quickly washed in 1 ml PTw to which 250 μl of Hybridization buffer was added, the solution was then removed and 1 ml Hybridization buffer was added and incubated at 65°C for 10 minutes. The solution was removed and 1 ml of fresh Hybridization buffer was

added and incubated at 65°C for 6 hours. The Hybridization-Mix was then replaced with 1 ml of new Hybridization buffer with 1 µg/ml of the appropriate Dig-labeled antisense RNA probes and incubated at 65°C overnight.

6.2.7.6 Washing steps

Step	Buffer	Temperature (°C)	Incubation (min)	No. of times
1	Hybridization buffer (500 µL)	65	10	1 x @
2	2 X SSC	65	20	3 x @
3	2 X SSC with 10µg/ml RNase A	37	30	2 x @
4	2 X SSC	RT	10	1 x @
5	0.2 X SSC	65	30	2 x @
6	1 X MAB	RT	15	2 x @

6.2.7.7 Antibody incubation

In this step, the embryos were incubated with Alkaline Phosphatase (AP)-linked anti Dig-antibody.

Step	Buffer	Temperature (°C)	Incubation (min)	No. of times
1	1 X MAB + 2% BMB	RT	60	1 x @
2	1 X MAB + 2% BMB + 20% horse serum	RT	60	1 x @
3	1 X MAB + 2% BMB + 20% horse serum +	RT	240	1 x @

	Antibody* (1:5000)			
4	1 X MAB (washing)	RT	30	2 x @
5	1 X MAB (washing)	4	O/N	1 x @

* Sheep-Anti Dig antibody linked to Alkaline Phosphatase

6.2.7.8 Color reaction

NBT/BCIP is the substrate for Alkaline Phosphatase, which converts it to a colored product.

Step	Buffer	Temperature (°C)	Incubation	No. of times
1	1 X MAB	RT	10 min	8 x @
2	APB	RT	5 min	2 x @
3	APB + NBT/BCIP*	Over ice, in dark	5min- 24 h	1 x @

* 1 µl NBT/ml APB; 3.5 µl BCIP/ml APB

6.2.7.9 Decolor reaction

After NBT/BCIP treatment, the embryos were washed once with water for 5 minutes, followed by destaining with 100% methanol for 2-3 minutes and with 50 % methanol for 5 minutes. Next, the embryos were washed again with water for 5 minutes and kept in MEMFA at room temperature for 30 minutes. Then the embryos were washed two times for 5 minutes, after this the embryos were decolored with bleaching solution for 30 min-2h. Again, the embryos were washed with 5 X SSC two times for 5 minutes. The embryos were stored in MEMFA at 4°C. Images were taken with a stereomicroscope.

6.2.8 Total RNA extraction (RNeasy Mini Kit (Qiagen))

5-8 embryos were transferred to a 1.5ml Eppendorf tube, and 700µl Qiazol lysis reagent was added. Embryos were immediately pipetted through a 1ml pipet tip to obtain a homogenized lysate. After 5 min incubation at room temperature, 200µl chloroform was added and samples were shaken vigorously. Subsequent steps of RNA isolation were performed using a Qiagen RNeasy Mini Kit according to the manufacturer's instructions.

6.2.9 qPCR (expression analysis)

cDNA was synthesized using Superscript II reverse transcriptase (Invitrogen) according to the manufacturer's instructions. Briefly, 500ng RNA, 1µl 10mM dNTPs and 2µl 100µM random primers were mixed in a final volume of 12µl. After denaturation for 5 min at 65°C, the mixture was cooled on ice. Then, 4µl 5x FS buffer, 2µl 0.1M DTT, 1 µl Ribolock and 1 µl Superscript II Polymerase were added and samples were incubated for 10 min at 25°C, 90 min at 42°C for cDNA synthesis and 5 min at 72°C for enzyme inactivation. Resulting cDNA was diluted 1:6 in ddH2O. All incubation steps were carried out in a PCR cycler.

For qPCR, 5µl cDNA, 5.5µl 2x Probes master, 0.055µl 100µM forward primer, 0.055µl 100µM reverse primer, 0.11µl UPL probe and 0.28µl ddH2O were mixed to a final volume of 11µl. PCR reactions were carried out in a 384-well format in the Roche Light Cycler 480 using the following PCR program:

	PCR step	**Temperature**	**Time**	**Ramp rate**
1	Denaturation	95°C	10 min	4.8 °C/sec
2	Denaturation	95°C	10s	4.8 °C/sec
3	Annealing	60°C	20s	2.5 °C/sec
4	Elongation + Signal acquisition	72°C	1s	4.8 °C/sec
5	Go to step [2], 49x times	-	-	-
6	Cooling	4°C	1s	2.5 °C/sec

Cp values were determined using the Roche Lightcycler software and relative expression values were calculated according to the ddCp method [293], and normalized to the housekeeping gene *histone h4*.

6.2.10 RNA sequencing

RNA from control MO and *neil2* MO injected embryos was purified as described in 6.2.2.7. Using an RNA 6000 Nano kit on a Bioanalyzer (Agilent), RNA integrity was assessed and deemed suitable with RIN values consistently above 8.1. 1µg total RNA of biological triplicates from control MO and *neil2* MO injected embryos at st23 were submitted for further processing. Stranded mRNA libraries were prepared with a TruSeq Stranded mRNA Sample Prep Kit (Illumina) according to the manufacturer's recommendations and sequenced on a HiSeq2500 high-throughput sequencer (Illumina). Quality controls, library preparation and

sequencing were performed in the IMB core facility genomics. Bioinformatic analysis was performed by Emil Karaulanov.

6.2.11 CRISPR/Cas9-mediated knockout

CRISPR/Cas9-mediated knockout in *Xenopus tropicalis* was carried out following a published protocol [294]. sgRNA was designed using an online tool CCTop (https://crispr.cos.uni-heidelberg.de/). Templates of sgRNA were assembled by PCR. PCR reactions were set up as described below:

Reagent	**Volume (µl)**
10 x Buffer	10
25 mM dNTP mixture	1.2
50 mM Mg_2SO_4	2
5' Primer (100 pmol/µl)	2
3' Primer (100 pmol/µl)	2
DNA polymerase	1
H_2O (DNAse/RNAse-free)	81.8

Following PCR conditions were used:

	PCR step	**Temperature**	**Time**
1	Initial denaturation	94°C	5 min
2	Denaturation	94°C	20s
3	Annealing	58°C	20s
4	Elongation	68°C	15s
5	Go to step [2], 19x times	-	-
6	Final extension	68°C	5min

The sgRNA template was purified using the QIAquick® PCR Purification Kit (Qiagen) according to the manufacturer's instructions. sgRNA was transcribed from 8µl of purified template (0.25–0.6µg) using 2µl T7 RNA polymerase (Ambion) in presence of 6.4µl dNTP mix, 2µl of reaction buffer and 1.6µl DNAse/RNAse-free H_2O for 2 hours at 37°C. After DNAseI digestion (1µl, Ambion) for 15 minutes at 37°C, sgRNAs were purified using the miRNeasy mini kit (Qiagen) according to the manufacturer's instructions. sgRNA quantity was estimated on a Nanodrop 2000 spectrophotometer and quality was examined on a 2% agarose gel.

Cas9 mRNA was prepared as described in 6.2.2.2. Each embryo was injected with 400pg Cas9 mRNA and 300pg gRNA at the 1-cell stage.

6.2.12 Western Blot

Embryos were harvested in 1.5ml Eppendorf tubes. Excess culture medium was removed as much as possible. 20µl NOP^+ buffer per embryo was added to the tube. Embryos were homogenized on ice by pipetting up and down through a pipet tip. 2X volume of Freon (1,1,2-Trichloro-1,2,2-trifluoroethane) was added to the homogenized lysate and mixed thoroughly. After centrifugation of samples for 15 min at 21,000g at 4°C, the upper phase of the supernatant was transferred into a fresh tube containing 1 parts of 4x Lämmli to 3 part sample. Then the mixture was boiled at 95°C for 5min and stored at -80°C.

Electrophoresis on precast 12% Criterion™ XT Bis-Tris Protein Gels, transfer to polyvinylidene difluoride (PVDF) membranes pretreated in methanol at RT for 10s and Western Blotting was performed according to standard protocols [291]. Signals were developed with SuperSignal West Pico or Femto Chemiluminescent Substrate (Thermo Scientific) and analyzed using a ChemiDoc (BioRad) with ImageLab software.

6.2.13 Pyocyanin treatment

Pyocyanin was dissolved in DMSO to yield a 10mM stock solution and stored at -20°C. Embryos were treated with 25µM pyocyanin diluted in 0.1X Barth's. Equivalent volumes of DMSO were added to 0.1X Barth's as a control.

For the synergy experiment, embryos were treated with 20ng/embryo of MO and 10 µM pyocyanin.

6.2.14 Alcian Blue cartilage staining

Embryos were fixed at st45. After washing in 100% ethanol for 2 times, embryos were stored in fresh 100% ethanol at -20°C. For cartilage staining, fixed embryos were incubated in Alcian Blue staining solution for 3 days. After staining, embryos were rinsed in 95% ethanol at RT for 3X 15min. Then, embryos were rehydrated in a decreasing series of 75%, 50%, and 25% ethanol in 2% KOH for 10min each. After another 3X 10min wash in 2% KOH, embryos were washed through an increasing series of 20%, 40%, 60%, and 80% glycerol in 2% KOH for 1h each. Stained cartilages were stored in 80% glycerol in 2% KOH at 4°C. Images were taken with a Zeiss stereomicroscope.

7. References

1. Handy DE, Castro R, Loscalzo J (2011) Epigenetic Modifications. Circulation 123(19): 2145. doi: 10.1161/circulationaha.110.956839
2. Colot Vincent, Rossignol Jean‐Luc (1999) Eukaryotic DNA methylation as an evolutionary device. BioEssays 21(5): 402–411. doi: 10.1002/(sici)1521-1878(199905)21:5<402:aid-bies7>3.0.co;2-b
3. Bird A (2002) DNA methylation patterns and epigenetic memory. Genes & Development 16(1): 6–21. doi: 10.1101/gad.947102
4. Jeltsch A, Jurkowska RZ (2014) New concepts in DNA methylation. Trends in Biochemical Sciences 39(7): 310–318. doi: 10.1016/j.tibs.2014.05.002
5. Probst AV, Dunleavy E, Almouzni G (2009) Epigenetic inheritance during the cell cycle. Nature Reviews Molecular Cell Biology 10: 192 EP -. doi: 10.1038/nrm2640
6. Nomura J, Hisatsune A, Miyata T et al. (2007) The role of CpG methylation in cell type-specific expression of the aquaporin-5 gene. Biochemical and Biophysical Research Communications 353(4): 1017–1022. doi: 10.1016/j.bbrc.2006.12.126
7. Aoyama T, Okamoto T, Nagayama S et al. (2004) Methylation in the Core-promoter Region of the Chondromodulin-I Gene Determines the Cell-specific Expression by Regulating the Binding of Transcriptional Activator Sp3. Journal of Biological Chemistry 279(27): 28789–28797. doi: 10.1074/jbc.M401273200
8. Bird AP, Wolffe AP (1999) Methylation-Induced Repression— Belts, Braces, and Chromatin. Cell 99(5): 451–454. doi: 10.1016/S0092-8674(00)81532-9
9. Hendrich B, Bird A (1998) Identification and Characterization of a Family of Mammalian Methyl-CpG Binding Proteins. Molecular and Cellular Biology 18(11): 6538–6547. doi: 10.1128/MCB.18.11.6538
10. Boyes J, Bird A (1991) DNA methylation inhibits transcription indirectly via a methyl-CpG binding protein. Cell 64(6): 1123–1134. doi: 10.1016/0092-8674(91)90267-3
11. Bahar Halpern K, Vana T, Walker MD (2014) Paradoxical role of DNA methylation in activation of FoxA2 gene expression during endoderm development. Journal of Biological Chemistry. doi: 10.1074/jbc.M114.573469
12. Bhattacharya SK, Ramchandani S, Cervoni N et al. (1999) A mammalian protein with specific demethylase activity for mCpG DNA. Nature 397: 579 EP -. doi: 10.1038/17533
13. Rougier N, Bourc'his D, Gomes DM et al. (1998) Chromosome methylation patterns during mammalian preimplantation development. Genes & Development 12(14): 2108–2113. doi: 10.1101/gad.12.14.2108
14. Kriaucionis S, Heintz N (2009) The Nuclear DNA Base 5-Hydroxymethylcytosine Is Present in Purkinje Neurons and the Brain. Science 324(5929): 929. doi: 10.1126/science.1169786
15. Tahiliani M, Koh KP, Shen Y et al. (2009) Conversion of 5-Methylcytosine to 5-Hydroxymethylcytosine in Mammalian DNA by MLL Partner TET1. Science 324(5929): 930. doi: 10.1126/science.1170116
16. Ito S, Shen L, Dai Q et al. (2011) Tet Proteins Can Convert 5-Methylcytosine to 5-Formylcytosine and 5-Carboxylcytosine. Science 333(6047): 1300. doi: 10.1126/science.1210597
17. Maiti A, Drohat AC (2011) Thymine DNA Glycosylase Can Rapidly Excise 5-Formylcytosine and 5-Carboxylcytosine: POTENTIAL IMPLICATIONS FOR ACTIVE DEMETHYLATION OF CpG SITES. Journal of Biological Chemistry 286(41): 35334–35338. doi: 10.1074/jbc.C111.284620

18. He Y-F, Li B-Z, Li Z et al. (2011) Tet-Mediated Formation of 5-Carboxylcytosine and Its Excision by TDG in Mammalian DNA. Science 333(6047): 1303. doi: 10.1126/science.1210944
19. Sun W, Zang L, Shu Q et al. (2014) From development to diseases: the role of 5hmC in brain. Genomics 104(5): 347–351. doi: 10.1016/j.ygeno.2014.08.021
20. Szulwach KE, Li X, Li Y et al. (2011) 5-hmC–mediated epigenetic dynamics during postnatal neurodevelopment and aging. Nature Neuroscience 14(12): 1607. doi: 10.1038/nn.2959
21. Spruijt CG, Gnerlich F, Smits AH et al. (2013) Dynamic Readers for 5-(Hydroxy)Methylcytosine and Its Oxidized Derivatives. Cell 152(5): 1146–1159. doi: 10.1016/j.cell.2013.02.004
22. Schomacher Lars, Niehrs Christof (2017) DNA repair and erasure of 5‐methylcytosine in vertebrates. BioEssays 39(3): 1600218. doi: 10.1002/bies.201600218
23. Lindahl T, Wood RD (1999) Quality Control by DNA Repair. Science 286(5446): 1897. doi: 10.1126/science.286.5446.1897
24. Lindahl T (1974) An N-glycosidase from Escherichia coli That Releases Free Uracil from DNA Containing Deaminated Cytosine Residues. Proceedings of the National Academy of Sciences 71(9): 3649. doi: 10.1073/pnas.71.9.3649
25. Jacobs AL, Schär P (2011) DNA glycosylases: in DNA repair and beyond. Chromosoma 121(1): 1–20. doi: 10.1007/s00412-011-0347-4
26. Meadows KL, Song B, Doetsch PW (2003) Characterization of AP lyase activities of Saccharomyces cerevisiae Ntg1p and Ntg2p: implications for biological function. Nucleic Acids Research 31(19): 5560–5567. doi: 10.1093/nar/gkg749
27. McCullough AK, Sanchez A, Dodson ML et al. (2001) The Reaction Mechanism of DNA Glycosylase/AP Lyases at Abasic Sites. Biochemistry 40(2): 561–568. doi: 10.1021/bi002404
28. Morgan HD, Dean W, Coker HA et al. (2004) Activation-induced Cytidine Deaminase Deaminates 5-Methylcytosine in DNA and Is Expressed in Pluripotent Tissues: IMPLICATIONS FOR EPIGENETIC REPROGRAMMING. Journal of Biological Chemistry 279(50): 52353–52360. doi: 10.1074/jbc.M407695200
29. Rai K, Huggins IJ, James SR et al. (2008) DNA Demethylation in Zebrafish Involves the Coupling of a Deaminase, a Glycosylase, and Gadd45. Cell 135(7): 1201–1212. doi: 10.1016/j.cell.2008.11.042
30. Zhu B, Zheng Y, Hess D et al. (2000) 5-Methylcytosine-DNA glycosylase activity is present in a cloned G/T mismatch DNA glycosylase associated with the chicken embryo DNA demethylation complex. Proceedings of the National Academy of Sciences 97(10): 5135. doi: 10.1073/pnas.100107597
31. Hashimoto H, Liu Y, Upadhyay AK et al. (2012) Recognition and potential mechanisms for replication and erasure of cytosine hydroxymethylation. Nucleic Acids Research 40(11): 4841–4849. doi: 10.1093/nar/gks155
32. Shimoda N, Hirose K, Kaneto R et al. (2014) No Evidence for AID/MBD4-Coupled DNA Demethylation in Zebrafish Embryos. PLoS ONE 9(12): e114816. doi: 10.1371/journal.pone.0114816
33. Guo JU, Su Y, Zhong C et al. (2011) Hydroxylation of 5-methylcytosine by TET1 promotes active DNA demethylation in the adult brain. Cell 145(3): 423–434. doi: 10.1016/j.cell.2011.03.022
34. Hazra TK, Izumi T, Boldogh I et al. (2002) Identification and characterization of a human DNA glycosylase for repair of modified bases in oxidatively damaged DNA. Proceedings of the National Academy of Sciences 99(6): 3523. doi: 10.1073/pnas.062053799

35. Hazra TK, Kow YW, Hatahet Z et al. (2002) Identification and Characterization of a Novel Human DNA Glycosylase for Repair of Cytosine-derived Lesions. Journal of Biological Chemistry 277(34): 30417–30420. doi: 10.1074/jbc.C200355200
36. Doublié S, Bandaru V, Bond JP et al. (2004) The crystal structure of human endonuclease VIII-like 1 (NEIL1) reveals a zincless finger motif required for glycosylase activity. Proceedings of the National Academy of Sciences of the United States of America 101(28): 10284. doi: 10.1073/pnas.0402051101
37. Wallace SS, Bandaru V, Kathe SD et al. (2003) The enigma of endonuclease VIII. DNA Repair 2(5): 441–453. doi: 10.1016/S1568-7864(02)00182-9
38. Englander EW, Ma H (2006) Differential modulation of base excision repair activities during brain ontogeny: Implications for repair of transcribed DNA. Mechanisms of Ageing and Development 127(1): 64–69. doi: 10.1016/j.mad.2005.09.008
39. Canugovi C, Yoon JS, Feldman NH et al. (2012) Endonuclease VIII-like 1 (NEIL1) promotes short-term spatial memory retention and protects from ischemic stroke-induced brain dysfunction and death in mice. Proceedings of the National Academy of Sciences 109(37): 14948. doi: 10.1073/pnas.1204156109
40. Shinmura K, Kato H, Kawanishi Y et al. (2016) Abnormal Expressions of DNA Glycosylase Genes NEIL1, NEIL2, and NEIL3 Are Associated with Somatic Mutation Loads in Human Cancer. Oxidative Medicine and Cellular Longevity 2016: 10. doi: 10.1155/2016/1546392
41. Chan MK, Ocampo-Hafalla MT, Vartanian V et al. (2009) Targeted deletion of the genes encoding NTH1 and NEIL1 DNA N-glycosylases reveals the existence of novel carcinogenic oxidative damage to DNA. DNA Repair 8(7): 786–794. doi: 10.1016/j.dnarep.2009.03.001
42. Vartanian V, Lowell B, Minko IG et al. (2006) The metabolic syndrome resulting from a knockout of the NEIL1 DNA glycosylase. Proceedings of the National Academy of Sciences of the United States of America 103(6): 1864. doi: 10.1073/pnas.0507444103
43. Gao D, Wei C, Chen L et al. (2004) Oxidative DNA damage and DNA repair enzyme expression are inversely related in murine models of fatty liver disease. American Journal of Physiology-Gastrointestinal and Liver Physiology 287(5): G1070-G1077. doi: 10.1152/ajpgi.00228.2004
44. Chakraborty A, Wakamiya M, Venkova-Canova T et al. (2015) Neil2-null Mice Accumulate Oxidized DNA Bases in the Transcriptionally Active Sequences of the Genome and Are Susceptible to Innate Inflammation. Journal of Biological Chemistry 290(41): 24636–24648. doi: 10.1074/jbc.M115.658146
45. Regnell CE, Hildrestrand GA, Sejersted Y et al. (2012) Hippocampal Adult Neurogenesis Is Maintained by Neil3-Dependent Repair of Oxidative DNA Lesions in Neural Progenitor Cells. Cell Reports 2(3): 503–510. doi: 10.1016/j.celrep.2012.08.008
46. Sejersted Y, Hildrestrand GA, Kunke D et al. (2011) Endonuclease VIII-like 3 (Neil3) DNA glycosylase promotes neurogenesis induced by hypoxia-ischemia. Proceedings of the National Academy of Sciences 108(46): 18802. doi: 10.1073/pnas.1106880108
47. Rolseth V, Luna L, Olsen AK et al. (2017) No cancer predisposition or increased spontaneous mutation frequencies in NEIL DNA glycosylases-deficient mice. Scientific Reports 7(1): 4384. doi: 10.1038/s41598-017-04472-4
48. Theveneau E, Mayor R (2012) Neural crest delamination and migration: From epithelium-to-mesenchyme transition to collective cell migration. Developmental Biology 366(1): 34–54. doi: 10.1016/j.ydbio.2011.12.041
49. Mayor R, Aybar MJ (2001) Induction and development of neural crest in Xenopus laevis. Cell and Tissue Research 305(2): 203–209. doi: 10.1007/s004410100369

50. Sauka-Spengler T, Bronner-Fraser M (2008) A gene regulatory network orchestrates neural crest formation. Nature Reviews Molecular Cell Biology 9: 557 EP -. doi: 10.1038/nrm2428
51. Sadaghiani B, Thiébaud CH (1987) Neural crest development in the Xenopus laevis embryo, studied by interspecific transplantation and scanning electron microscopy. Developmental Biology 124(1): 91–110. doi: 10.1016/0012-1606(87)90463-5
52. Schroeder TE (1970) Neurulation in Xenopus laevis. An analysis and model based upon light and electron microscopy. Journal of Embryology and Experimental Morphology 23(2): 427
53. Nichols DH (1987) Ultrastructure of neural crest formation in the midbrain/rostral hindbrain and preotic hindbrain regions of the mouse embryo. The American journal of anatomy 179 2: 143–154
54. Théveneau E, Duband J-L, Altabef M (2007) Ets-1 Confers Cranial Features on Neural Crest Delamination. PLoS ONE 2(11): e1142. doi: 10.1371/journal.pone.0001142
55. Franz Thomas (1992) Neural tube defects without neural crest defects in Splotch mice. Teratology 46(6): 599–604. doi: 10.1002/tera.1420460609
56. Estibeiro JP, Brook FA, Copp AJ (1993) Interaction between splotch (Sp) and curly tail (ct) mouse mutants in the embryonic development of neural tube defects. Development 119(1): 113
57. Kos R, Reedy MV, Johnson RL et al. (2001) The winged-helix transcription factor FoxD3 is important for establishing the neural crest lineage and repressing melanogenesis in avian embryos. Development 128(8): 1467
58. LaBonne C, Bronner-Fraser M (1998) Neural crest induction in Xenopus: evidence for a two-signal model. Development 125(13): 2403
59. Hong C-S, Park B-Y, Saint-Jeannet J-P (2008) Fgf8a induces neural crest indirectly through the activation of Wnt8 in the paraxial mesoderm. Development 135(23): 3903. doi: 10.1242/dev.026229
60. Crozé N de, Maczkowiak F, Monsoro-Burq AH (2011) Reiterative AP2a activity controls sequential steps in the neural crest gene regulatory network. Proceedings of the National Academy of Sciences 108(1): 155. doi: 10.1073/pnas.1010740107
61. Monsoro-Burq A-H, Fletcher RB, Harland RM (2003) Neural crest induction by paraxial mesoderm in Xenopus embryos requires FGF signals. Development 130(14): 3111. doi: 10.1242/dev.00531
62. Steventon B, Araya C, Linker C et al. (2009) Differential requirements of BMP and Wnt signalling during gastrulation and neurulation define two steps in neural crest induction. Development 136(5): 771. doi: 10.1242/dev.029017
63. Nichane M, Ren X, Bellefroid EJ (2010) Self‐regulation of Stat3 activity coordinates cell‐cycle progression and neural crest specification. The EMBO Journal 29(1): 55. doi: 10.1038/emboj.2009.313
64. Pegoraro Caterina, Monsoro‐Burq Anne H. (2012) Signaling and transcriptional regulation in neural crest specification and migration: lessons from xenopus embryos. WIREs Dev Biol 2(2): 247–259. doi: 10.1002/wdev.76
65. Wang Y, Fu Y, Gao L et al. (2010) Xenopus Skip Modulates Wnt/β-Catenin Signaling and Functions in Neural Crest Induction. Journal of Biological Chemistry 285(14): 10890–10901. doi: 10.1074/jbc.M109.058347
66. Abu-Elmagd M, Garcia-Morales C, Wheeler GN (2006) Frizzled7 mediates canonical Wnt signaling in neural crest induction. Developmental Biology 298(1): 285–298. doi: 10.1016/j.ydbio.2006.06.037

67. Meulemans D, Bronner-Fraser M (2004) Gene-Regulatory Interactions in Neural Crest Evolution and Development. Developmental Cell 7(3): 291–299. doi: 10.1016/j.devcel.2004.08.007
68. Monsoro-Burq A-H, Wang E, Harland R (2005) Msx1 and Pax3 Cooperate to Mediate FGF8 and WNT Signals during Xenopus Neural Crest Induction. Developmental Cell 8(2): 167–178. doi: 10.1016/j.devcel.2004.12.017
69. Nichane M, Crozé N de, Ren X et al. (2008) Hairy2–Id3 interactions play an essential role in Xenopus neural crest progenitor specification. Developmental Biology 322(2): 355–367. doi: 10.1016/j.ydbio.2008.08.003
70. Bellmeyer A, Krase J, Lindgren J et al. (2003) The Protooncogene c-Myc Is an Essential Regulator of Neural Crest Formation in Xenopus. Developmental Cell 4(6): 827–839. doi: 10.1016/S1534-5807(03)00160-6
71. Simões-Costa M, Bronner ME (2015) Establishing neural crest identity: a gene regulatory recipe. Development (Cambridge, England) 142(2): 242–257. doi: 10.1242/dev.105445
72. Gross Joshua B., Hanken James (2004) Cranial neural crest contributes to the bony skull vault in adult Xenopus laevis: Insights from cell labeling studies. J. Exp. Zool. 304B(2): 169–176. doi: 10.1002/jez.b.21028
73. Vega-Lopez GA, Cerrizuela S, Tribulo C et al. (2018) Neurocristopathies: New insights 150 years after the neural crest discovery. Developmental Biology. doi: 10.1016/j.ydbio.2018.05.013
74. Trainor PA (2010) Craniofacial Birth Defects: The Role of Neural Crest Cells in the Etiology and Pathogenesis of Treacher Collins Syndrome and the Potential for Prevention. American journal of medical genetics. Part A 0(12): 2984–2994. doi: 10.1002/ajmg.a.33454
75. Treacher Collins E (1900) Case with symmetrical congenital notches in the outer partofeach lower lid and defective development of the malar bones. Trans Opthalmol Soc UK: 20:90
76. Sakai D, Trainor PA (2009) Treacher Collins syndrome: Unmasking the role of Tcof1/treacle. The International Journal of Biochemistry & Cell Biology 41(6): 1229–1232. doi: 10.1016/j.biocel.2008.10.026
77. Katsanis SH, Jabs EW (1993) GeneReviews®: Treacher Collins Syndrome, Seattle (WA)
78. Matsumoto N, Kaneko M, Watanabe N et al. (2018) Treacher Collins syndrome 3 (TCS3)-associated POLR1C mutants are localized in the lysosome and inhibits chondrogenic differentiation. Biochemical and Biophysical Research Communications 499(1): 78–85. doi: 10.1016/j.bbrc.2018.03.136
79. Marszałek-Kruk BA, Śmigiel R, Sąsiadek MM (2014) Novel mutation in the TCOF1 gene in a patient with Treacher Collins syndrome. Pediatria Polska 89(6): 462–465. doi: 10.1016/j.pepo.2014.09.006
80. Hedera P, Toriello HV, Petty EM (2002) Novel autosomal dominant mandibulofacial dysostosis with ptosis: clinical description and exclusion of TCOF1. J Med Genet 39(7): 484–488
81. Noack Watt KE, Achilleos A, Neben CL et al. (2016) The Roles of RNA Polymerase I and III Subunits Polr1c and Polr1d in Craniofacial Development and in Zebrafish Models of Treacher Collins Syndrome. PLoS Genet 12(7). doi: 10.1371/journal.pgen.1006187
82. Thiffault I, Wolf NI, Forget D et al. (2015) Recessive mutations in POLR1C cause a leukodystrophy by impairing biogenesis of RNA polymerase III. Nature Communications 6: 7623 EP -. doi: 10.1038/ncomms8623
83. Dauwerse JG, Dixon J, Seland S et al. (2010) Mutations in genes encoding subunits of RNA polymerases I and III cause Treacher Collins syndrome. Nature Genetics 43: 20 EP -. doi: 10.1038/ng.724

84. Schaefer E, Collet C, Genevieve D et al. (2014) Autosomal recessive POLR1D mutation with decrease of TCOF1 mRNA is responsible for Treacher Collins syndrome. Genetics In Medicine 16: 720 EP -. doi: 10.1038/gim.2014.12
85. Valdez BC, Henning D, So RB et al. (2004) The Treacher Collins syndrome (TCOF1) gene product is involved in ribosomal DNA gene transcription by interacting with upstream binding factor. Proceedings of the National Academy of Sciences 101(29): 10709–10714. doi: 10.1073/pnas.0402492101
86. Hayano T, Yanagida M, Yamauchi Y et al. (2003) Proteomic Analysis of Human Nop56p-associated Pre-ribosomal Ribonucleoprotein Complexes. Journal of Biological Chemistry 278(36): 34309–34319. doi: 10.1074/jbc.M304304200
87. Dixon J, Jones NC, Sandell LL et al. (2006) Tcof1/Treacle is required for neural crest cell formation and proliferation deficiencies that cause craniofacial abnormalities. Proceedings of the National Academy of Sciences 103(36): 13403–13408. doi: 10.1073/pnas.0603730103
88. Yelick PC, Trainor PA (2015) Ribosomopathies: Global process, tissue specific defects. Rare Diseases 3(1): e1025185. doi: 10.1080/21675511.2015.1025185
89. Trainor PA, Merrill AE (2014) Ribosome biogenesis in skeletal development and the pathogenesis of skeletal disorders. Biochimica et Biophysica Acta (BBA) - Molecular Basis of Disease 1842(6): 769–778. doi: 10.1016/j.bbadis.2013.11.010
90. Pestov DG, Strezoska Z, Lau LF (2001) Evidence of p53-Dependent Cross-Talk between Ribosome Biogenesis and the Cell Cycle: Effects of Nucleolar Protein Bop1 on G1/S Transition. Molecular and Cellular Biology 21(13): 4246–4255. doi: 10.1128/MCB.21.13.4246-4255.2001
91. Chakraborty A, Uechi T, Kenmochi N (2011) Guarding the 'translation apparatus': defective ribosome biogenesis and the p53 signaling pathway. WIREs RNA 2(4): 507–522. doi: 10.1002/wrna.73
92. Sakai D, Dixon J, Achilleos A et al. (2016) Prevention of Treacher Collins syndrome craniofacial anomalies in mouse models via maternal antioxidant supplementation. Nature Communications 7. doi: 10.1038/ncomms10328
93. Weiner AMJ, Scampoli NL, Calcaterra NB (2012) Fishing the Molecular Bases of Treacher Collins Syndrome. PLoS ONE 7(1): e29574. doi: 10.1371/journal.pone.0029574
94. Jones NC, Lynn ML, Gaudenz K et al. (2008) Prevention of the neurocristopathy Treacher Collins syndrome through inhibition of p53 function. Nature Medicine 14: 125 EP -. doi: 10.1038/nm1725
95. Hoeijmakers JHJ (2009) DNA Damage, Aging, and Cancer. N Engl J Med 361(15): 1475–1485. doi: 10.1056/NEJMra0804615
96. Ciccia A, Elledge SJ (2010) The DNA Damage Response: Making It Safe to Play with Knives. Molecular Cell 40(2): 179–204. doi: 10.1016/j.molcel.2010.09.019
97. Jackson SP, Bartek J (2009) The DNA-damage response in human biology and disease. Nature 461: 1071 EP -. doi: 10.1038/nature08467
98. Polo SE, Jackson SP (2011) Dynamics of DNA damage response proteins at DNA breaks: a focus on protein modifications. Genes & Development 25(5): 409–433. doi: 10.1101/gad.2021311
99. Khanna KK, Jackson SP (2001) DNA double-strand breaks: signaling, repair and the cancer connection. Nature Genetics 27: 247 EP -. doi: 10.1038/85798
100. Pfeifer GP, Besaratinia A (2012) UV wavelength-dependent DNA damage and human non-melanoma and melanoma skin cancer. Photochem. Photobiol. Sci. 11(1): 90–97. doi: 10.1039/C1PP05144J

101. Mouret S, Baudouin C, Charveron M et al. (2006) Cyclobutane pyrimidine dimers are predominant DNA lesions in whole human skin exposed to UVA radiation. Proceedings of the National Academy of Sciences 103(37): 13765–13770. doi: 10.1073/pnas.0604213103
102. Murray HC, Maltby VE, Smith DW et al. (2016) Nucleotide excision repair deficiency in melanoma in response to UVA. Exp Hematol Oncol 5. doi: 10.1186/s40164-016-0035-4
103. Wiseman H, Halliwell B (1996) Damage to DNA by reactive oxygen and nitrogen species: role in inflammatory disease and progression to cancer. Biochem J 313(Pt 1): 17–29
104. Radi R (2013) Peroxynitrite, a Stealthy Biological Oxidant. J. Biol. Chem. 288(37): 26464–26472. doi: 10.1074/jbc.R113.472936
105. Di Meo S, Reed TT, Venditti P et al. (2016) Role of ROS and RNS Sources in Physiological and Pathological Conditions. Oxidative Medicine and Cellular Longevity 2016(22): 1–44. doi: 10.1155/2016/1245049
106. Balasubramanian B, Pogozelski WK, Tullius TD (1998) DNA strand breaking by the hydroxyl radical is governed by the accessible surface areas of the hydrogen atoms of the DNA backbone. Proceedings of the National Academy of Sciences 95(17): 9738–9743. doi: 10.1073/pnas.95.17.9738
107. Halliwell B, Whiteman M (2004) Measuring reactive species and oxidative damage in vivo and in cell culture: how should you do it and what do the results mean? British Journal of Pharmacology 142(2): 231–255. doi: 10.1038/sj.bjp.0705776
108. Collins AR, Cadet J, Mőller L et al. (2004) Are we sure we know how to measure 8-oxo-7,8-dihydroguanine in DNA from human cells? Archives of Biochemistry and Biophysics 423(1): 57–65. doi: 10.1016/j.abb.2003.12.022
109. Yoshihara M, Jiang L, Akatsuka S et al. (2014) Genome-wide Profiling of 8-Oxoguanine Reveals Its Association with Spatial Positioning in Nucleus. DNA Research 21(6): 603–612. doi: 10.1093/dnares/dsu023
110. (2014) Correction: Replicative Bypass of Abasic Site in Escherichia coli and Human Cells: Similarities and Differences. PLoS ONE 9(10): e112506. doi: 10.1371/journal.pone.0112506
111. Yu S-L, Lee S-K, Johnson RE et al. (2003) The Stalling of Transcription at Abasic Sites Is Highly Mutagenic. Molecular and Cellular Biology 23(1): 382–388. doi: 10.1128/MCB.23.1.382-388.2003
112. Kow YW (2002) Repair of deaminated bases in DNA. Free Radic Biol Med 33(7): 886–893
113. Phaniendra A, Jestadi DB, Periyasamy L (2015) Free Radicals: Properties, Sources, Targets, and Their Implication in Various Diseases. Ind J Clin Biochem 30(1): 11–26. doi: 10.1007/s12291-014-0446-0
114. Kawanishi S, Hiraku Y, Pinlaor S et al. (2006) Oxidative and nitrative DNA damage in animals and patients with inflammatory diseases in relation to inflammation-related carcinogenesis. Biol Chem 387(4): 365–372. doi: 10.1515/BC.2006.049
115. Zhang X-P, Liu F, Wang W (2011) Two-phase dynamics of p53 in the DNA damage response. Proceedings of the National Academy of Sciences of the United States of America 108(22): 8990–8995. doi: 10.1073/pnas.1100600108
116. Speidel D (2015) The role of DNA damage responses in p53 biology. Archives of Toxicology 89(4): 501–517. doi: 10.1007/s00204-015-1459-z
117. Vousden KH, Lane DP (2007) p53 in health and disease. Nature Reviews Molecular Cell Biology 8: 275 EP -. doi: 10.1038/nrm2147
118. Freed-Pastor WA, Prives C (2012) Mutant p53: one name, many proteins. Genes & Development 26(12): 1268–1286. doi: 10.1101/gad.190678.112

119. Lakin ND, Jackson SP (1999) Regulation of p53 in response to DNA damage. Oncogene 18(53): 7644. doi: 10.1038/sj.onc.1203015
120. Batchelor E, Loewer A, Lahav G (2009) The ups and downs of p53: Understanding protein dynamics in single cells. Nat Rev Cancer 9(5): 371–377. doi: 10.1038/nrc2604
121. Kruse J-P, Gu W (2008) SnapShot: p53 posttranslational modifications. Cell 133(5): 930-30.e1. doi: 10.1016/j.cell.2008.05.020
122. Liu Y (2001) p53 protein at the hub of cellular DNA damage response pathways through sequence-specific and non-sequence-specific DNA binding. Carcinogenesis 22(6): 851–860. doi: 10.1093/carcin/22.6.851
123. Appella E, Anderson CW (2001) Post-translational modifications and activation of p53 by genotoxic stresses. European Journal of Biochemistry 268(10): 2764–2772. doi: 10.1046/j.1432-1327.2001.02225.x
124. Meek DW, Anderson CW (2009) Posttranslational modification of p53: cooperative integrators of function. Cold Spring Harb Perspect Biol 1(6): a000950. doi: 10.1101/cshperspect.a000950
125. Xu Y (2003) Regulation of p53 responses by post-translational modifications. Cell Death And Differentiation 10: 400 EP -. doi: 10.1038/sj.cdd.4401182
126. Kruse J-P, Gu W (2009) Modes of p53 regulation. Cell 137(4): 609–622. doi: 10.1016/j.cell.2009.04.050
127. Toledo F, Wahl GM (2006) Regulating the p53 pathway: in vitro hypotheses, in vivo veritas. Nature Reviews Cancer 6: 909 EP -. doi: 10.1038/nrc2012
128. Chehab NH, Malikzay A, Stavridi ES et al. (1999) Phosphorylation of Ser-20 mediates stabilization of human p53 in response to DNA damage. Proceedings of the National Academy of Sciences 96(24): 13777–13782. doi: 10.1073/pnas.96.24.13777
129. Haupt Y, Maya R, Kazaz A et al. (1997) Mdm2 promotes the rapid degradation of p53. Nature 387(6630): 296–299. doi: 10.1038/387296a0
130. Kubbutat MH, Jones SN, Vousden KH (1997) Regulation of p53 stability by Mdm2. Nature 387(6630): 299–303. doi: 10.1038/387299a0
131. Midgley CA, Lane DP (1997) p53 protein stability in tumour cells is not determined by mutation but is dependent on Mdm2 binding. Oncogene 15(10): 1179–1189. doi: 10.1038/sj.onc.1201459
132. Dai C, Gu W (2010) p53 post-translational modification: deregulated in tumorigenesis. Trends Mol Med 16(11): 528–536. doi: 10.1016/j.molmed.2010.09.002
133. Grossman SR (2001) p300/CBP/p53 interaction and regulation of the p53 response. European Journal of Biochemistry 268(10): 2773–2778. doi: 10.1046/j.1432-1327.2001.02226.x
134. Ito A, Lai C-H, Zhao X et al. (2001) p300/CBP-mediated p53 acetylation is commonly induced by p53-activating agents and inhibited by MDM2. The EMBO Journal 20(6): 1331–1340. doi: 10.1093/emboj/20.6.1331
135. Brooks CL, Gu W (2011) The impact of acetylation and deacetylation on the p53 pathway. Protein Cell 2(6): 456–462. doi: 10.1007/s13238-011-1063-9
136. Contreras AU, Mebratu Y, Delgado M et al. (2013) Deacetylation of p53 induces autophagy by suppressing Bmf expression. J Cell Biol 201(3): 427–437. doi: 10.1083/jcb.201205064
137. Luo J, Su F, Chen D et al. (2000) Deacetylation of p53 modulates its effect on cell growth and apoptosis. Nature 408(6810): 377–381. doi: 10.1038/35042612
138. Ting P-C, Wu L-H, Wang DL (2017) Sirtuin-1 deacetylation of p53 plays a role in shear stress-induced autophagy in endothelial cells. The FASEB Journal 31(1_supplement): lb662-lb662. doi: 10.1096/fasebj.31.1_supplement.lb662

139. Chuikov S, Kurash JK, Wilson JR et al. (2004) Regulation of p53 activity through lysine methylation. Nature 432(7015): 353–360. doi: 10.1038/nature03117
140. Huang J, Perez-Burgos L, Placek BJ et al. (2006) Repression of p53 activity by Smyd2-mediated methylation. Nature 444(7119): 629–632. doi: 10.1038/nature05287
141. Shi X, Kachirskaia I, Yamaguchi H et al. (2007) Modulation of p53 function by SET8-mediated methylation at lysine 382. Molecular Cell 27(4): 636–646. doi: 10.1016/j.molcel.2007.07.012
142. Lee M-H, Na H, Kim E-J et al. (2012) Poly(ADP-ribosyl)ation of p53 induces gene-specific transcriptional repression of MTA1. Oncogene 31: 5099 EP -. doi: 10.1038/onc.2012.2
143. Simbulan-Rosenthal CM, Rosenthal DS, Luo R et al. (2001) Poly(ADP-ribosyl)ation of p53 In Vitro and In Vivo Modulates Binding to its DNA Consensus Sequence1. Neoplasia 3(3): 179–188
144. Wang L, Wu Q, Qiu P et al. (2001) Analyses of p53 target genes in the human genome by bioinformatic and microarray approaches. J. Biol. Chem. 276(47): 43604–43610. doi: 10.1074/jbc.M106570200
145. Wei C-L, Wu Q, Vega VB et al. (2006) A Global Map of p53 Transcription-Factor Binding Sites in the Human Genome. Cell 124(1): 207–219. doi: 10.1016/j.cell.2005.10.043
146. SÃ¡nchez Y, Segura V, MarÃ-n-BÃ©jar O et al. (2014) Genome-wide analysis of the human p53 transcriptional network unveils a lncRNA tumour suppressor signature. Nature Communications 5: 5812 EP -. doi: 10.1038/ncomms6812
147. Bayer FE, Zimmermann M, Fischer P et al. (2017) p53 and cyclin G cooperate in mediating genome stability in somatic cells of Drosophila. Scientific Reports 7(1): 17890. doi: 10.1038/s41598-017-17973-z
148. Kimura SH, Nojima H (2002) Cyclin G1 associates with MDM2 and regulates accumulation and degradation of p53 protein. Genes Cells 7(8): 869–880
149. Okamoto K, Li H, Jensen MR et al. (2002) Cyclin G recruits PP2A to dephosphorylate Mdm2. Molecular Cell 9(4): 761–771
150. Zhao L, Samuels T, Winckler S et al. (2003) Cyclin G1 has growth inhibitory activity linked to the ARF-Mdm2-p53 and pRb tumor suppressor pathways. Mol Cancer Res 1(3): 195–206
151. Fischer M (2017) Census and evaluation of p53 target genes. Oncogene 36: 3943 EP -. doi: 10.1038/onc.2016.502
152. Ford JM, Kastan MB (2014) 10 - DNA Damage Response Pathways and Cancer. In: Niederhuber JE, Armitage JO, Doroshow JH et al. (eds) Abeloff's Clinical Oncology (Fifth Edition). Content Repository Only!, Philadelphia, 142-153.e3
153. Zhang D, Tang B, Xie X et al. (2015) The interplay between DNA repair and autophagy in cancer therapy. Cancer Biology & Therapy 16(7): 1005–1013. doi: 10.1080/15384047.2015.1046022
154. Chen X, Ko LJ, Jayaraman L et al. (1996) p53 levels, functional domains, and DNA damage determine the extent of the apoptotic response of tumor cells. Genes & Development 10(19): 2438–2451. doi: 10.1101/gad.10.19.2438
155. Bartek J, Lukas J (2001) Pathways governing G1/S transition and their response to DNA damage. FEBS Letters 490(3): 117–122. doi: 10.1016/S0014-5793(01)02114-7
156. Hyun S-Y, Jang Y-J (2014) p53 activates G1 checkpoint following DNA damage by doxorubicin during transient mitotic arrest. Oncotarget 6(7): 4804–4815
157. D'Orazi G, Cecchinelli B, Bruno T et al. (2002) Homeodomain-interacting protein kinase-2 phosphorylates p53 at Ser 46 and mediates apoptosis. Nat Cell Biol 4(1): 11–19. doi: 10.1038/ncb714
158. Okamura S, Arakawa H, Tanaka T et al. (2001) p53DINP1, a p53-inducible gene, regulates p53-dependent apoptosis. Molecular Cell 8(1): 85–94

159. Feng L, Hollstein M, Xu Y (2006) Ser46 phosphorylation regulates p53-dependent apoptosis and replicative senescence. Cell Cycle 5(23): 2812–2819. doi: 10.4161/cc.5.23.3526
160. Sykes SM, Stanek TJ, Frank A et al. (2009) Acetylation of the DNA binding domain regulates transcription-independent apoptosis by p53. J Biol Chem 284(30): 20197–20205. doi: 10.1074/jbc.M109.026096
161. Collins HM, Abdelghany MK, Messmer M et al. (2013) Differential effects of garcinol and curcumin on histone and p53 modifications in tumour cells. BMC Cancer 13: 37. doi: 10.1186/1471-2407-13-37
162. Dasika GK, Lin S-CJ, Zhao S et al. (1999) DNA damage-induced cell cycle checkpoints and DNA strand break repair in development and tumorigenesis. Oncogene 18(55): 7883. doi: 10.1038/sj.onc.1203283
163. Bartek J, Lukas C, Lukas J (2004) Checking on DNA damage in S phase. Nature Reviews Molecular Cell Biology 5(10): 792. doi: 10.1038/nrm1493
164. Mailand N (2000) Rapid Destruction of Human Cdc25A in Response to DNA Damage. Science 288(5470): 1425–1429. doi: 10.1126/science.288.5470.1425
165. Molinari M, Mercurio C, Dominguez J et al. (2000) Human Cdc25 A inactivation in response to S phase inhibition and its role in preventing premature mitosis. EMBO reports 1(1): 71–79. doi: 10.1093/embo-reports/kvd018
166. Iyer DR, Rhind N (2017) The Intra-S Checkpoint Responses to DNA Damage. Genes (Basel) 8(2). doi: 10.3390/genes8020074
167. Willis N, Rhind N (2009) Regulation of DNA replication by the S-phase DNA damage checkpoint. Cell Div 4: 13. doi: 10.1186/1747-1028-4-13
168. Lamb JR, Petit-Frère C, Broughton BC et al. (1989) Inhibition of DNA replication by ionizing radiation is mediated by a trans-acting factor. Int J Radiat Biol 56(2): 125–130
169. Lopes M, Cotta-Ramusino C, Pellicioli A et al. (2001) The DNA replication checkpoint response stabilizes stalled replication forks. Nature 412(6846): 557–561. doi: 10.1038/35087613
170. Szyjka SJ, Aparicio JG, Viggiani CJ et al. (2008) Rad53 regulates replication fork restart after DNA damage in Saccharomyces cerevisiae. Genes & Development 22(14): 1906–1920. doi: 10.1101/gad.1660408
171. Guha G, Lu W, Li S et al. (2015) Novel Pactamycin Analogs Induce p53 Dependent Cell-Cycle Arrest at S-Phase in Human Head and Neck Squamous Cell Carcinoma (HNSCC) Cells. PLoS ONE 10(5): e0125322. doi: 10.1371/journal.pone.0125322
172. Agarwal ML, Agarwal A, Taylor WR et al. (1998) A p53-dependent S-phase checkpoint helps to protect cells from DNA damage in response to starvation for pyrimidine nucleotides. PNAS 95(25): 14775–14780
173. Shimura T, Inoue M, Taga M et al. (1998) p53-Dependent S-Phase Damage Checkpoint and Pronuclear Cross Talk in Mouse Zygotes with X-Irradiated Sperm. Mol. Cell. Biol. 95(25): 14775–14780. doi: 10.1128/MCB.22.7.2220-2228.2002
174. Calonge TM, O'Connell MJ (2008) Turning off the G2 DNA damage checkpoint. DNA Repair 7(2): 136–140. doi: 10.1016/j.dnarep.2007.07.017
175. DiPaola RS (2002) To Arrest or Not To G2-M Cell-Cycle Arrest : Commentary re: A. K. Tyagi et al., Silibinin Strongly Synergizes Human Prostate Carcinoma DU145 Cells to Doxorubicin-induced Growth Inhibition, G2-M Arrest, and Apoptosis. Clin. Cancer Res., 8: 3512–3519, 2002. Clin Cancer Res 8(11): 3311–3314. doi: 10.1385/1-59259-788-2:051
176. Schönthal AH (ed) (2004) Checkpoint controls and cancer. Methods in molecular biology, 280-281. Human Press, Totowa, N.J.

177. Stark GR, Taylor WR (2004) Analyzing the G2/M Checkpoint. In: Schönthal AH (ed) Checkpoint controls and cancer. Human Press, Totowa, N.J., pp 51–82
178. Rouse J, Jackson SP (2002) Interfaces between the detection, signaling, and repair of DNA damage. Science 297(5581): 547–551. doi: 10.1126/science.1074740
179. Houtgraaf JH, Versmissen J, van der Giessen WJ (2006) A concise review of DNA damage checkpoints and repair in mammalian cells. Cardiovasc Revasc Med 7(3): 165–172. doi: 10.1016/j.carrev.2006.02.002
180. Sancar A, Lindsey-Boltz LA, Unsal-Kaçmaz K et al. (2004) Molecular mechanisms of mammalian DNA repair and the DNA damage checkpoints. Annu Rev Biochem 73: 39–85. doi: 10.1146/annurev.biochem.73.011303.073723
181. Fielder E, Zglinicki T von, Jurk D (2017) The DNA Damage Response in Neurons: Die by Apoptosis or Survive in a Senescence-Like State? J Alzheimers Dis 60(s1): S107-S131. doi: 10.3233/JAD-161221
182. Plesca D, Mazumder S, Almasan A (2008) DNA Damage Response and Apoptosis. Methods Enzymol 446: 107–122. doi: 10.1016/S0076-6879(08)01606-6
183. Roos WP, Thomas AD, Kaina B (2016) DNA damage and the balance between survival and death in cancer biology. Nat Rev Cancer 16(1): 20–33. doi: 10.1038/nrc.2015.2
184. Rosen DB, Putta S, Covey T et al. (2010) Distinct patterns of DNA damage response and apoptosis correlate with Jak/Stat and PI3kinase response profiles in human acute myelogenous leukemia. PLoS ONE 5(8): e12405. doi: 10.1371/journal.pone.0012405
185. Haupt S, Berger M, Goldberg Z et al. (2003) Apoptosis - the p53 network. J Cell Sci 116(Pt 20): 4077–4085. doi: 10.1242/jcs.00739
186. Schuler M, Green DR (2001) Mechanisms of p53-dependent apoptosis. Biochem Soc Trans 29(Pt 6): 684–688
187. Amaral JD, Xavier JM, Steer CJ et al. (2010) The role of p53 in apoptosis. Discov Med 9(45): 145–152
188. Attardi LD, Reczek EE, Cosmas C et al. (2000) PERP, an apoptosis-associated target of p53, is a novel member of the PMP-22/gas3 family. Genes & Development 14(6): 704–718
189. Bennett M, Macdonald K, Chan SW et al. (1998) Cell surface trafficking of Fas: a rapid mechanism of p53-mediated apoptosis. Science 282(5387): 290–293
190. Owen-Schaub LB, Zhang W, Cusack JC et al. (1995) Wild-type human p53 and a temperature-sensitive mutant induce Fas/APO-1 expression. Mol. Cell. Biol. 15(6): 3032–3040. doi: 10.1128/MCB.15.6.3032
191. Yada S, Takamura N, Inagaki-Ohara K et al. (2005) The Role of p53 and Fas in a Model of Acute Murine Graft-versus-Host Disease. The Journal of Immunology 174(3): 1291–1297. doi: 10.4049/jimmunol.174.3.1291
192. Certo M, Moore VDG, Nishino M et al. (2006) Mitochondria primed by death signals determine cellular addiction to antiapoptotic BCL-2 family members. Cancer Cell 9(5): 351–365. doi: 10.1016/j.ccr.2006.03.027
193. Schuler M, Bossy-Wetzel E, Goldstein JC et al. (2000) p53 Induces Apoptosis by Caspase Activation through Mitochondrial Cytochrome c Release. J Biol Chem 275(10): 7337–7342. doi: 10.1074/jbc.275.10.7337
194. Zhang Y, Xing D, Liu L (2009) PUMA promotes Bax translocation by both directly interacting with Bax and by competitive binding to Bcl-X L during UV-induced apoptosis. Mol Biol Cell 20(13): 3077–3087. doi: 10.1091/mbc.e08-11-1109
195. Roy S, Nicholson DW (2000) Cross-Talk in Cell Death Signaling. J Exp Med 192(8): f21-6

196. Wei MC, Lindsten T, Mootha VK et al. (2000) tBID, a membrane-targeted death ligand, oligomerizes BAK to release cytochrome c. Genes Dev. 14(16): 2060–2071. doi: 10.1101/gad.14.16.2060
197. Saraste A (2000) Morphologic and biochemical hallmarks of apoptosis. Cardiovascular Research 45(3): 528–537. doi: 10.1016/S0008-6363(99)00384-3
198. Häcker G (2000) The morphology of apoptosis. Cell and Tissue Research 301(1): 5–17
199. Kerr JFR, Wyllie AH, Currie AR (1972) Apoptosis: A Basic Biological Phenomenon with Wide-ranging Implications in Tissue Kinetics. Br J Cancer 26(4): 239–257
200. Collins JA, Schandl CA, Young KK et al. (1997) Major DNA Fragmentation Is a Late Event in Apoptosis. Journal of Histochemistry & Cytochemistry 45(7): 923–934. doi: 10.1177/002215549704500702
201. Sgonc R, Gruschwitz MS, Dietrich H et al. (1996) Endothelial cell apoptosis is a primary pathogenetic event underlying skin lesions in avian and human scleroderma. J Clin Invest 98(3): 785–792
202. Gorczyca W, Gong J, Darzynkiewicz Z (1993) Detection of DNA strand breaks in individual apoptotic cells by the in situ terminal deoxynucleotidyl transferase and nick translation assays. Cancer Res 53(8): 1945–1951
203. Sgonc R, Gruber J (1998) Apoptosis detection: an overview. Experimental Gerontology 33(6): 525–533. doi: 10.1016/S0531-5565(98)00031-X
204. Porter AG, Jänicke RU (1999) Emerging roles of caspase-3 in apoptosis. Cell Death And Differentiation 6(2): 99–104. doi: 10.1038/sj.cdd.4400476
205. Wolf BB, Schuler M, Echeverri F et al. (1999) Caspase-3 Is the Primary Activator of Apoptotic DNA Fragmentation via DNA Fragmentation Factor-45/Inhibitor of Caspase-activated DNase Inactivation. J Biol Chem 274(43): 30651–30656. doi: 10.1074/jbc.274.43.30651
206. Jacobson MD, Weil M, Raff MC (1997) Programmed Cell Death in Animal Development. Cell 88(3): 347–354. doi: 10.1016/S0092-8674(00)81873-5
207. Tata JR (1966) Requirement for RNA and protein synthesis for induced regression of the tadpole tail in organ culture. Developmental Biology 13(1): 77–94
208. Elmore S (2007) Apoptosis: a review of programmed cell death. Toxicol Pathol 35(4): 495–516. doi: 10.1080/01926230701320337
209. Grodzicky T, Elkon KB (2002) Apoptosis: a case where too much or too little can lead to autoimmunity. Mt Sinai J Med 69(4): 208–219
210. Kerr JF, Winterford CM, Harmon BV (1994) Apoptosis. Its significance in cancer and cancer therapy. Cancer 73(8): 2013–2026
211. Halliwell B, Gutteridge JMC (2007) Free radicals in biology and medicine, 4th ed. Oxford University Press, Oxford
212. Halliwell B (2006) Reactive species and antioxidants. Redox biology is a fundamental theme of aerobic life. Plant Physiol 141(2): 312–322. doi: 10.1104/pp.106.077073
213. Sturmey RG, Hawkhead JA, Barker EA et al. (2009) DNA damage and metabolic activity in the preimplantation embryo. Hum Reprod 24(1): 81–91. doi: 10.1093/humrep/den346
214. Fischer B, Bavister BD (1993) Oxygen tension in the oviduct and uterus of rhesus monkeys, hamsters and rabbits. J Reprod Fertil 99(2): 673–679
215. Gardner DK, Lane M (1996) Alleviation of the '2-cell block' and development to the blastocyst of CF1 mouse embryos: role of amino acids, EDTA and physical parameters. Hum Reprod 11(12): 2703–2712

216. Thompson JG, Simpson AC, Pugh PA et al. (1990) Effect of oxygen concentration on in-vitro development of preimplantation sheep and cattle embryos. J Reprod Fertil 89(2): 573–578
217. Yedwab GA, Paz G, Homonnai TZ et al. (1976) The temperature, pH, and partial pressure of oxygen in the cervix and uterus of women and uterus of rats during the cycle. Fertil Steril 27(3): 304–309
218. Takahashi M, Keicho K, Takahashi H et al. (2000) Effect of oxidative stress on development and DNA damage in in-vitro cultured bovine embryos by comet assay. Theriogenology 54(1): 137–145. doi: 10.1016/S0093-691X(00)00332-0
219. Park SY, Kim EY, Cui XS et al. (2006) Increase in DNA fragmentation and apoptosis-related gene expression in frozen-thawed bovine blastocysts. Zygote 14(2): 125–131. doi: 10.1017/S0967199406003649
220. Rausell F, Pertusa JF, Gómez-Piquer V et al. (2007) Beneficial effects of dithiothreitol on relative levels of glutathione S-transferase activity and thiols in oocytes, and cell number, DNA fragmentation and allocation at the blastocyst stage in the mouse. Mol Reprod Dev 74(7): 860–869. doi: 10.1002/mrd.20569
221. Lamarre SG, Le François NR, Driedzic WR et al. (2009) Protein synthesis is lowered while 20S proteasome activity is maintained following acclimation to low temperature in juvenile spotted wolffish (Anarhichas minor Olafsen). J Exp Biol 212(Pt 9): 1294–1301. doi: 10.1242/jeb.028290
222. Hermes-Lima M, Zenteno-Savín T (2002) Animal response to drastic changes in oxygen availability and physiological oxidative stress. Comparative Biochemistry and Physiology Part C: Toxicology & Pharmacology 133(4): 537–556. doi: 10.1016/S1532-0456(02)00080-7
223. Inupakutika MA, Sengupta S, Devireddy AR et al. (2016) The evolution of reactive oxygen species metabolism. J Exp Bot 67(21): 5933–5943. doi: 10.1093/jxb/erw382
224. Sakai D, Trainor PA (2016) Face off against ROS: Tcof1/Treacle safeguards neuroepithelial cells and progenitor neural crest cells from oxidative stress during craniofacial development. Dev Growth Differ 58(7): 577–585. doi: 10.1111/dgd.12305
225. Rinon A, Molchadsky A, Nathan E et al. (2011) p53 coordinates cranial neural crest cell growth and epithelial-mesenchymal transition/delamination processes. Development (Cambridge, England) 138(9): 1827–1838. doi: 10.1242/dev.053645
226. Lee K-C, Goh WLP, Xu M et al. (2008) Detection of the p53 response in zebrafish embryos using new monoclonal antibodies. Oncogene 27(5): 629–640. doi: 10.1038/sj.onc.1210695
227. Zhang Z, Lei A, Xu L et al. (2017) Similarity in gene-regulatory networks suggests that cancer cells share characteristics of embryonic neural cells. J Biol Chem 292(31): 12842–12859. doi: 10.1074/jbc.M117.785865
228. Xia Z, Tong X, Liang F et al. (2013) Eif3ba regulates cranial neural crest development by modulating p53 in zebrafish. Developmental Biology 381(1): 83–96. doi: 10.1016/j.ydbio.2013.06.009
229. Kitami K, Kitami M, Kaku M et al. (2018) BRCA1 and BRCA2 tumor suppressors in neural crest cells are essential for craniofacial bone development. PLoS Genet 14(5): e1007340. doi: 10.1371/journal.pgen.1007340
230. Gessert S, Maurus D, Rössner A et al. (2007) Pescadillo is required for Xenopus laevis eye development and neural crest migration. Developmental Biology 310(1): 99–112. doi: 10.1016/j.ydbio.2007.07.037
231. Morgan SC, Lee H-Y, Relaix F et al. (2008) Cardiac outflow tract septation failure in Pax3-deficient embryos is due to p53-dependent regulation of migrating cardiac neural crest. Mech Dev 125(9-10): 757–767. doi: 10.1016/j.mod.2008.07.003

232. Pani L, Horal M, Loeken MR (2002) Rescue of neural tube defects in Pax-3-deficient embryos by p53 loss of function: implications for Pax-3- dependent development and tumorigenesis. Genes & Development 16(6): 676–680. doi: 10.1101/gad.969302
233. Konstantinidou C, Taraviras S, Pachnis V (2016) Geminin prevents DNA damage in vagal neural crest cells to ensure normal enteric neurogenesis. BMC Biol 14(1): 94. doi: 10.1186/s12915-016-0314-x
234. Burstyn-Cohen T, Kalcheim C (2002) Association between the cell cycle and neural crest delamination through specific regulation of G1/S transition. Developmental Cell 3(3): 383–395
235. Paglini MG, Rovasio RA (1994) Cell cycle of neural crest cells in the early migratory stage in vivo. Cell Prolif 27(9): 571–578. doi: 10.1111/j.1365-2184.1994.tb01494.x
236. Wainwright LJ, Lasorella A, Iavarone A (2001) Distinct mechanisms of cell cycle arrest control the decision between differentiation and senescence in human neuroblastoma cells. Proceedings of the National Academy of Sciences of the United States of America 98(16): 9396–9400. doi: 10.1073/pnas.161288698
237. Hörmanseder E, Tischer T, Mayer TU (2013) Modulation of cell cycle control during oocyte-to-embryo transitions. The EMBO Journal 32(16): 2191–2203. doi: 10.1038/emboj.2013.164
238. Strathmann RR, Staver JM, Hoffman JR (2002) Risk and the evolution of cell-cycle durations of embryos. Evolution 56(4): 708–720
239. Newport J, Kirschner M (1982) A major developmental transition in early Xenopus embryos: II. Control of the onset of transcription. Cell 30(3): 687–696
240. Kappas NC, Savage P, Chen KC et al. (2000) Dissection of the XChk1 Signaling Pathway in Xenopus laevis Embryos. Mol Biol Cell 11(9): 3101–3108
241. Nakajo N, Oe T, Uto K et al. (1999) Involvement of Chk1 kinase in prophase I arrest of Xenopus oocytes. Developmental Biology 207(2): 432–444. doi: 10.1006/dbio.1998.9178
242. Hensey C, Gautier J (1997) A developmental timer that regulates apoptosis at the onset of gastrulation. Mech Dev 69(1): 183–195. doi: 10.1016/S0925-4773(97)00191-3
243. Stack JH, Newport JW (1997) Developmentally regulated activation of apoptosis early in Xenopus gastrulation results in cyclin A degradation during interphase of the cell cycle. Development (Cambridge, England) 124(16): 3185–3195
244. Sible JC, Anderson JA, Lewellyn AL et al. (1997) Zygotic transcription is required to block a maternal program of apoptosis in Xenopus embryos. Developmental Biology 189(2): 335–346. doi: 10.1006/dbio.1997.8683
245. Zhang M, Kothari P, Mullins M et al. (2014) Regulation of zygotic genome activation and DNA damage checkpoint acquisition at the mid-blastula transition. Cell Cycle 13(24): 3828–3838. doi: 10.4161/15384101.2014.967066
246. Chakraborti S, Chakraborty S, Saha S et al. (2017) PEG-functionalized zinc oxide nanoparticles induce apoptosis in breast cancer cells through reactive oxygen species-dependent impairment of DNA damage repair enzyme NEIL2. Free Radic Biol Med 103: 35–47. doi: 10.1016/j.freeradbiomed.2016.11.048
247. Sarker AH, Chatterjee A, Williams M et al. (2014) NEIL2 protects against oxidative DNA damage induced by sidestream smoke in human cells. PLoS ONE 9(3): e90261. doi: 10.1371/journal.pone.0090261
248. Gato WE, McGee SR, Hales DB et al. (2014) Time-Dependent Regulation of Apoptosis by AEN and BAX in Response to 2-Aminoanthracene Dietary Consumption. Toxicol Int 21(1): 57–64. doi: 10.4103/0971-6580.128796

249. Kawase T, Ichikawa H, Ohta T et al. (2008) p53 target gene AEN is a nuclear exonuclease required for p53-dependent apoptosis. Oncogene 27: 3797 EP -. doi: 10.1038/onc.2008.32
250. Brosh R, Sarig R, Natan EB et al. (2010) p53-dependent transcriptional regulation of EDA2R and its involvement in chemotherapy-induced hair loss. FEBS Letters 584(11): 2473–2477. doi: 10.1016/j.febslet.2010.04.058
251. Tanikawa C, Ri C, Kumar V et al. (2010) Crosstalk of EDA-A2/XEDAR in the p53 signaling pathway. Mol Cancer Res 8(6): 855–863. doi: 10.1158/1541-7786.MCR-09-0484
252. Liu J, Yu H, Hu W (2015) LIF is a new p53 negative regulator. J Nat Sci 1(7): e131-
253. Yu H, Yue X, Zhao Y et al. (2014) LIF negatively regulates tumour-suppressor p53 through Stat3/ID1/MDM2 in colorectal cancers. Nature Communications 5: 5218. doi: 10.1038/ncomms6218
254. Tarsounas M, Davies AA, West SC (2004) RAD51 localization and activation following DNA damage. Philos Trans R Soc Lond , B, Biol Sci 359(1441): 87–93. doi: 10.1098/rstb.2003.1368
255. Chae H-D, Mitton B, Lacayo NJ et al. (2015) Replication factor C3 is a CREB target gene that regulates cell cycle progression through the modulation of chromatin loading of PCNA. Leukemia 29(6): 1379–1389. doi: 10.1038/leu.2014.350
256. Takashima K, Oshiumi H, Takaki H et al. (2015) RIOK3-mediated phosphorylation of MDA5 interferes with its assembly and attenuates the innate immune response. Cell Reports 11(2): 192–200. doi: 10.1016/j.celrep.2015.03.027
257. Joachim J, Jefferies HBJ, Razi M et al. (2015) Activation of ULK Kinase and Autophagy by GABARAP Trafficking from the Centrosome Is Regulated by WAC and GM130. Molecular Cell 60(6): 899–913. doi: 10.1016/j.molcel.2015.11.018
258. Jiang K, Pereira E, Maxfield M et al. (2003) Regulation of Chk1 includes chromatin association and 14-3-3 binding following phosphorylation on Ser-345. J Biol Chem 278(27): 25207–25217. doi: 10.1074/jbc.M300070200
259. Liu Q, Guntuku S, Cui X-S et al. (2000) Chk1 is an essential kinase that is regulated by Atr and required for the G2/M DNA damage checkpoint. Genes & Development 14(12): 1448–1459
260. Zachos G, Black EJ, Walker M et al. (2007) Chk1 is required for spindle checkpoint function. Developmental Cell 12(2): 247–260. doi: 10.1016/j.devcel.2007.01.003
261. Zhao H, Piwnica-Worms H (2001) ATR-Mediated Checkpoint Pathways Regulate Phosphorylation and Activation of Human Chk1. Molecular and Cellular Biology 21(13): 4129–4139. doi: 10.1128/MCB.21.13.4129-4139.2001
262. Muller M (2002) Pyocyanin induces oxidative stress in human endothelial cells and modulates the glutathione redox cycle. Free Radical Biology and Medicine 33(11): 1527–1533. doi: 10.1016/S0891-5849(02)01087-0
263. Ran H, Hassett DJ, Lau GW (2003) Human targets of Pseudomonas aeruginosa pyocyanin. PNAS 100(24): 14315–14320. doi: 10.1073/pnas.2332354100
264. Calo E, Gu B, Bowen ME et al. (2018) Tissue-selective effects of nucleolar stress and rDNA damage in developmental disorders. Nature 554(7690): 112. doi: 10.1038/nature25449
265. Love NR, Chen Y, Ishibashi S et al. (2013) Amputation-induced reactive oxygen species are required for successful Xenopus tadpole tail regeneration. Nat Cell Biol 15(2): 222–228. doi: 10.1038/ncb2659
266. Nathan C, Cunningham-Bussel A (2013) Beyond oxidative stress: an immunologist's guide to reactive oxygen species. Nature Reviews Immunology 13(5): 349. doi: 10.1038/nri3423
267. Yang Y, Bazhin AV, Werner J et al. (2013) Reactive oxygen species in the immune system. Int Rev Immunol 32(3): 249–270. doi: 10.3109/08830185.2012.755176

268. Han Y, Ishibashi S, Iglesias-Gonzalez J et al. (2018) Ca2+-Induced Mitochondrial ROS Regulate the Early Embryonic Cell Cycle. Cell Reports 22(1): 218–231. doi: 10.1016/j.celrep.2017.12.042
269. Tadros W, Lipshitz HD (2009) The maternal-to-zygotic transition: a play in two acts. Development (Cambridge, England) 136(18): 3033–3042. doi: 10.1242/dev.033183
270. Schultz RM (1993) Regulation of zygotic gene activation in the mouse. Bioessays 15(8): 531–538. doi: 10.1002/bies.950150806
271. Kobayashi GS, Alvizi L, Sunaga DY et al. (2013) Susceptibility to DNA Damage as a Molecular Mechanism for Non-Syndromic Cleft Lip and Palate. PLOS ONE 8(6): e65677. doi: 10.1371/journal.pone.0065677
272. Hall S, McDermott C, Anoopkumar-Dukie S et al. (2016) Cellular Effects of Pyocyanin, a Secreted Virulence Factor of Pseudomonas aeruginosa. Toxins (Basel) 8(8). doi: 10.3390/toxins8080236
273. Jacox L, Sindelka R, Chen J et al. (2014) The extreme anterior domain is an essential craniofacial organizer acting through Kinin-Kallikrein signaling. Cell Reports 8(2): 596–609. doi: 10.1016/j.celrep.2014.06.026
274. Choi B-M, Pae H-O, Jang SI et al. (2002) Nitric oxide as a pro-apoptotic as well as anti-apoptotic modulator. J Biochem Mol Biol 35(1): 116–126
275. Messmer UK, Brüne B (1996) Nitric oxide-induced apoptosis: p53-dependent and p53-independent signalling pathways. Biochem J 319(Pt 1): 299–305
276. Xu Y, Xu C, Kato A et al. (2012) Tet3 CXXC Domain and Dioxygenase Activity Cooperatively Regulate Key Genes for Xenopus Eye and Neural Development. Cell 151(6): 1200–1213. doi: 10.1016/j.cell.2012.11.014
277. Nakatani T, Yamagata K, Kimura T et al. (2015) Stella preserves maternal chromosome integrity by inhibiting 5hmC-induced γH2AX accumulation. EMBO reports 16(5): 582–589. doi: 10.15252/embr.201439427
278. An J, González-Avalos E, Chawla A et al. (2015) Acute loss of TET function results in aggressive myeloid cancer in mice. Nature Communications 6: 10071. doi: 10.1038/ncomms10071
279. Kafer GR, Li X, Horii T et al. (2016) 5-Hydroxymethylcytosine Marks Sites of DNA Damage and Promotes Genome Stability. Cell Reports 14(6): 1283–1292. doi: 10.1016/j.celrep.2016.01.035
280. Cimmino L, Dawlaty MM, Ndiaye-Lobry D et al. (2015) TET1 is a tumor suppressor of hematopoietic malignancy. Nature Immunology 16: 653 EP -. doi: 10.1038/ni.3148
281. Jiang D, Wei S, Chen F et al. (2017) TET3-mediated DNA oxidation promotes ATR-dependent DNA damage response. EMBO reports 18(5): 781–796. doi: 10.15252/embr.201643179
282. Cortázar D, Kunz C, Selfridge J et al. (2011) Embryonic lethal phenotype reveals a function of TDG in maintaining epigenetic stability. Nature 470(7334): 419–423. doi: 10.1038/nature09672
283. Cortellino S, Xu J, Sannai M et al. (2011) Thymine DNA glycosylase is essential for active DNA demethylation by linked deamination-base excision repair. Cell 146(1): 67–79. doi: 10.1016/j.cell.2011.06.020
284. Hassan HM, Kolendowski B, Isovic M et al. (2017) Regulation of Active DNA Demethylation through RAR-Mediated Recruitment of a TET/TDG Complex. Cell Reports 19(8): 1685–1697. doi: 10.1016/j.celrep.2017.05.007
285. Ito K, Morita T (1995) Role of retinoic acid in mouse neural crest cell development in vitro. Dev Dyn 204(2): 211–218. doi: 10.1002/aja.1002040212
286. Jones NC, Trainor PA (2005) Role of morphogens in neural crest cell determination. J Neurobiol 64(4): 388–404. doi: 10.1002/neu.20162

287. Li N, Kelsh RN, Croucher P et al. (2010) Regulation of neural crest cell fate by the retinoic acid and Pparg signalling pathways. Development (Cambridge, England) 137(3): 389–394. doi: 10.1242/dev.044164
288. Nakamura T, Murakami K, Tada H et al. (2017) Thymine DNA glycosylase modulates DNA damage response and gene expression by base excision repair-dependent and independent mechanisms. Genes Cells 22(4): 392–405. doi: 10.1111/gtc.12481
289. Glassner BJ, Rasmussen LJ, Najarian MT et al. (1998) Generation of a strong mutator phenotype in yeast by imbalanced base excision repair. Proceedings of the National Academy of Sciences of the United States of America 95(17): 9997–10002
290. Kidane D, Murphy DL, Sweasy JB (2014) Accumulation of abasic sites induces genomic instability in normal human gastric epithelial cells during Helicobacter pylori infection. Oncogenesis 3: e128. doi: 10.1038/oncsis.2014.42
291. Sambrook J, Russell DW (2001) Molecular cloning: A laboratory manual / Joseph Sambrook, David W. Russell. Vol. 3, 3rd ed. Cold Spring Harbor Laboratory Press, Cold Spring Harbor, N.Y.
292. Nieuwkoop PD, Faber J (1994) Normal table of Xenopus laevis (Daudin): A systematical and chronological survey of the development from the fertilized egg till the end of metamorphosis / edited by P.D. Nieuwkoop and J. Faber ; with a new foreword by John Gerhart and Marc Kirschner. Garland Pub, New York, London
293. Livak KJ, Schmittgen TD (2001) Analysis of relative gene expression data using real-time quantitative PCR and the 2(-Delta Delta C(T)) Method. Methods 25(4): 402–408. doi: 10.1006/meth.2001.1262
294. Nakayama T, Blitz IL, Fish MB et al. (2014) Cas9-based genome editing in Xenopus tropicalis. Methods Enzymol 546: 355–375. doi: 10.1016/B978-0-12-801185-0.00017-9

8. List of abbreviations

$^{\bullet}OH$	Hydroxyl radical
$^{1}O2$	Singlet oxygen
5caC	5-carboxylcytosine
5fC	5-formylcytosine
5hmC	5-hydroxymethylcytosine
5hmU	5-hydroxymethyluracil
5mC	5-methylcytosine
ACS	Auriculo Condylar syndrome
AID/APOBEC	Activation Induced Deaminase/ Apolipoprotein B mRNA-editing Enzyme Complex
AP	Apurinic/apyrimidinic
APAF-1	Apoptotic protease-activating factor 1
APE1/Apex1	AP endonuclease
ATM	Ataxia telangiectasia mutated
ATR	Ataxia telangiectasia and Rad3-related protein
BA	Basihyal cartilage
BER	Base excision repair
BMP	Bone morphogenetic protein
BR	Branchial streams
BR	Branchial cartilage
CBP	CREB-binding protein
CE	Ceratohyal cartilage
ChIP-Seq	Chromatin immunoprecipitation sequencing
CPD	Cyclobutane pyrimidine dimer
CpG	Cytidine-guanosine
CS	Craniosynostosis
cyt c	cytochrome c
DDR	DNA damage response
DISC	Death inducing signaling complex
DNMT	DNA methyltransferase
DSB	Double strand break
EMT	Epithelial to mesenchymal transition
ENS	Enteric nervous system
ESC	Embryonic stem cell

FADD	Fas-associated death domain
FapyA	4,6-diamino-5-formamidopyrimidine
FapyG	2,6-diamino-4-hydroxy-5-formamidopyrimidine
FGF	Fibroblast growth factor
Gadd45	Growth Arrest and DNA Damage 45
GO	Gene ontology
H_2O_2	Hydrogen peroxide
HDAC	Histone deacetylase
HY	Hyoid
IR	Ionizing irradiation
MA	Mandibular
MBD2	Methyl-CpG-binding domain protein 2
MBT	Mid-blastula transition
MDM2	Mouse double minute protein 2
ME	Meckel's cartilage
MMR	Mismatch repair
MO	Morpholino
MutS	Mutator S
NCC	Neural crest cell
NCP	Neurocristopathy
NEIL	Nei-like DNA glycosylases
NER	Nuclear excision repair
NK	Natural killer
$NO^{\bullet}$	Nitric oxide
$NO_2^{\bullet}$	Nitric dioxide
NOS1	Nitric oxide synthase 1
$ONOO^{-}$	Peroxynitrite
$O^{\bullet -}_2$	Superoxide anion
POLR1C	RNA polymerase I and III subunit C
POLR1D	RNA polymerase I and III subunit D
PUMA	p53 upregulated modulator of apoptosis
RA	Retinoic acid
RNS	Reactive nitric species
ROS	Reactive oxygen species
SIRT1	Sirtuin1

SSB	Single strand break
St	Stage
T	Thymine
tBid	Truncated Bid
Tcof1	Treacle ribosome biogenesis factor 1
TCS	Treacher-Collins-Syndrome
TDG	Thymine DNA glycosylase
Tet	Ten-eleven translocation
TUNEL	Terminal deoxynucleotidyl transferase dUTP nick end labeling
UBF1	Upstream-binding factor 1
UV	Ultraviolet
Wnt	Wingless-type MMTV integration site family member
XPC	Xeroderma pigmentosum, complementation group C
ZGA	Zygotic genome activation

9. Acknowledgements

10. Lebenslauf